R-09-39

Examination of the Excavation Damaged Zone in the TASS tunnel, Äspö HRL

Mats Olsson, Swebrec

Ingemar Markström, Anders Pettersson, Malin Sträng
Golder Associates

October 2009

Svensk Kärnbränslehantering AB
Swedish Nuclear Fuel
and Waste Management Co

Box 250, SE-101 24 Stockholm
Phone +46 8 459 84 00

ISSN 1402-3091
SKB Rapport R-09-39

Examination of the Excavation Damaged Zone in the TASS tunnel, Äspö HRL

Mats Olsson, Swebrec

Ingemar Markström, Anders Pettersson, Malin Sträng
Golder Associates

October 2009

Summary

The question of an existing continuous Excavation Damage Zone (EDZ) is very important for SKB. Is it possible to use drilling and blasting in the planned repository for spent nuclear fuel? Could fractures from blasting form a continuous EDZ?

In order to increase the understanding of the EDZ and the possibility of an existing continuous EDZ along the deposition tunnel, SKB decided to examine the fracturing in a selected area of the TASS tunnel and to create a 3D model of the fractures in the investigated area. It was of special interest to study the transition zones between the blast rounds to examine if the EDZ from the bottom charges could form a continuous EDZ from one round to another.

The TASS-tunnel is situated at the 450-m level in the Äspö Hard Rock Laboratory. The tunnel, with a cross-section area of 20 m^2, was planned to be 90 m long. In a subproject called Excavation the purpose was to test different plans for drilling, charging and initiation in order to give recommendations on how the final repository of spent fuel should be excavated.

The test methodology used in this investigation comprised the following steps: selecting test area, drilling and wire sawing of blocks, surveying the blocks, removal and transportation of the blocks to the surface, cutting the blocks into slabs, fracture identification with penetrants, positioning and photographing the slabs, digitizing and 3D modelling of the fractures.

The test area for EDZ consisted of an 8 m long and 1.5 m high section in excavation sequence no 4. The selected section covered the end of round 9, the entire round 10 and the start of round 11. In the contour and the helpers small diameter charges for smooth blasting were used (decoupled charges). These charges also have a relatively low detonation velocity (VOD) and this, together with the decoupling, gives short fracture lengths i.e. a small EDZ. The contour holes and the helpers were initiated with electronic detonators to achieve a simultaneous initiation, which also results in shorter fracture lengths in the remaining wall after blasting.

Eight adjacent blocks were excavated from the tunnel wall using wire sawing. The blocks were 1 m wide, 1.5 m high and c. 0.7 m deep. The blocks were transported to the surface for investigation, surveying and wire sawing into slabs. Of the 8 blocks, 5 were sawed into 9 slabs and 3 were sawed into 10 slabs. This makes a total of 75 slabs. One side of each slab was surveyed, cleaned and examined using penetrant fluid, which enabled detection of fractures with an aperture down to 20 µm. After this each slab side was photographed from a fixed position and the sawing of the next slab could start.

The digitalization of the fracture traces was done on screen in Quantum GIS and the fractures were classified into three different types of fractures: direct blast fractures, blast induced fractures and natural fractures. Direct blast fractures are fractures formed by the blasting process and these fractures originate from the borehole. Blast induced fractures are also caused by the blasting although they do not originate from the borehole itself. Natural fractures are fractures that existed in the rock before the blasting. They could be completely closed and/or filled, wide open or partly open. All visible fracture traces were digitized, except traces within crush zones. A total of 2,509 fracture traces were identified in the eight blocks.

After digitalization the 3D modelling was done in SKB's Rock Visualization System (RVS). A model volume was setup, covering the investigated area. In RVS the fracture traces were connected to form fracture planes in 3D space. All modelled fractures were assigned one of the three types Blast Fracture (direct), Blast Induced Fracture or Natural Fracture. All modelled fractures were confidence classed regarding geometry. Using this function a fracture model of the investigated volume was created. Fracture traces that could not be connected to any other fracture trace were modelled as small, planar fractures with unknown orientation.

In the model there are a total of 1,218 modelled fractures. There are 773 modelled natural fractures, 260 blast fractures and 185 blast induced fractures.

To verify the model, six areas were selected for a detailed investigation. The lesson learned from the detailed investigation was that the modelling was quite successful for the blast fractures and that no major revision of the model was necessary.

The following conclusions regarding the EDZ are drawn from the main investigation.

- No evidence is found of a continuous EDZ in the investigated area. No evidence is found that blasting fractures from different rounds are connected.
- Blasting fractures are strongly influenced by the presence of natural fractures as they are drawn towards the natural fractures.
- Since the blasting fractures do not form a continuous network, the capacity of the longer natural fractures is the limit of potential water flow in the rock mass.

Sammanfattning

Frågan om en kontinuerlig skadezon är av stor vikt för SKB vid val av uttagsmetod för ett slutförvar. Kan man använda borrning och sprängning för att göra tunnlarna utan att riskera att sprickor från sprängningen bildar en sammanhängande skadezon?

För att öka förståelsen för detta problem genomförde SKB en undersökning av sprickutbredningen i en utvald sektion i TASS tunneln i Äspö och att skapa en 3D-modell av sprickorna i området. Det var av specifikt intresse att studera övergångszonen mellan salvorna för att ta reda på om sprängskadorna från bottenladdningen i en salva åstadkommer en kontinuerlig skadezon till följande salva.

TASS-tunneln ligger på 450 m nivån i Äspö-laboratoriet. Tunneln, som har en tvärsnittsarea av ca 20 m^2 och planerades vara 90 m lång, drevs under 2008 i SKB-projektet ”Fintätning på stort djup”. Ett av delprojekten här gick ut på att undersöka om olika borr- och laddplaner för att senare kunna lämna rekommendationer till berguttaget i slutförvaret för högaktivt avfall.

Testmetodiken som användes i dessa försök omfattar; val av testområde, sågning av block, inmätning av block, uttag och transport av block till ytan, sågning av block till skivor, sprickdetektering med hjälp av penetranter, positionering och fotografering av skivor, digitalisering och 3D-modellering av sprickorna.

En 8 m lång och 1,5 m hög sektion av tunnelväggen valdes som försöksplats för att undersöka sprickutbredningen. Den utvalda sektionen täckte tre halvpipor i konturen och omfattade slutet av salva 9, hela salva 10 samt första delen av salva 11. Salvorna sprängdes skonsamt med patronerade och frikopplade sprängämnen i kontur och hjälpare. De valda laddningarna har också en låg detonationshastighet viket tillsammans med frikopplingen ger en kort sprickbildning. Dessa hål initierades med elektroniska sprängkapslar för att uppnå momentan initiering och därmed kortast möjliga sprickbildning.

I tunnelväggen togs 8 närliggande block ut med hjälp av wiresågning. Blocken var 1 m breda, 1,5 m höga och ca 0,7 m djupa. Blocken transporterades upp ovan jord där en speciell sågplats iordningställts. Blocken undersöktes, mättes in och varje block sågades därefter i 10–11 cm tjocka skivor. Av de 8 blocken sågades 5 till 9 skivor och 3 till 10 skivor, vilket ger totalt 75 skivor. Den ena sidan av varje skiva mättes in och undersöktes genom att den sågade skivytan rengjordes, torkades noggrant och påfördes penetrantvätska. Sprickor med en sprickvidd ner till 20 µm kunde på så sätt detekteras. Varje skiva fotograferades därefter med en fast kamera ovanför blocket varefter sågning av en ny skiva kunde påbörjas.

Sprickspåren i samtliga skivor digitaliserades i Quantum GIS och sprickorna indelades och färgkodades i tre kategorier, direkta sprängsprickor, spränginducerade sprickor samt naturliga sprickor. Direkta sprängsprickor är sprickor som uppstått av sprängningen och som direkt utgår från ett borrhål. Spränginducerade sprickor är sprickor som uppstått till följd av sprängningen men de har inte kontakt med borrhålet. Naturliga sprickor är sprickor som fanns i berget innan sprängningen. De kan vara slutna, helt öppna eller delvis öppna. Alla synliga sprickspår digitaliserades, utom inom krosszoner. Totalt identifierades 2 509 st sprickspår i de åtta blocken.

Efter digitaliseringen vidtog 3D-modellering och här användes SKB:s Rock Visualization System (RVS). En modellvolym skapades som täckte uttagsområdet. De digitaliserade tvärsnitten kopplades som referensfiler till RVS-modellen med inmätta fixpunkter och sprickplanen skapades genom att utvalda linjesträngar knöts till ytor. De modellerade sprickorna klassades, på samma sätt som sprickspåren som sprängsprickor (direkta), spränginducerade sprickor samt naturliga sprickor. Alla modellerade sprickor konfidensklassades också rörande geometri. På detta sätt skapades en sprickmodell i den undersökta bergvolymen. Sprickspår som inte kunde knytas till något annat sprickspår modellerades som små, plana sprickor med okänd orientering.

I modellen identifierades 1 218 sprickor varav 773 st naturliga sprickplan, 260 plan av sprängsprickor samt 185 st plan från spränginducerade sprickor.

För att verifiera modelleringen valdes sex områden ut för detaljundersökningar. Resultaten från dessa undersökningar verifierade i stort sett modelleringen och medförde att endast mindre justeringar av modellen behövde göras.

Slutsatserna om sprängskadezonen (EDZ) kan sammanfattas med:

- Det finns inget som tyder på en kontinuerlig EDZ i det undersökta området. Inget tyder på att sprängsprickor knyts samman mellan olika salvor.
- Sprängsprickor påverkas starkt av närheten till naturliga sprickor då sprängsprickorna dras mot de naturliga sprickorna.
- Eftersom sprängsprickorna inte bildar ett sammanhängande spricknätverk så är det kapaciteten för de långa naturliga sprickplanen som utgör begränsningen för potentiella vattenflöden i berget.

Contents

Attached to the printed report is a DVD containing:
1 Tunnel wall before and after sampling
2 Overview of the blocks (back side and top views)
3 Dry samples (without dye)
4 Images (same as Appendix 1)

1 Introduction

1.1 Background

In 2003 a tunnel was driven by SKB in their Hard Rock Laboratory in Äspö in order to examine the pillar stability /Andersson 2007/. In some of the rounds electronic detonators were tested and the Excavation Damage Zone (EDZ) was examined in the walls and floor of the tunnel /Olsson et al. 2004/. The EDZ was examined by cutting slabs from the wall and then by spraying dye penetrant on the remaining slot surface causing all of the fractures in the rock to appear very clearly. The result of this examination showed no continuous EDZ in the wall.

The question of an existing continuous EDZ is very important for SKB. Is it possible to use drilling and blasting in the planned repository for spent nuclear fuel? Could fractures from blasting form a continuous EDZ? In order to increase the understanding of the EDZ and the possibility of an existing continuous EDZ along the tunnel a methodology study was made to examine if it was possible to produce a 3D model of blast induced fractures around a tunnel /Olsson et al. 2008/. The result of the study was so positive that it was decided to use the same methodology for an examination of the EDZ in the TASS tunnel.

1.2 Scope of the study

The purpose of this project was to examine the EDZ in an 8 m long section of the wall in the TASS tunnel and to create a 3D model of the fractures in the investigated area. It was of special interest to study the transition zones between the rounds to conclude if the EDZ from the bottom charges could form a continuous EDZ from one round to the next.

1.3 Terminology

In this report the terms Fracture and Fracture traces are used. It is vital that the reader appreciates the difference between the two concepts.

A Fracture is a 3D object and can be an observed structure in field or on an investigated slab as well as a 3D modelled object created by connecting Fracture traces to a surface.

A Fracture trace is a 2D object and is the imprint of a Fracture on a planar surface. When the investigated slab surface is photographed, and digitized, 2D Fracture traces are created.

Since the Fracture traces are connected into Fractures when modelling, the number of Fracture traces, section 7.1, will be higher than the number of modelled Fractures, see section 7.2. Still, all Fracture traces are used for modelling Fractures.

2 Site conditions

2.1 Location

The TASS-tunnel is situated at the 450 m level in the Äspö underground laboratory, see Figure 2-1. The tunnel, with an area of 20 m^2, was planned to be 90 m long. The purpose of the tunnel was mainly to confirm that silica sol is a useful grout. The TASS-tunnel was therefore placed in an area with water bearing fractures. The direction of the tunnel was perpendicular to the zones of water bearing fractures. The area was classified as consisting of fresh Äspödiorite, see section 2.2.1, with steep water bearing fractures with a NW-NNW direction.

The test area for the EDZ covers an 8 m long section of the right wall starting at the end of round 9 in length section 36 m and stops in round 11 in length section 43 m, see Figure 2-2. The driving direction is from right to left in the figure. The block numbering coincides with the chainage at the end of the 1 m blocks. Thus block 37B covers the transition from round 9 to 10 and block 41B the transition from round 10–11. Each 1 m block was sawn into 9 or 10 vertical slabs. The slabs are consecutively numbered, e.g. 37B-01, 37B-02 etc. Of the 8 blocks, 5 were sawed into 9 slabs and 3 were sawed into 10 slabs. This makes a total of 75 slabs.

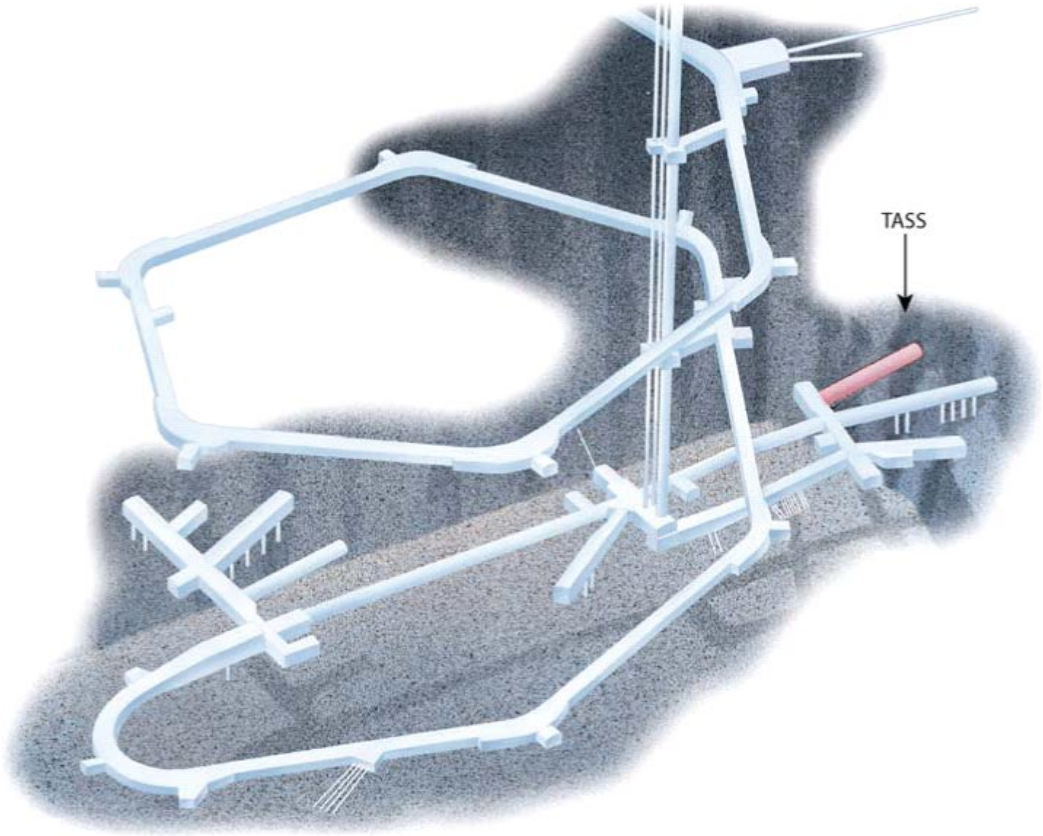

Figure 2-1. *The underground laboratory in Äspö /Malmtorp et al. 2008/.*

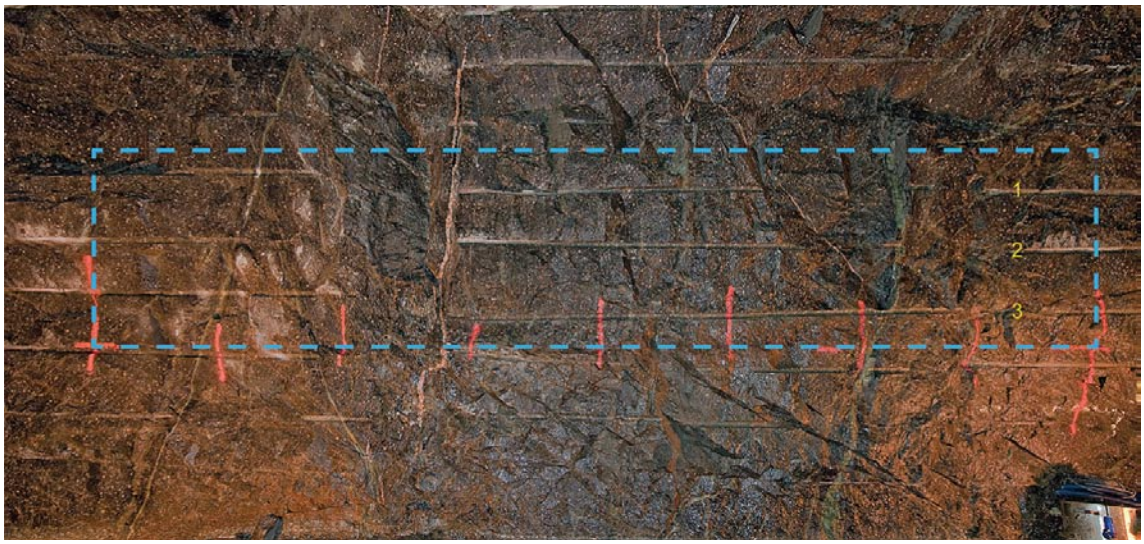

Figure 2-2. *The test area, for block numbers see Figure 4-1.*

2.2 Geology

2.2.1 Overview of the lithology

The bedrock in south-eastern Sweden is dominated by igneous rocks that belong to the c. 1.8 Ga generation of the Transcandinavian Igneous Belt (TIB). The main rock types are granite-syenitoid-dioritoid-gabbroid and associated volcanic rocks. The youngest rocks are dykes and irregular intrusions of fine-grained granite as well as fine-grained mafic dykes that commonly constitute composite intrusions together with fine-grained granite.

The dominant rock type at Äspö is the so-called Äspödiorite, a medium-grained, sparsely to strongly porphyritic rock that vary in composition mainly between quartz monzodiorite and granodiorite, but granitic, quartz monzonitic, tonalitic and quartz dioritic varieties occur as well. Another lithological component of importance is the so-called Ävrö granite, a medium-grained rock that vary in composition between granite and granodiorite. Dykes, patches and irregular intrusions of fine-grained granite are frequently occurring. Additional subordinate rock types are mafic rocks, including both diorite/gabbro and fine-grained composite intrusions as well as fine-grained dioritoid and pegmatite.

2.2.2 Lithological observations in the blocks

All blocks are dominated by red to grey, coarsely porphyritic Äspö diorite. Near a fractured zone in the bottom of the blocks, see Figure 4-4 the diorite is more fine grained and less porphyritic.

There are smaller occurrences in all blocks of fine-grained, dark grey mafic rock fragments, in the size range 5–30 cm, generally with an elongation axis concordant with the foliation. The boundaries between the host diorite and the fine-grained mafic rock are diffuse indicating a similar age of formation.

There are no occurrences of the Ävrö granite in any of the blocks.

In slab 37B-08 a bigger fine-grained mafic rock fragment appears the part visible in the slab is 90 cm×30 cm. This fragment cuts the foliation of the diorite. The fragment is possible to follow from slab 37B-08 to slab 38B-04, see Figure 2-3.

A 1–2 cm thin aplite dyke cuts through the Äspö diorite and a fine-grained mafic rock from slab 38B-01 to slab 38B-08, see Figure 2-3.

A 2–5 cm thin dyke of fine grained, weak porphyritic aplite cuts from slab 41B-05 to 41B-08.

In slab 42B-07 to 43B-03 a 10–20 cm wide aplitic dyke appears. This aplite is fine grained, grey to green and massive. In the contact area (3 cm wide) with the aplite the Äspö diorite is more foliated (ductile deformation), less porhyritic and contains more mica and epidote than usual, see Figure 2-4.

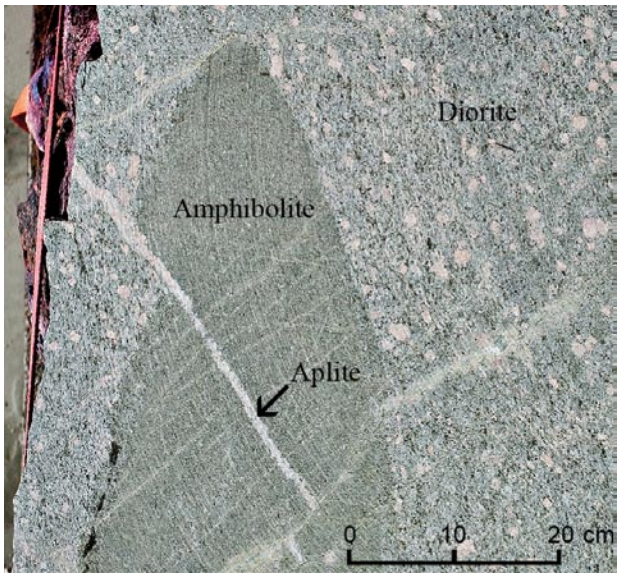

Figure 2-3. *Diorite with a fine-grained mafic rock fragment and a 1–2 cm wide aplite dyke in block 38.*

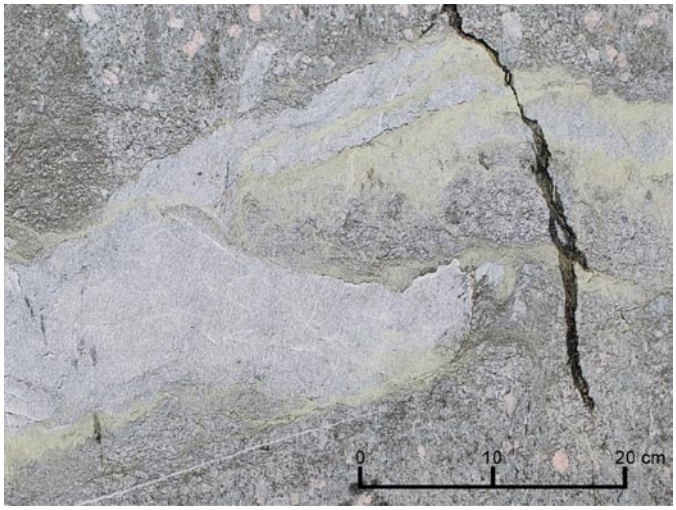

Figure 2-4. *Aplite dyke and Äspö diorite in block 42B. The contact area is 3 cm wide.*

In block 43B, more fine-grained mafic rock fragments appear. The Äspö diorite is less porhyritic and has a more intermediate composition compared to the other blocks.

2.2.3 Overview of structures

The bedrock at Äspö, is post-tectonic in relation to the regional, penetrative deformation that is related to the peak of the Svecokarelian orogeny. The bedrock is affected by a system of ductile deformation zones. The 1,810–1,760 Ma TIB rocks locally display a more or less well developed internal fabric /Berglund et al. 2003/.

A large scale network of shear zones of ductile to semi ductile character is located in the coastal area of Äspö. Most of these shear zones are often thinner than 1 meter, but the Äspö shear zone (EW1) is c. 100 m wide in the central part of Äspö.

During the last ca 1,450 Ma only brittle deformation has affected the bedrock in the Oskarshamn region /Berglund et al. 2003/.

The oldest fractures are epidote- and quartz-bearing, and with decreasing age, chlorite, prehnite and calcite appear as fracture filling /Drake and Tullborg 2007/.

The NE-SW trending structures are the oldest, followed by the E-W trending systems. The youngest system is the N-S trends /Nisca 1987/.The large scale semi-ductile deformation zones in the area generally have a steep NE direction.

Figure 2-5 shows a Schmidt diagram in the TASS tunnel. The orientations are given relative to the magnetic north.

SKB:s tunnel mapping from the actual section of the TASS-tunnel has identified 128 fractures. The cut-off for tunnel mapping is 1 m fracture length. In Figure 2-6 the fractures have been plotted showing classifications of type (top) and mineral generation (bottom) as classified when mapped.

Natural fractures re-opened by blasting appear to follow the in situ stress patterns in terms of orientation, see section 2.2.5. A majority of natural fractures re-opened by blasting ('Blast Open Nat Fra' in Figure 2-6) appear to be subvertically dipping, with a wide range of strikes that are generally subparallel to the orientation of σ_1 (W to WNW) (the diagram at top in Figure 2-6).

A tentative assessment of the age/generation of minerals filling fractures suggests some interesting correlations. The terminology of /Drake and Tullborg 2007/ is used (cf. Table 3-7 in /Wahlgren et al. 2008/). There is a slight tendency for fractures hosting Generation 3B minerals (prehnite and calcite) to have subhorizontal dips. There also appears to be a slight tendency towards east-west strike for fractures hosting Generation 3A minerals (quartz, epidote, chlorite, calcite, pyrite, flourite, and muscovite). The Generation 2A minerals (cataclasite; epidote, quartz and chlorite) in Figure 2-6 are older than 1,450 Ma. Class 3A/3B indicates that it has been impossible to decide if the minerals belong to Generation 3A or 3B. UNK stands for 'unknown'.

However, none of these tendencies have been subjected to rigorous statistical testing; in addition, there are a large number of fractures for which it was not possible to uniquely identify a specific mineral generation (the diagram at bottom in Figure 2-6).

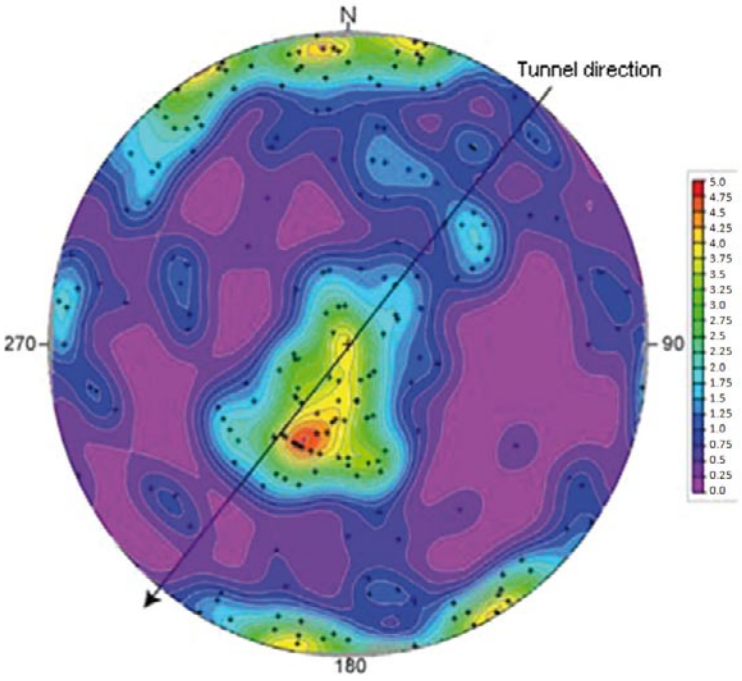

Figure 2-5. *Stereogram (Schmidt) of fracture orientation /Malmtorp et al. 2008/.*

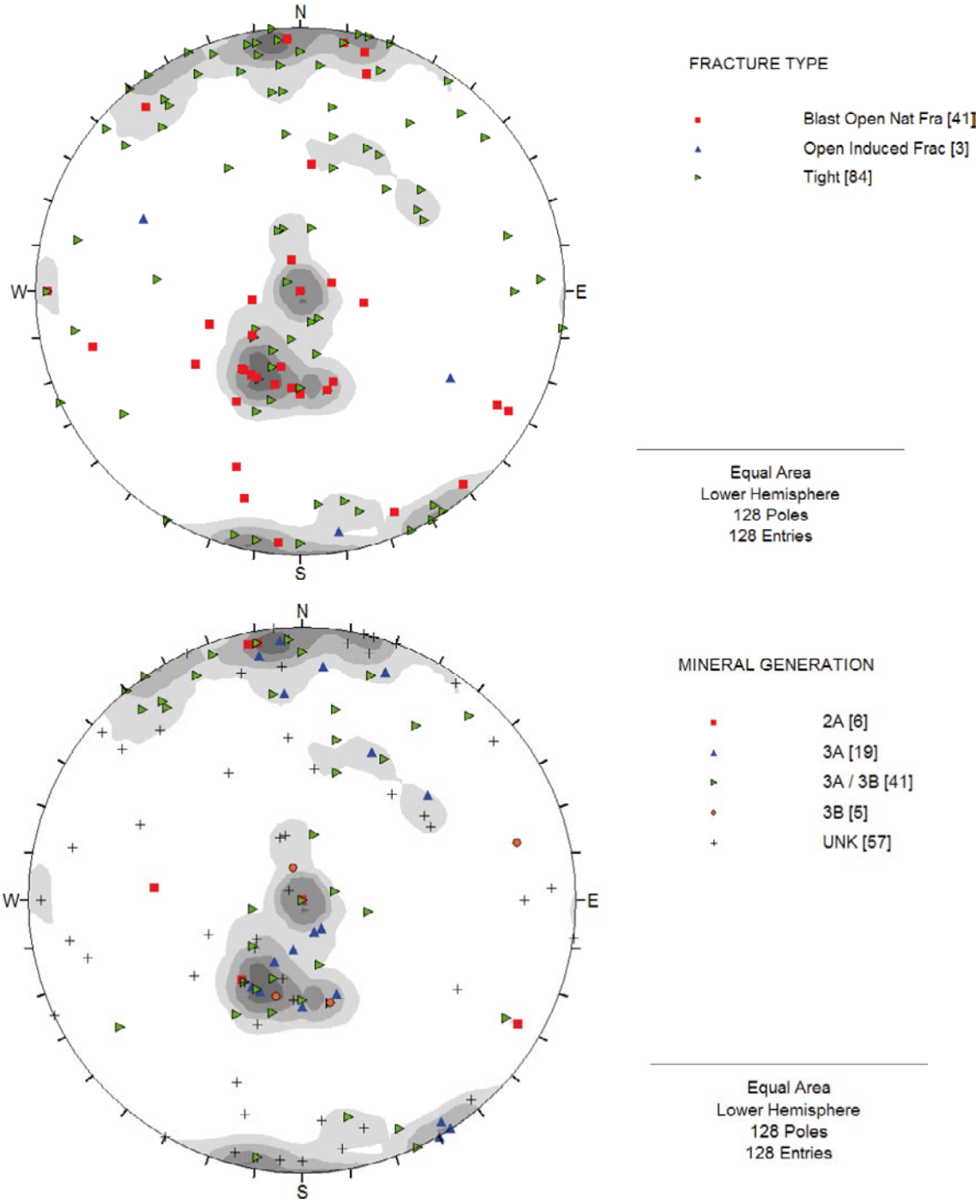

Figure 2-6. *Fractures from SKB:s tunnel mapping plotted in stereo diagrams. The classification of the fractures was made by SKB site geologists when mapping. The mineral generation classes in the lower diagram are explained in the text below.*

2.2.4 Observations of structures in the blocks

A larger fractured zone is possible to follow in the bottom of block no 36B to block no 40B. The zone is more than 20 cm wide (Figure 2-7).

There are many natural fractures in the blocks, both open fractures, sealed fractures with different minerals and old sealed fractures, which have opened during the blasting and transportation of the blocks. Observed fracture fillings from the project area are epidote (slab 38B-05–308B-06, 40B-05–41B-08 and 43B-01–43B-03), calcite (slab 39B-03), chlorite (slab 36B-05), quartz (slab 38B-02), pyrite (slab 42B-10) and oxidation around the fractures.

A large open fracture (observed in slab 38B-07 to 38B-09), which caused a big part of the block to fall off during the sawing, contains chlorite and calcite. Another big, calcite filled fracture stretches from slab 39B-04 to 39B-07. The filling in this fracture is about 2 cm thick, see Figure 2-8.

2.2.5 State of stress

The maximum compressive principle stress (σ_1) at Oskarshamn is generally WNW, with the minimum principle compressive stress (σ_3) oriented vertically, see Table 2-1. Note that trend orientations in this table are given towards Äspö96 north which is oriented approx. 12° west of RT90 north.

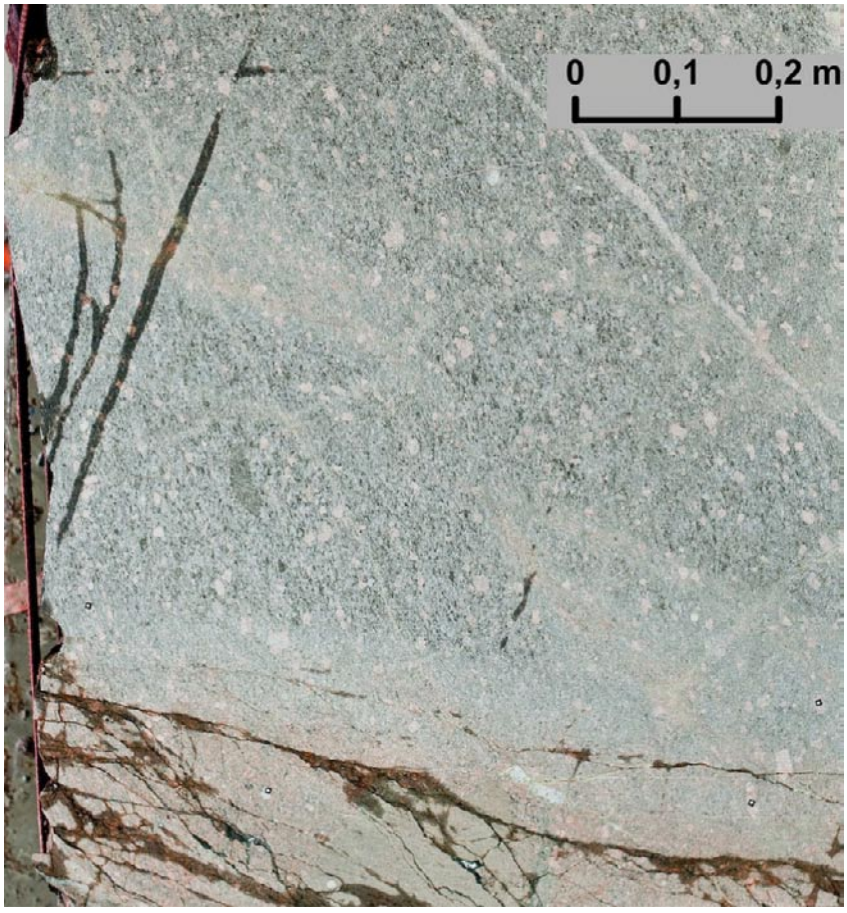

Figure 2-7. *20 cm wide fractured zone in bottom of the block (and photo), which is possible to follow from block no 36B to block no 40B. Note half-casts on left side of slab. This gently dipping fracture is noted all the way to the collar of the tunnel, i.e. it is more than 40 m long.*

Figure 2-8. *An open, 2 cm thick fracture filled with calcite in block 39. Note half-casts on left side of slab.*

Table 2-1. Probable stress tensor for the adjacent TASQ tunnel /Andersson 2007/.

	σ_1	σ_2	σ_3
Magnitude [MPa]	25–35	15	10
Trend (Äspö96)	310	090	208
Plunge (degrees from horizontal)	30	53	20

3 Excavation method

Within the main project “Fintätning på stort djup” (Sealing of tunnels at great depth) there was a subproject called Excavation. In this subproject the purpose was to test different plans for drilling, charging and initiation in order to give recommendations on how the final repository should be excavated. The result of the excavation is published in the report “Berguttag i TASS-tunneln” /Malmtorp et al. 2008/ (Excavation of the TASS-tunnel). It was also planned to examine the damage zone from blasting, EDZ, under different circumstances along the tunnel wall. However during the project it was decided to focus the examination of the EDZ to a specific area of the tunnel, see chapter 2.1.

The planned 90-m excavation of the TASS tunnel was divided into 7 sections and each of the sections consisted of 2-4 rounds. Smooth blasting techniques were used in all the rounds when excavating the TASS tunnel. The test area for EDZ consisted of an 8 m long section in excavation section no 4 and covered parts of round 9–11. Test section 4 consisted of four rounds, round 9–12 and it was situated between length sections 32.47–48.47 m along the tunnel, see Figure 3-1.

3.1 Drilling

There were 92 charged boreholes in a round and their diameter was 48 mm, see Figure 3-2. The hole length for all holes was planned to be 4.6 m. Table 3-1 shows spacing and burden values for the all of the charged holes. The lookout angle was planned to be less than 25 cm for all of the contour holes.

The opening consisted of 13 holes of which four holes were reamed to 100 mm and were left uncharged, see Figure 3-3. The originally planned location of the opening was in the middle of the tunnel but during the excavation the opening was moved towards the right wall.

The opening sequence in tunnelling is very important. This opening worked very well, was reliable and was an important reason for the successful advance values of the tunnel.

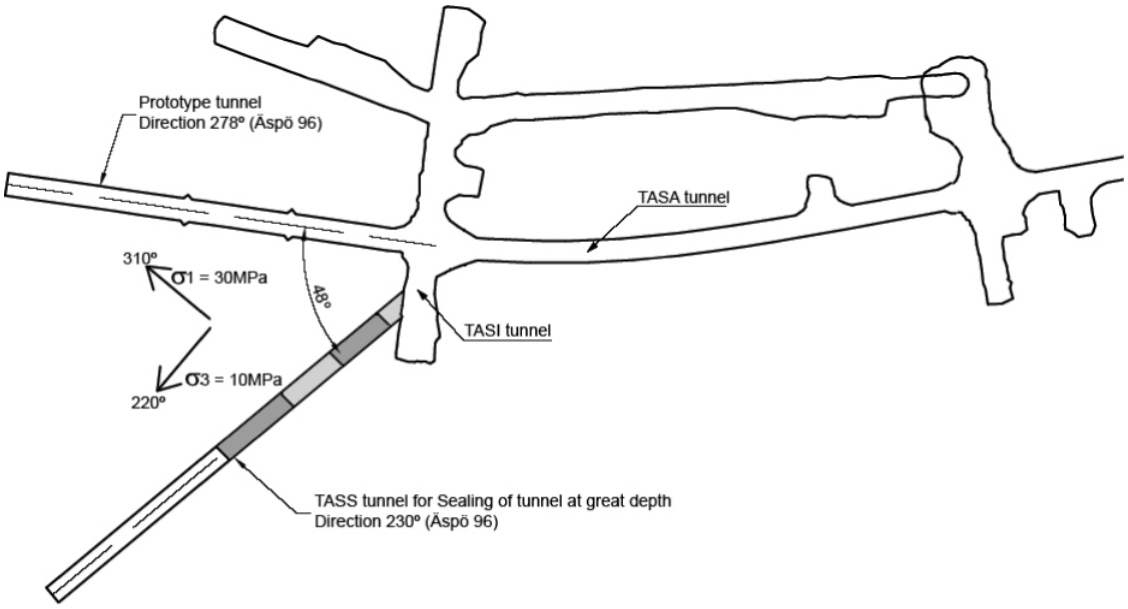

Figure 3-1. *A horizontal plan of the TASS tunnel /Malmtorp et al. 2008/.*

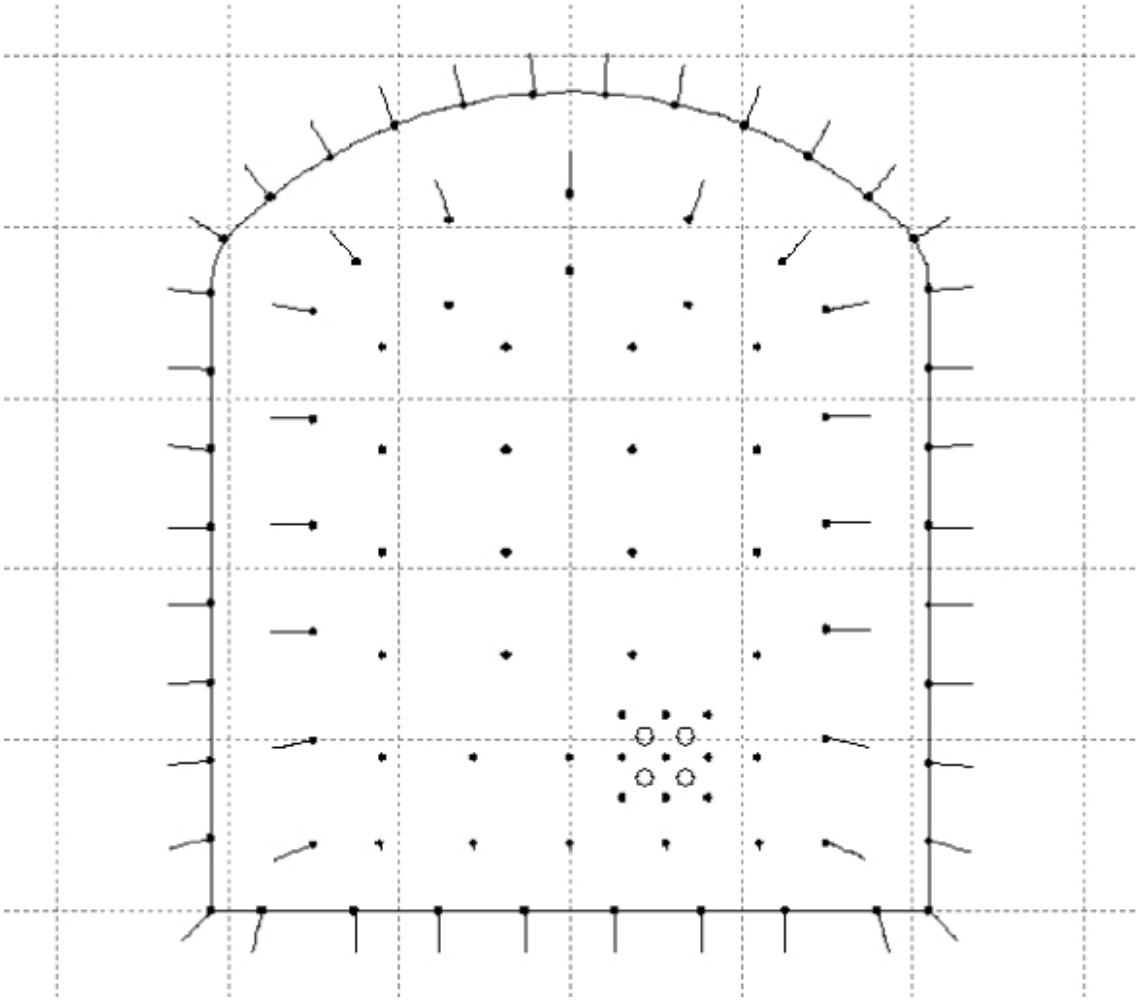

Figure 3-2. *Drilling plan for excavation section 4 (1 m grid).*

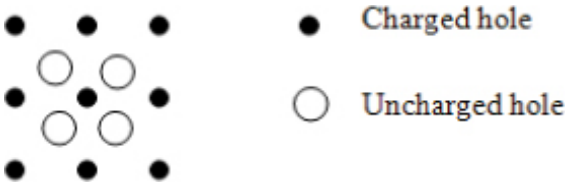

Figure 3-3. *A detail of the opening holes.*

Table 3-1. Borehole data.

Hole	No of holes	Spacing (m)	Burden (m)
Opening	9		
Stoping	28	0.60	0.60
Lifter	10	0.50	0.45
Helper	17	0.60	0.55
Contour	28	0.45	0.60

There was a collaring requirement for the contour holes, which stated that the centre of the borehole should stay within a theoretical box of 100×100 mm, see Figure 3-4. Furthermore the bottoms of the contour holes and the helpers should not deviate more than +/– 50 mm from the theoretical toe end of the hole.

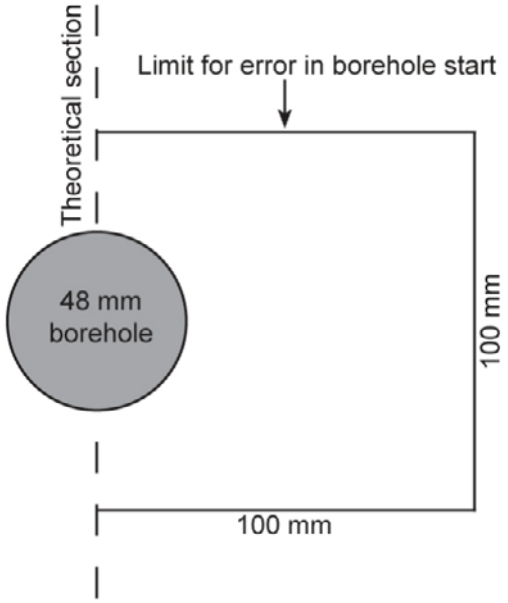

Figure 3-4. *The demand of collaring /Malmtorp et al. 2008/.*

3.2 Charging

All of the blast holes were charged with cartridged explosives from Orica, see Table 3-2. In the contour and the helpers small diameter charges for smooth blasting were used. In smooth blasting it is very important to use decoupled charges, charge diameter down to 1/3 of the hole diameter. The charges used also have a rather low detonation velocity (VOD) and this together with the decoupling gives a short fracture length i.e. a small EDZ /Olsson and Bergqvist 1995/. In Table 3-3 the characteristics of the used explosives are shown.

In Table 3-4 the charging plan for rounds 9–11 is shown. The explosive for the bottom charge is the same for all of the holes but the amount was cut to half in the contour holes, 190 mm instead of 380 mm. During charging these bottom charges were tamped to a length of 0.1 m for the contour holes and to roughly 0.2 m for the other holes. A total charge per round of 193 kg of explosives was used. The specific charge became 2.22 kg/m^3. With a total drill length per hole of 4.6 m and a planned charge length of 4.4 m roughly 0.2 m of the contour holes were left uncharged. A short stopper of cellulose plastic was used to lock the charges and then the collars of the holes were filled with gravel.

Table 3-2. Explosives used in rounds 9–11.

Hole	Bottom charge		Column charge	
	Name	Dimension (mm) diameter × length	Name	Dimension (mm) diameter × length
Opening	Dynomit	30×380	Dynorex	25×1,100
Stoping	Dynomit	30×380	Dynorex	25×1,100
Lifter	Dynomit	30×380	Dynorex	25×1,100
Helper	Dynomit	30×380	Dynotex 1	22×1,000
Contour	Dynomit	30×190	Dynotex 1	17×460

Table 3-3. Characteristics of used explosives, AN = ammonium nitrate.

Explosives	Components	Density (kg/dm^3)	VOD (m/s)	Gas volume (l/kg)	Energy (MJ/kg)
Dynotex 1	Nitro glycol, AN	1.0	2,300	930	3.4
Dynomite	Nitro glycol, AN	1.4	2,900–6,200	890	4.5
Dynorex	Nitro glycerine, nitro glycol, AN	1.4	>4,000	885	4.4

Table 3-4. Charging plan for rounds 9-11 (theoretical).

Hole	Charge weight (kg/hole)	Total charge (kg)	Charge length (m) Bottom	Column	Uncharged length (m)
Opening	2.8	25.2	0.38	3.92	0.3
Stoping	2.8	75.6	0.38	3.92	0.5
Lifter	2.9	29.0	0.38	4.02	0.2
Helper	1.8	32.4	0.38	3.92	0.2
Contour	1.1	30.8	0.19	4.21	0.2

There were however some changes made from the original charging plan. Instead of cutting the cartridges to fit the charged hole lengths the holes were charged with uncut cartridges, hence the length of the uncharged part of the holes differed between the holes.

3.3 Initiation

In all of the rounds of excavation no 4 the contour holes and the helpers were initiated with i-kon® electronic detonators from Orica, see initiation plan in Figure 3-5. The i-kon® detonators could be programmed within 0–15,000 ms in steps of 1 ms.

The accuracy is ± 0.05 ms within 0–500 ms and ± 0.01% within 501–15,000 ms. This accuracy results in a near simultaneous initiation of the holes of the same number. A simultaneous initiation of contour holes well within 1 ms results in shorter fracture length in the remaining wall after blasting /Olsson and Ouchterlony 2003/.

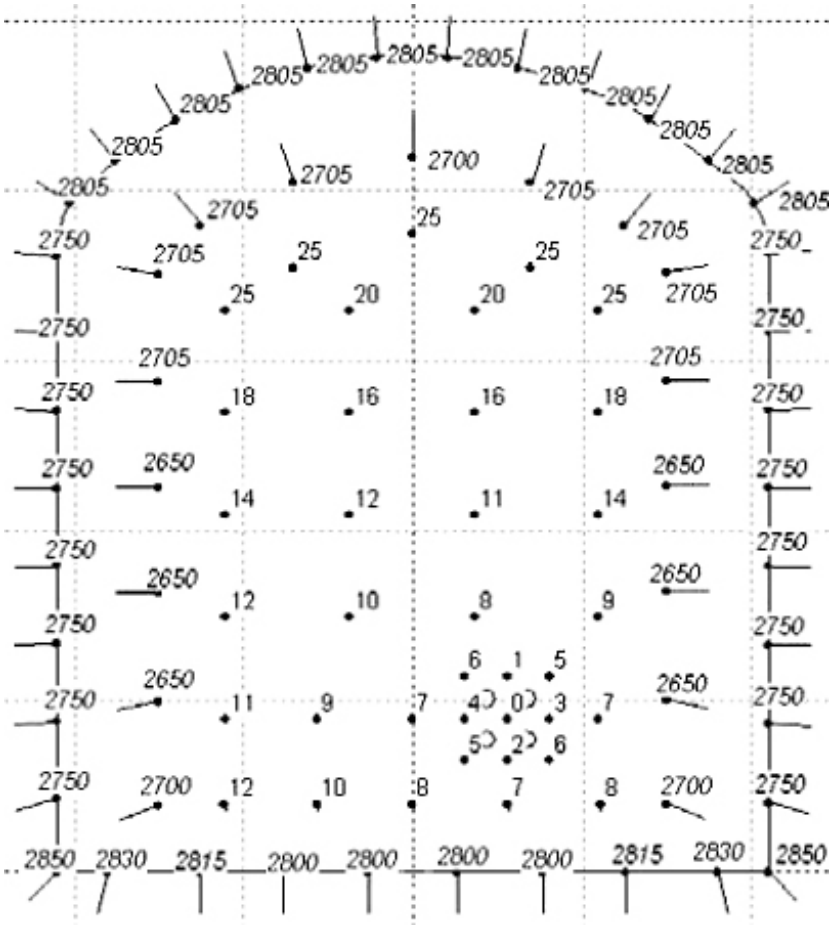

Figure 3-5. *Initiation plan for the holes in rounds 9–11.*

All of the wall holes were initiated simultaneously at interval 2,750 ms and all of the roof holes as well but on interval 2,805 ms. The helpers close to the wall were also initiated simultaneously at interval 2,650 ms. The expected accuracy is ± 0.28 ms.

3.4 Tunnel excavation

All holes were logged by the drill rig. Knowing the lengths of the contour holes and the lengths of the bottom charges and the number of column charges, the uncharged lengths for each round could in principle be calculated. However there is no detailed information available as there was no detailed follow up of the charging. The result for all of the three rounds is shown in Table 3-5, 3-6 and 3-7. Of interest for the EDZ study is the length of the bottom charges in rounds 9 and 10, the uncharged length in round 10 and 11 and the column charge length in round 10. Round 11 was the shortest round and also a round where the length of the holes varied quite much. This will of course have an important effect on the charge length but unfortunately there is a lack of information for round 11. There is no information concerning how many charges that were put in the holes and as a consequence the uncharged length is unknown. Therefore Table 3-7 is incomplete.

The start and end positions of the contour holes are also of great interest. The situation is about the same as for the charge lengths, i.e. a lack of information of the positions for the holes, see more in chapter 7.

A follow-up of the advance for these rounds resulted in advance of 101% for round 9 and 10 and 94% for round 11. A number of holes in the helpers and contour in round 9 had to be recharged and reblasted

Table 3-5. Some details for round 9.

Contour hole [1]	Hole length [2] (m)	Charge length (m)		Uncharged [5] (m)
		Bottom [3]	Column [4]	
1	4.56	0.14	4.14	0.28
2	4.56	0.14	4.14	0.28
3	4.56	0.14	4.14	0.28

Notes:
1) Hole number according to Figure 2-2.
2) Hole length from rig log.
3) Bottom charge compressed 50 mm reduce charge length to 190–50 = 140 mm.
4) Number of charges multiplied by charge length (example 9×460 mm = 4,140 mm).
5) Uncharged = length contour hole-bottom length-column length.

Table 3-6. Some details for round 10.

Contour hole [1]	Hole length [2] (m)	Charge length (m)		Uncharged [5] (m)
		Bottom [3]	Column [4]	
1	4.61	0.14	4.14	0.33
2	4.61	0.14	4.14	0.33
3	4.60	0.14	4.14	0.32

Table 3-7. Some details for round 11.

Contour hole [1]	Hole length [2] (m)	Charge length (m)		Uncharged [5] (m)
		Bottom [3]	Column [4]	
1	4.30	0.14	n.a.	n.a.
2	4.16	0.14	n.a.	n.a.
3	3.85	0.14	n.a.	n.a.

due to remaining rock in the bottom of the holes and also due to one undetonated electronic detonator, see Figure 3-6. The holes were re-charged with one 30×380 mm cartridge of Dynomit each and initiated with Nonel detonators. The hole marked as green corresponds to hole 3 in Figure 2-2 and it is the lowest hole in the test area. Certainly this re-blast has influenced the EDZ in this area but it is not clear how.

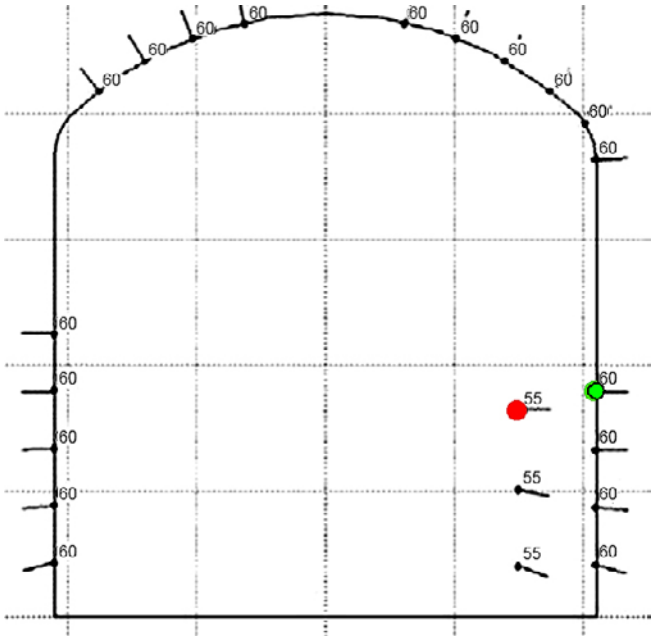

Figure 3-6. *Re-charged holes. The red marked hole contained the uncharged detonator.*

4 Test methodology

The earlier tested methodology of EDZ detection in Äspö consisted of cutting slabs in the wall of a tunnel and spraying dye penetrants onto the surface to visualize clearly the fractures /Olsson et al. 2004/. A pre-test to find out if it was possible to produce a 3D model of blast induced fractures around a tunnel had also been successful /Olsson et al. 2008/.

The test methodology used in this investigation comprised the following steps: selecting test area, drilling and wire sawing of blocks, surveying the blocks, extacting and transportation of the blocks to surface, cutting the blocks into slabs, fracture identification with penetrants, positioning and photographing the slabs, digitizing and 3D modelling.

4.1 Selecting the test area

The test area was selected on the following criteria:

1. The rounds in the test area were smooth blasted and initiated with electronic detonators. This always gives shortest fractures from blasting /Olsson and Bergqvist 1996/.
2. The presence of visible half-pipes. In order to measure the fracture length from a blast hole remaining half-pipes must exist.
3. At least three parallel half-pipes should be visible in order to be able to see the interaction between holes.
4. The test area had to cover at least two transition zones between the rounds.

The test area could be seen in Figure 4-1. The outer borders were marked on the tunnel wall together with proposed positions for the blocks to be cut. Eight sections were marked. The test area covers the end part of round 9, the hole length of round 10 and the first part of round 11. The length of the test area was 8 m and the height was 1.5 m. Each block was planned to be 1 m wide and it was required that the depth of the block was at least 0.5 m.

Note that it is very hard to find out exactly where rounds start and stop. The reason for this is that parts of the borehole collars and sockets have disappeared due to the blasting or scaling. Also notice that a vertical wedge has fallen out from the transition zone between round 10 and round 11.

The technique chosen to excavate the blocks was wire sawing. A Norwegian contractor DWireTeknikk, with a good reputation for this kind of work, was selected for the job.

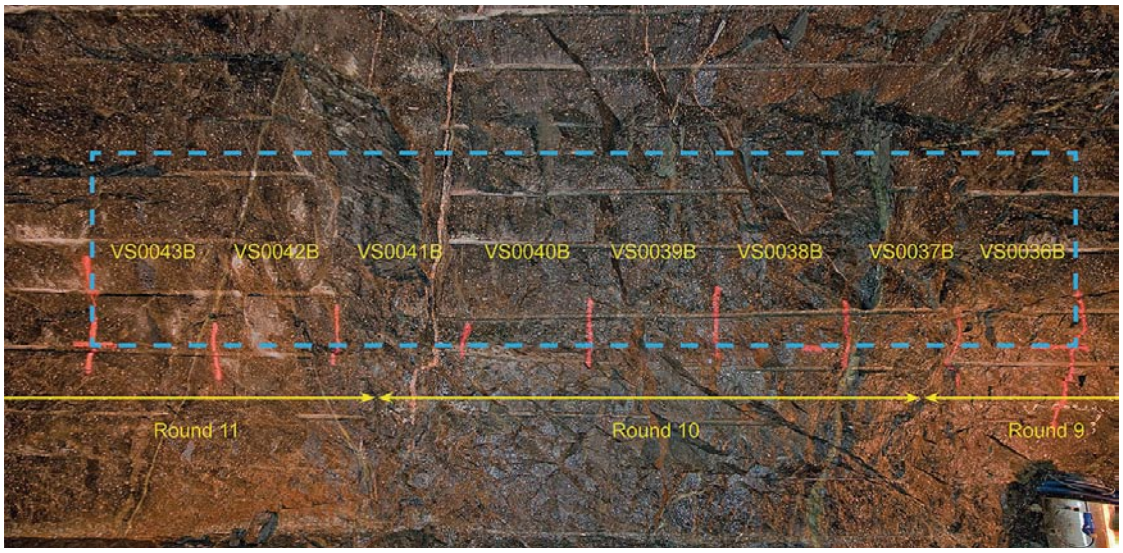

Figure 4-1. *The test area and the different rounds.*

4.2 Drilling of wire sawing holes

In order to extract the blocks without disturbing the ongoing grouting experiments there was a very strict requirement from the TASS organisation to stay within a restricted area. The contractor had suggested a technique with two drilled holes in the wall parallel to tunnel but this was not accepted. Instead it was decided to drill 18, Ø 250 mm, 2.5 m deep holes with core drilling, see Figure 4-2.

The exact position for each borehole was surveyed before drilling. The cores from drilling were transported, mapped and stored. The result of this mapping was also saved in the SKB system SICADA. Drilling of the lower row of holes was more difficult due to geological conditions and the cores from these holes fell apart into many pieces. Figure 4-3 shows a picture from the core drilling.

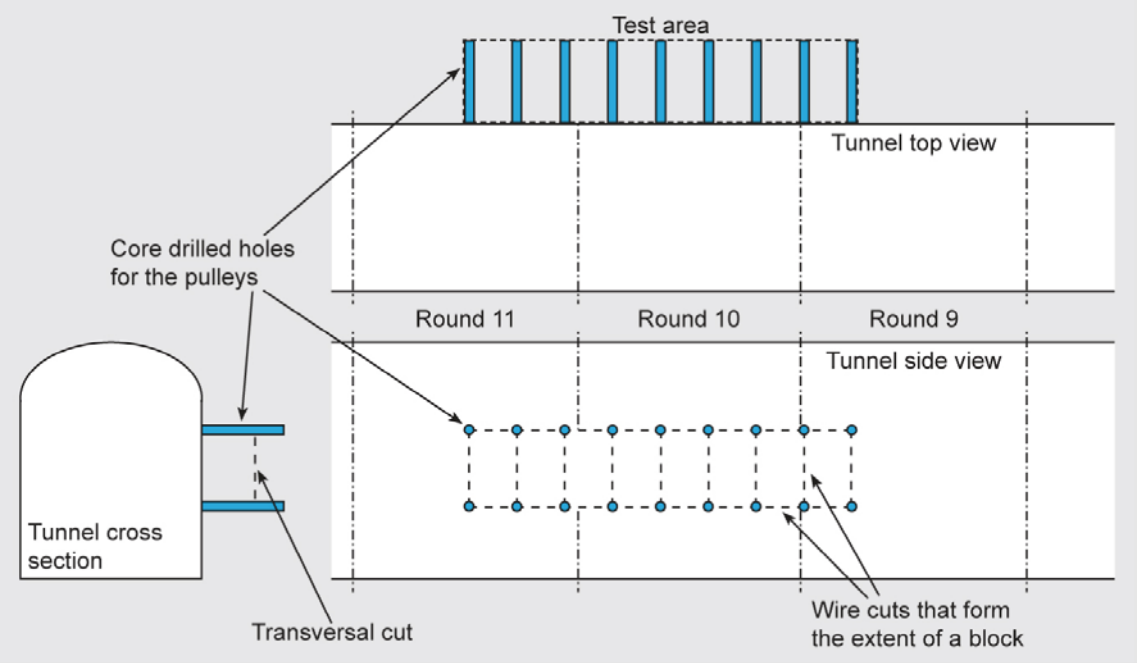

Figure 4-2. *The drilling/wire sawing principle.*

Figure 4-3. *Core drilling of wire sawing holes.*

4.3 Wire sawing

After drilling of the holes the wire sawing started. A pulley wheel was fixed close to the bottom of the holes and the wire was thread round the wheel, see Figure 4-4. The saw rig with its hydraulic motor and gear is mounted on a rail to enable it to slide backwards when sawing to create the tension on the wire that is needed.

The rotating speed of the wire and the traction force could be changed. The normal traction force is roughly 800 N. Figure 4-5 shows a picture from the wire sawing. Water is added to cool the wire and assist in the removal of the cuttings. In this way the wire cuts the rock from the tunnel wall and into the rock.

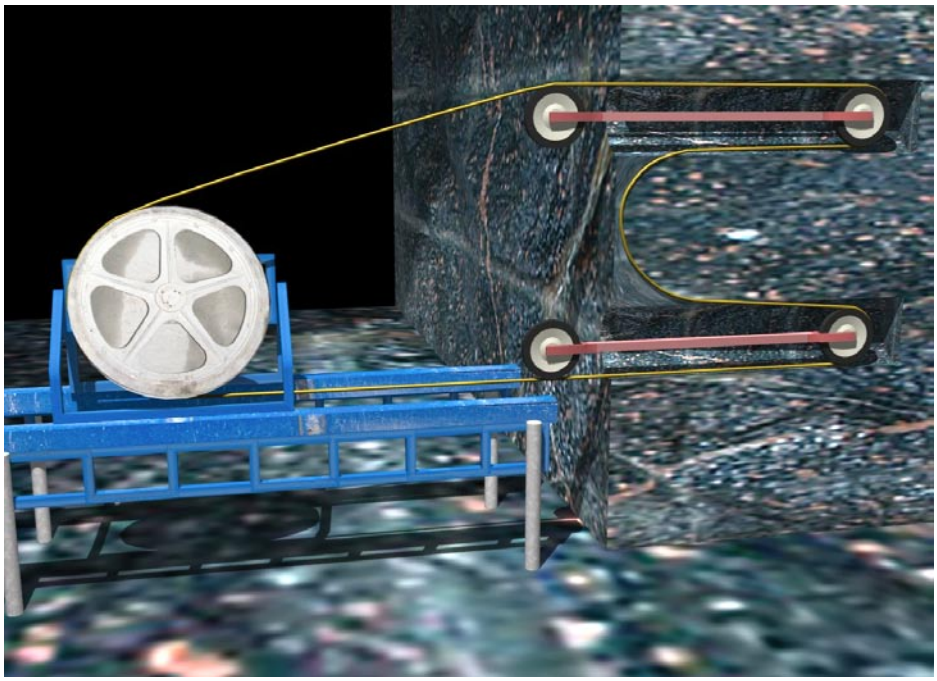

Figure 4-4. *The principle for wire sawing of vertical cuts.*

Figure 4-5. *Wire sawing of a horizontal cut.*

After sawing a lower horizontal cut a steel plate was inserted in the cut. After the steel plate was inserted, the vertical cuts separating the blocks and the upper horizontal cut were made. Finally the wire was threaded through the bottom horizontal cut and into the outer vertical cut and then back through the upper horizontal cut. The rig was then moved to the inner vertical cut where the wire was tread out via pulley wheels in the bottom of the holes and onto the gear of the rig. In this way the backsides of the blocks were cut loose. When the block was cut loose it dropped down some 3 mm onto the steel plate.

In order to be able to position the finished slabs in the 3D model, surveyed reference points were needed. The points were provided by marking the blocks with fix point markers before the blocks were extracted from the tunnel wall. The tunnel wall surface was also marked with white dots on black background as fix point markers that were surveyed with a total station to get their exact position in the tunnel. As the side of the next block became available when the previous block was removed, the side of this block was marked with markers that also were surveyed with a total station. When the survey was completed the block was cut loose from the wall.

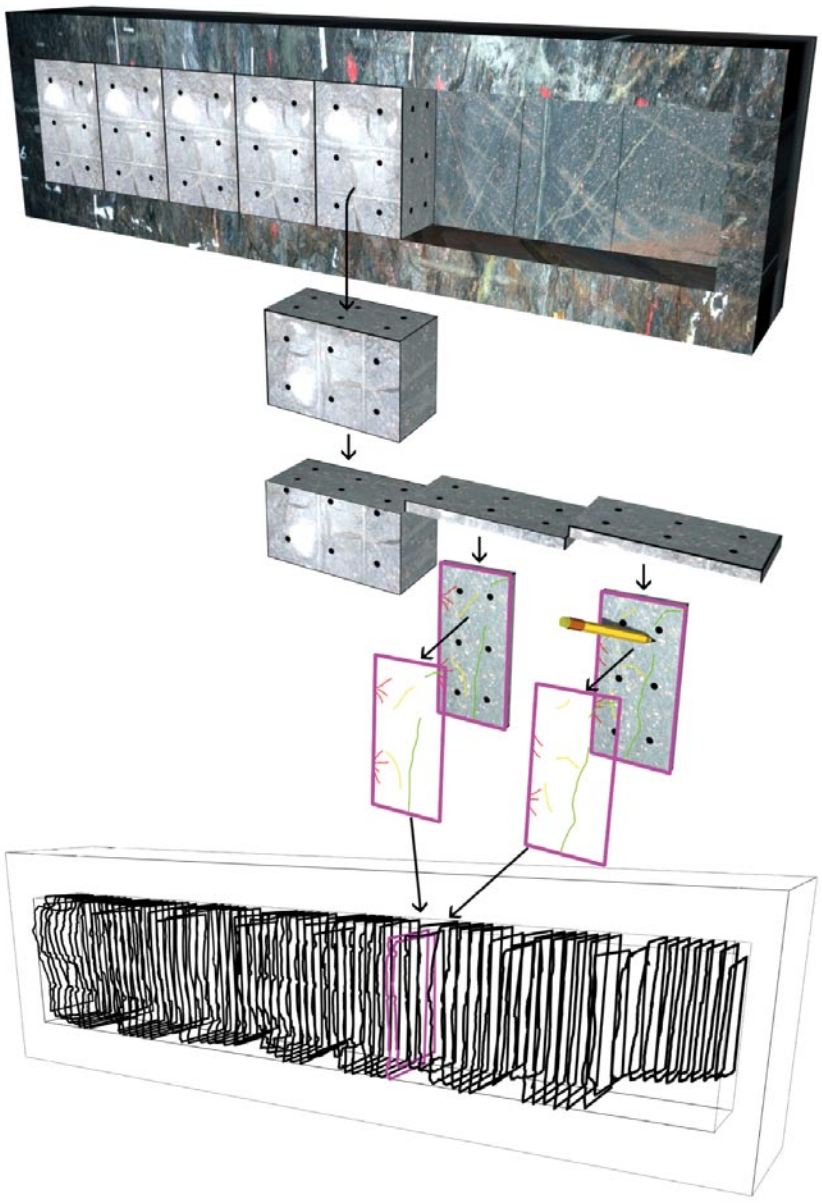

Figure 4-6. *Illustration of the process of extracting blocks, sawing into slabs, photographing, digitizing and referencing digitalization in 3D.The black dots represents fix point markers and the contour holes are shown as lighter lines.*

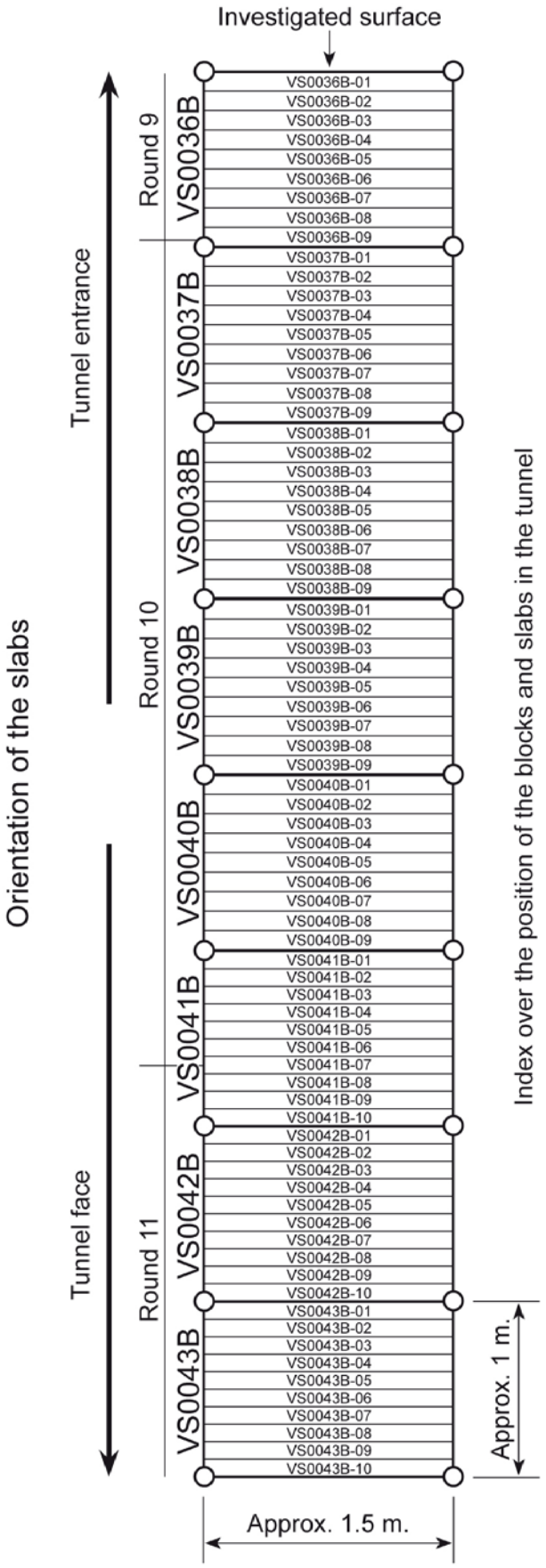

Figure 4-7. *Overview of the investigated blocks and slabs. All slab sides are presented in Appendix 1.*

This procedure made it possible to calculate the original position of the markers on the image of a slab in the tunnel. First the blocks were marked and surveyed before they were extracted. The next survey is done relatively to the marks already on the blocks, thereby establishing a relationship between the marks placed on the slabs while cutting them and the original places of the reference markings in the tunnel. This relationship between the different markings was then used to position the new slab surfaces, created when sawing, in 3D space.

Since this is multi step operation it is very important that the surveys have the highest possible accuracy and to have redundant points when positioning the surveying instrument. The additive nature of the errors when measuring in multiple steps also has to be taken into account, see section 6.2.2.

4.4 Extracting blocks

A custom made rig mounted on a front loader was placed so the blocks could be slid out from the tunnel wall and onto the rig. After this, a geared chain pulley was placed between the steel plate and the rig. Two persons then carefully pulled the steel plate with a block onto the rig.

The reason for doing this by hand was that the pull on the steel plate needed to be adjusted continuously to make sure that the block came out straight onto the rig. By pulling by hand the force could be adjusted more precisely than if motorized pulleys had been used.

The block was then packed and strapped up to make sure that no part of the block could fall off during the transport to the surface. The block was also securely strapped to the rig.

When all the blocks had been brought to the surface the first step was to photograph the top and backside of the block for future reference. There were two photos taken of each block surface, one when the surface was dry and one when it was wet in order to better see different features.

4.5 Preparing for fracture investigation

The blocks were tipped over so that the cutting could be done horizontally and to make it easier to move and transport the slab once the cut was made. The block was tipped over by strapping a large steel plate on to the rig and the block, securing it in to one package and then tipping it over with a truck and a front loader. The plate with the block was then moved with the front loader to the place where the sawing and surveying were done and the block was carefully positioned under the camera.

Figure 4-8. *Removal of a block from the tunnel wall.*

Figure 4-9. *Gently tipping a block.*

Figure 4-10. *The block positioned at the sawing/investigation place.*

When the block was in place, the position of the fix point markers placed on the blocks (made before they were removed from the tunnel) were surveyed using a total station. The purpose of this survey was to establish reference points for the positioning of the slabs in the model. Reference points were also established on the ground to be able to reposition the instrument even if the blocks moved during sawing.

4.6 Fracture investigation

When the markers on the block were surveyed the top side of the block was investigated.

Cleaning

The surface was cleaned with water and then dried using hot-air guns. It was very important to dry all the fractures on the surface completely since water significantly affects the penetration efficiency of the dye penetrant by preventing it from making contact with the rock surface and entering the fractures.

Colouring

After cleaning the block surface was sprayed with Bycotest RP 20 dye penetrant. The dye reveals fractures that are not visible to the naked eye by entering the fractures and colouring them red. This makes it possible to indentify fractures down 20 µm width (according to product specifications from Bycotest AB). Narrower fractures and fractures sealed with non-absorbing filling material cannot be detected. The dye needs approximately five to ten minutes to be absorbed in to the rock, depending on the ambient temperature and the structure of the rock.

After the dye was absorbed, excess dye was washed away with water and the surface was dried, first by using a window wiper blade and paper towels. To get the surface completely dry hot-air guns were used.

When the surface was dried the fractures immediately started to bleed out the dye absorbed in the fractures. There is a short time span where the fractures show up as thin lines on the surface of the slab but the dye can bleed quite heavily, soon making the fractures appear wider than they really are. Hence, the finer details of the fractures are usually lost within minutes, which is a problem when using dye penetrant. The problem is worsened if the fractures have not been dried enough as the water forces the dye out from the fractures. When fractures cluster close together they tend to show up as a coloured blob as the dye from several fractures meet and blur the picture. In some cases this could be remedied by washing the surface with Bycotest BC10 cleaner to remove the dye and letting new dye emerge from the fractures.

Documenting

For easier fracture identification and estimation of their orientation and constitution when 3D modelling, the slab was examined before it was cut from the block. Sketches of the surface were made and interesting details like width, fillings etc. were noted.

A number of free hand photos were also taken of the block sides at different angles, showing both the top surface and the sides of the block at the same time, see Figure 6-12 e.g. The purpose of these images was to show how the fractures near the edges of the surface continued further down in the block. These photos were taken during the whole slab sawing process and were found to be very useful when digitizing and 3D modelling.

During the processing of the surface the camera was aligned with the current surface. The realignment was done to compensate for the reduced height when removing a slab from the block. The reason for doing the alignment during the preparation process was to be ready to take the photo immediately after the surface of the slab became dry to make sure that the blurring in the images was kept to a minimum.

The images were taken at a perpendicular angle from a position directly above the surface of the block. Two sets of images were taken, one with and one without a reference scale placed on the surface.

Figure 4-11. *Photographing. From left to right: The camera, image from above showing camera and dyed surface, the investigated surface photographed without and with a reference scale.*

4.7 Sawing

When the investigation was completed the equipment was covered and the block was prepared for the cut. The first step of the cutting was to cut marks in the corners of the block to prevent the wire from slipping when starting the cut.

Before the cutting started the wire was placed in the marks and the saw was started. When the cut was half way through a steel plate was inserted into the cut. When the stone was cut through the slab had settled onto the steel plate and was then transferred onto a fork lift for transport to the storage.

The same saw that was used to cut out the blocks in the tunnel was used to slice the blocks into slabs.

4.8 Preparing for the next investigation

After the slab had been cut and removed from the block, the new surface of the block was prepared for investigation. New fix point markers were placed on it so that each piece of rock that could be suspected to fall apart would have at least two markers.

The total station was again setup using the reference points on the ground to reposition the instrument. Then the markers on the new surface were surveyed to get the new slab surface position in relation to the block's original place in the tunnel wall. The remains of the markers on the tunnel side of the block were also surveyed to make sure that the block had not moved.

When the survey of the surface was completed the surface was investigated as described above and then sawed again. This process was repeated with all slabs from a block 9 to 10 times per block depending on the quality of the rock.

4.9 Specification of photgraphic equipment

The equipment used was a Nikon D200 digital SLR camera with a Nikkor 35-mm lens attached. The camera was mounted on a geared tripod head to give the best possibilities to make fine corrections when aiming the camera to take the images. The tripod was attached to a threaded pole that was used to adjust the camera position in the vertical plane. A remote shutter control was used to make sure that the images were as free from movement blur as possible. A bubble level was mounted in the flash shoe on the camera to ensure that the camera was kept as level as possible.

Figure 4-12. *Preparing for sawing and the actual sawing.*

The main light source on most of the images was natural daylight. There were lights mounted in the tent at the sawing area, their main purpose was to lighten up the shadows from the tent and scaffolding and create a more even light on the slab.

The effective resolution of the images of the slabs is approx 2 pixels per millimetre.

The images were taken in NEF (Nikon Electronic Format). This is a raw format that represents the sensor data rather than the final image. One of the benefits of the NEF format is that the images can be reprocessed from the original data for different purposes. It also preserves maximum amount of details in the photo. The NEF files need to be interpolated to create RGB data from the sensor data. During the interpolation process some parameters were set like white balance and colour depth. In the next step contrast, colour enhancement and sharpening operations were applied. The goal of the process was not to create natural looking images but rather to emphasize the fractures. After the processing the images were exported to a tiff file for later use in Quantum GIS where the fractures were digitized, see chapter 5.

4.10 Revision of investigation process

After the first slab was cut it became apparent that the planned way of taking the images of the slabs by removing the finished slab and transporting it to a photo booth indoors, preparing the surface and taking the image of the surface there, was not going to work in a satisfactory way. The reason being that the slabs would risk falling apart when they were removed it from the block and even more so during the transport. This would make it impossible to distinguish fractures from the blasting from fractures originating from cutting and transport.

The solution to this problem was to photograph and investigate the block surface before cutting the slab. This ensured that only fractures that were present in the block when it was removed from the tunnel were recorded and that the fractures did not open up more than they had been in the tunnel.

To create a weather-proof investigation place a tent was raised over the sawing place and scaffolding was raised inside to create a platform for the camera and the photographer, see Figure 4-10 above. Due to the limited height in the tent a change in the camera setup was made. The lens was changed from one with 50 mm to one with 35 mm focal length, giving a small degradation in the geometry in the image. This degradation is measurable, within the mm range, but so small that it has no significant effect on our application.

5 Digitizing

The measured control points of each slab were transferred block by block to 2D reference files, one for each slab. These were later used to geo-reference the images. This part of the work was done in ArcGIS® 9.2 from ESRI, and each image was rectified to an image file in the GeoTIFF format. The relationship between the control points was very good, within ± 1.5 mm, and the necessary rectification was with small exceptions limited to rotation and scaling.

The digitizing of the fracture traces was done on screen in Quantum GIS. This application, often abbreviated to QGIS, is a free software desktop Geographic Information Systems (GIS) application that provides data viewing, editing, and analysis capabilities.

All the fracture traces were digitized and each fracture trace was given its own identification. The fracture identification was classified into three different types of fractures, blasting fractures (red), blast induced fractures (yellow) and natural fractures (green), see Figure 5-1. The classification is done by the blasting expert using the criteria described in sections 5.1–5.3. An example of fracture identification from photo is shown in Figure 5-2. On the left is the photo of the slab 40B-01 after the dye penetration process and on the right shows the same fractures digitalized. Notice the different types of fractures and how they are orientated.

For the digitization, the reference files and the rectified image files of each block were delivered as pre-prepared QGIS projects. The material for each block used a common coordinate system, which allowed simultaneous examination of adjacent slabs during the digitization in order to identify possibly related fractures.

After validation of data, and completion of the fractures with unique identities, the digitized files were converted to the MicroStation dgn format for the following modelling work. All format conversions were done with FME (The Feature Manipulation Engine), a tool for spatial data transformation and data translation. Unfortunately, the identities created in QGIS were not kept in the FME conversion to the dgn-file where the fractures got new id-numbers. This made the modelling a bit more difficult as the fracture identification was more time-consuming.

The bottom of block 36 could not be digitized as the rock here was so crushed that it fell apart. In the remaining part of the bottom of block 36, the rock also was so crushed that digitizing was impossible. A line was drawn marking the un-digitized area. This part was extended from slab 4 to slab 9 in block 36. When modelling, a surface was modelled to represent the upper border of the zone; under this surface no fractures are modelled.

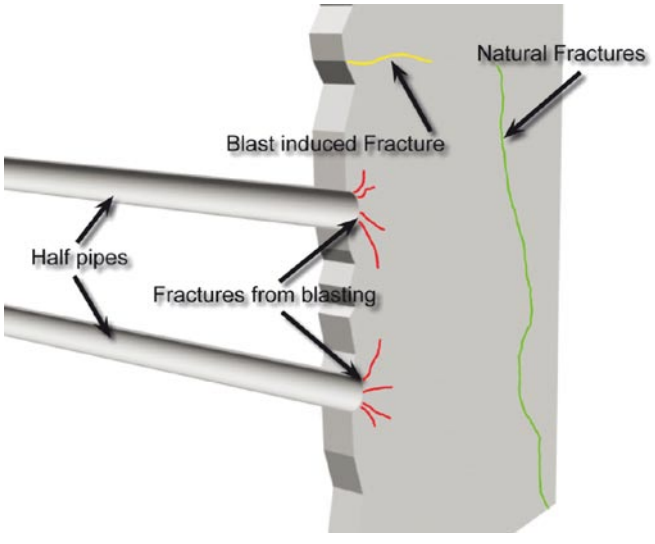

Figure 5-1. *Typical fracture pattern /Olsson et al. 2004/.*

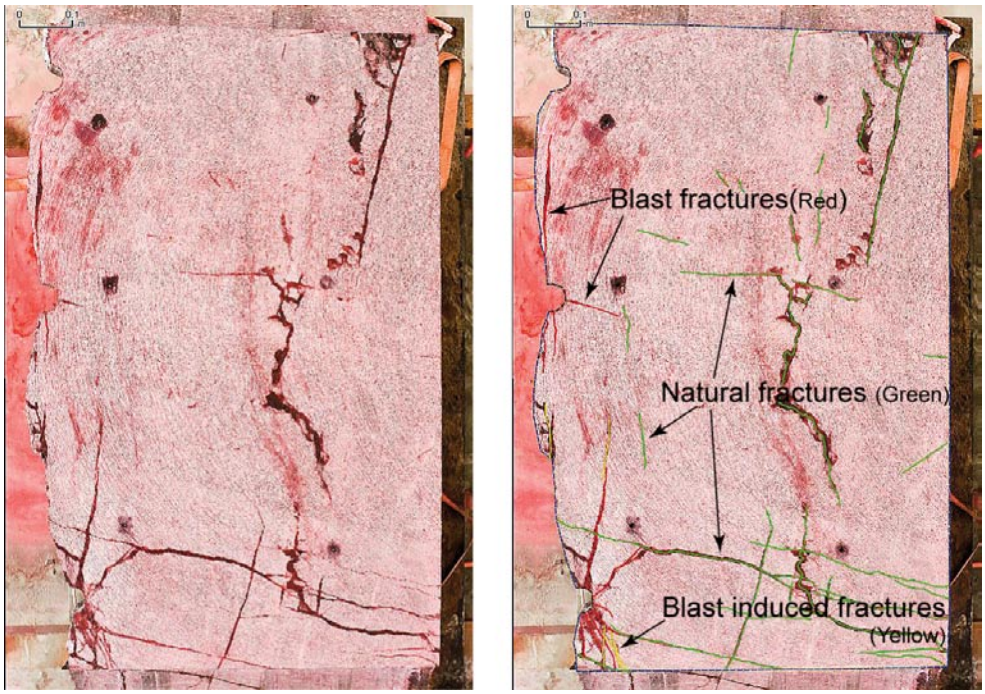

Figure 5-2. *Slab 40B-01; photo without and with digitized fractures on the right.*

5.1 Blast fractures

Blast Fractures are fractures formed by the blasting process and these fractures originate from the borehole perimeter or very close to it. Their direction is initially nearly radial. The length, intensity and width of these fractures are among other things dependent of the used explosive, the coupling ratio (diameter of charge/diameter of hole), the delay time of the detonators, spacing, nearby natural fractures, the rock and presence of water. These fractures are often rather easy to classify. In Quantum Gis they are marked as red fractures.

In this project the columns of the contour holes were charged with 17 mm Dynotex1 and initiated simultaneously. According to a huge number of earlier examinations the fracture length with this combination should be less than 15 cm /Olsson and Bergqvist 1997/. The fracture pattern from 17 mm Dynotex consists mostly of just a few radial fractures. The bottom charge was Dynomit and this cause another fracture pattern due to the explosive itself and the fact that the explosive was compacted to fill up the hole. An explosive with a high detonation velocity causes more and longer fractures and also a number of shorter shear fractures, due to the high borehole pressure around the borehole. If the bottom charge was used as column charge with same charge length, this would correspond to a charge weight of 5 times the charge weight for 17 mm Dynotex. The corresponding fracture length for the bottom charge then would be some 40 cm. Blasting fractures have a tendency to be drawn to natural fractures once the fracture tip comes close. They might stop there but in some cases they pass the natural fracture and continue further into the rock mass. Blasting fractures have the capacity to open up a closed natural fracture because they connect them with the blast hole, which contains high pressure gases from the explosive's detonation.

5.2 Blast induced fractures

Blast induced fractures are also caused by the blasting although they do not originate at the boreholes. Their directions are often pointing towards the borehole but they could appear in other directions as well. They could be parallel to the tunnel wall and they could appear as shorter fractures between natural fractures closer to the tunnel wall. These fractures are probably caused by the high stresses that are released by the blasting process or by the redistribution of stresses due to the excavation of the tunnel. These fractures are the most difficult fractures to classify as they can be hard to distinguish from natural fractures. In Quantum Gis they are marked as yellow fractures.

5.3 Natural fractures

Natural fractures are fractures that existed in the rock before the blasting. They could be completely closed and/or filled, wide open or partly open. They could often be identified on the sides of the blocks. Further they are often fairly easy to identify, the fracture surfaces are not fresh and often show evidence of oxidation and/or fracture filling. They often appear as long fractures parallel to the tunnel or as zones with crushed rock. Furthermore fractures far from the hole are most likely natural fractures. In this tunnel many of the natural fractures were flat dipping fractures. In Quantum Gis they are marked as green fractures.

5.4 Uncertainties

There are a number of uncertainties with the interpretation of fractures and how they should be classified. Below some typical questions to be considered and how they are handled are presented:

- How a cluster of fractures close to a borehole should be classified.

  If a fracture is in contact with the borehole it should normally be classified as a blasting fracture. A fracture near the borehole could be classified as natural or induced depending on geometry and the situation for other nearby fractures. The fracture surfaces, the slab sides and the fracture pattern of surrounding slabs are investigated to improve the interpretation.

- How the blasting fractures are affected by natural fractures.

  Blasting fractures are produced as radial cracks round the borehole due to the high pressure. If there are disturbances in the vicinity of the borehole, could be another borehole or other fractures, the blast fractures expand and the disturbances act like a free face. Tensile waves (returning waves) are produced and will cause scabbing of a part of the rock near the surface. All disturbances in the vicinity of the borehole will act like a magnet to the blasting fractures; they are hence generally drawn towards natural fractures.

- How the uncertainties in position of the boreholes affects the interpretation of the fractures.

  If the position of the borehole is not seen it is difficult to classify blasting fractures. As the position for the contour hole bottoms are very inexact it is very difficult to predict how long the fractures from a bottom charge are and how they will affect the next round. However, when the digitized sections are fitted into 3D space, visible half-pipes in surrounding sections facilitate the estimation of borehole positions within a round.

- How to follow and connect the right fracture if many fractures cross each other or to follow individual fractures that occur close to or within a complex network of natural fractures.

  This is not easy, nobody can be really sure. It is our interpretation; other persons could well have another opinion. Re-cutting the slabs in detailed investigations gives more information. Fracture characteristics are used to help the interpretation. When the digitized sections are fitted into 3D space the fracture pattern of surrounding sections will also help and could sometimes trigger re-evaluation of the interpretation made when digitizing.

- How to interpret fractures not indicated by the penetrant (i.e. a complete filled fracture).

  This is also tricky; a closed, narrow or sealed fracture can be lost. Generally very thin fractures are not affected by the penetrant. Wider filled fractures could be detected if the fill material in the fractures is soft and permeable for the penetrant. In some slabs there were thin visible lines in parts of the filled fracture and there it was possible to see and follow the filled fracture and tie the visible lines together to a longer fracture trace. The fracture pattern of surrounding sections is helpful when modelling; see the paragraph concerning re-evaluation when modelling in section 6.2.3.

6 Modelling

6.1 Conceptual model – fractures originating from blasting

6.1.1 Fracture propagation in general

Fractures have a tendency to go straight ahead if the state of stress is constant, i.e. static and if the material allows. Brittle materials are weakest in tension and in a homogeneous and isotropic material a fracture under symmetric static load goes straight ahead until it approaches a hole, or a fracture or something that disturbs the symmetry.

Anisotropic materials, e.g. gneiss, might be weaker along a schistosity plane than across it. The fracture will then no longer propgate perpendicular to the largest tensile stress but it is more likely to propagate along the schist plane. Local hard or strong areas are likely to force the fracture towards another plane parallel to the first.

A free surface or an open fracture attracts growing fractures but the fractures stops as they reach the surface. If a fracture is not fully open and the incidence angle is near 90 degrees the growing fracture can take a jump to the side and continue on the other side of the fracture.

If a fracture is formed under dynamic tensile conditions and then, when the dynamic stresses have subsided, is affected by superposed static (or dynamic) tensile stresses the fracture attempts to orient itself perpendicular to the new direction of maximum tensile stress. What might happen then is that the fracture front splits up into smaller fractures that on a plane surface look like a number of shorter parallel fractures ("en echelon"). This may possibly be interpreted as a single wavy fracture but it may well be a number of fracture fingers with its common root over or under the observation plane.

Then we have several dynamic effects. One is that a static fracture subjected to dynamic loading can begin to grow in an oblique direction; another is e.g. a borehole wall of rock where the strength varies from point to point. For dynamic loading, fracture growth initiates at the weakest place. Then the area around this fracture is unloaded and no new fractures are created there. But this suppression process takes some time. The faster the loading rate, the more fractures are initiated before the unloading effect takes over. A static load in a borehole normally creates two diametrical fractures along the borehole perimeter. By shooting e.g. high-pressure water slugs in a hole in a rock boulder, it is possible to regulate the number of fractures to between two and four fractures just by regulating velocity of the water slug.

In rock blasting many short fractures are formed around the blast hole but only a few (6–8) may grow to a significant length /Johansson and Persson 1970/. Such a crack system with many arms in 2D could be called a star crack /Ouchterlony 1983/). To assume that these arms continue along the whole length of a blast hole is in most cases false. The angle between the arms and the arm directions varies along the hole. In two cuts through the hole the fractures appear to start in different places. The blast hole in 3D looks rather like a hole with many semielliptic 'ears' attached to it. Figure 6-1 shows an example for isotropic rock. The trace length of an ear along the hole is probably longer than its depth in the lateral direction. When the blast fumes pressurize the ear cracks they grow and interconnect with each

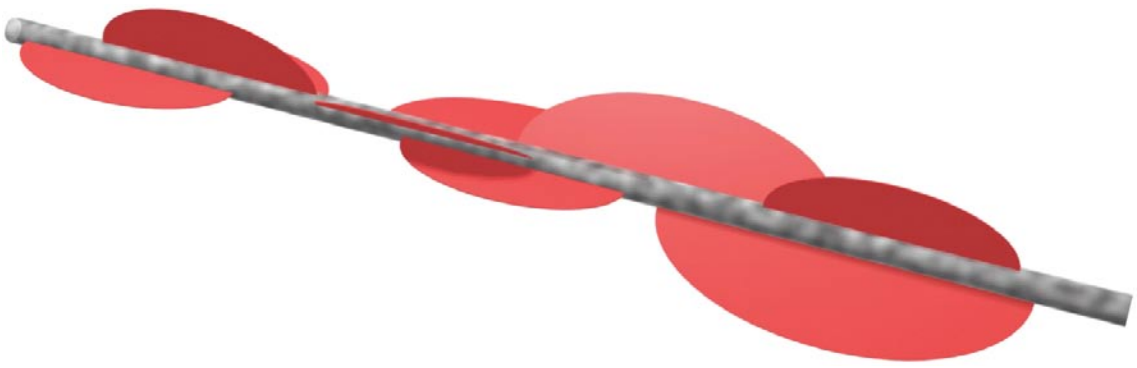

Figure 6-1. *Illustration of blast fracture formation.*

other, with cracks emanating from other blast holes, with natural fractures, with reflected stress waves from open fractures and other free surfaces and with the pre-existing stress field. This process creates the large through going cracks that separate the broken burden from the remaining rock mass. For an anisotropic rock the ears' traces along the blast hole are probably skewed already to begin with.

6.1.2 The blasting process

The phases of a blast essentially consist of

1. Detonation of individual charges.
2. Shock/stress wave propagation.
3. Fracture propagation.
4. Gas expansion and mass movement.

The detonation phase in turn consists of the following steps:

- the detonator plus a primer initiates a detonation in the charge,
- the detonation front moves up the charge with a characteristic, the VOD (velocity of detonation), which lies in the range 2,000–6,000 m/s for civil explosives,
- the pressure rises very fast and the reaction starts directly behind the detonation front, and,
- high pressure (up to several GPa for a fully charged blast-hole) and high temperature gases (several thousand K) are generated in the reaction, about 500–1,000 liters per kg of explosive after an expansion to atmospheric conditions.

The shock/stress wave propagation phase consists of the following steps:

- an initially radially symmetric shock wave moves out into the rock,
- the blast-hole wall simultaneously starts moving outwards, allowing the gases to do work,
- the rock surrounding a blast-hole is first, because of inertia, subjected to polyaxial compression of a more than sufficient magnitude to crush it if the hole is fully charged,
- then, as the shock wave moves out and radial movement of the blast-hole wall increases, the tangential compression relaxes and tends to go tensile, and,
- with the tensile stress radial cracking, which normally starts outside the wall of the blast-hole becomes possible.

These radial blasting fractures interact with the blast induced fractures and the natural fractures to form the rock fragments that define the breakage of primarily the burden. The gases in the blast-hole may penetrate into the cracks, widen them and increase the movement of the burden.

In normal smooth blasting the contour holes are typically initiated at delay numbers 50, 55 or 60 with a delay scatter of about ± 150 ms. The breakage process for each hole is more or less individual. The reflected wave from the free surface, where the compression was converted into tension, will favor the growth of cracks that are tangential to the wave front, i.e. more or less along the connection line between the contour holes. Their preferential growth will dominate the breakage.

When the contour holes are initiated simultaneously with electronic detonators, scatter of the order ± 0.1 ms, the primary waves from neighboring holes can interact with each other and with the growing fractures, see Figure 6-2. As the hole spacing normally is smaller than the burden, the first waves to arrive are now the compressive wave fronts from neighboring blast-holes. They first tend to close the growing blasting fractures and then their tensile tangential tails tend to favor growth of fractures that connect the blast-holes, leaving relatively short blasting cracks in other directions in the remaining rock. This fracture or damage suppression effect explains why the blasting cracks tend to be shorter when the spacing is smaller.

When the reflected primary wave from the free face arrives it will like before favor the growth of fractures that lie tangential to the crack front. This scenario will of course be modified by geometrical imperfections, jointing (natural fractures) and rock anisotropy.

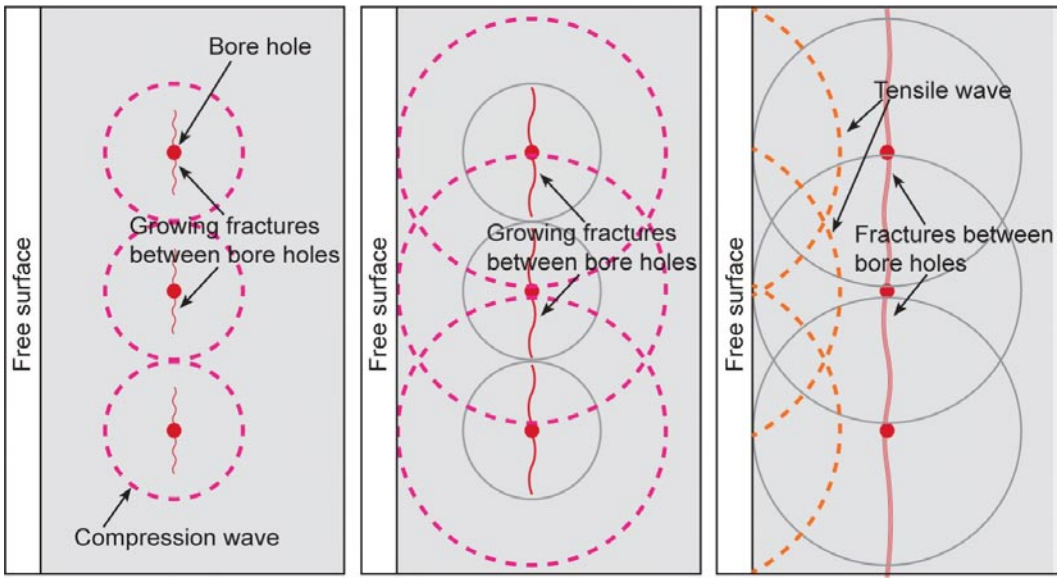

Figure 6-2. *Principal layout for different waves causing fractures.*

Experience shows that many blasting fractures in the blast damage zone have three properties that would counteract fluid flow /Olsson and Bergquist 1993, 1996, Ouchterlony et al. 2002/:

- They are usually partial fractures in the sense of having rock bridges and not having completely separated fracture surfaces. They are thus more like fracture zones than open fractures.
- They usually do not continue for very long along the blast-hole axis.
- Many of them are too short to connect with any natural fractures, i.e. the blast damage is local.

Around the heavier bottom charge, the blasting cracks are longer and not only radial but conchoidal. On the other hand the blast-hole toes of one round are facing the uncharged collars of the blast-holes of the next round and their lateral positions differ by at least the look-out distance. There thus seems to be a very low possibility of getting a continuous fracture plane along the blast-hole. The blasting fractures would in most cases be partially closed, non-continuous and local.

6.1.3 Blasting fractures-blast damage

Since many years a table is used in Sweden to design blast damage caused by blasting. /Olsson and Ouchterlony 2003/. Commonly used explosives for smooth blasting are listed in order of their equivalent linear charge concentration in terms of kg Dynamex per meter. The table suffers from many shortcomings and is only verified for very few explosives under specific circumstances. A clear definition of damage is lacking. Furthermore it does not take in consideration the influence of blast hole pattern, scatter in initiation and coupling ratio but has been a practical tool to design smooth blasting. So there was a strong demand for a new table.

An intensive research of how fractures are caused by blasting has been carried out at SveBeFo and Swebrec. A large number of holes have been blasted, in quarries as well as in tunnels, and the fractures in the remaining rock have been examined. The technique is based on cutting blocks or slots perpendicular to the blast holes and spraying dye penetrants on the surfaces causing fractures to appear very clearly.

Coupling ratio (charged diameter/hole diameter), spacing, water in the holes, scatter in the initiation and the influence of different explosives on fracture lengths are some of the examined factors. Figure 6-3 illustrates the influence of decoupling. On the left the fracture pattern from 22 mm Dynotex in a 64 mm hole is shown and on the right the fracture pattern from an identical charge in a 24 mm hole. In the tests groups of 3–5 holes with a simultaneous initiation were shot. Notice the large difference in fracture lengths, 25–30 cm behind the 64 mm hole and 90–100 cm behind the 24 mm hole. Notice also the many blast induced fractures behind the 24 mm holes.

Figure 6-4 shows the influence of an increased spacing, a larger distance between holes than the burden could result in long fractures sub-parallel to the surface.

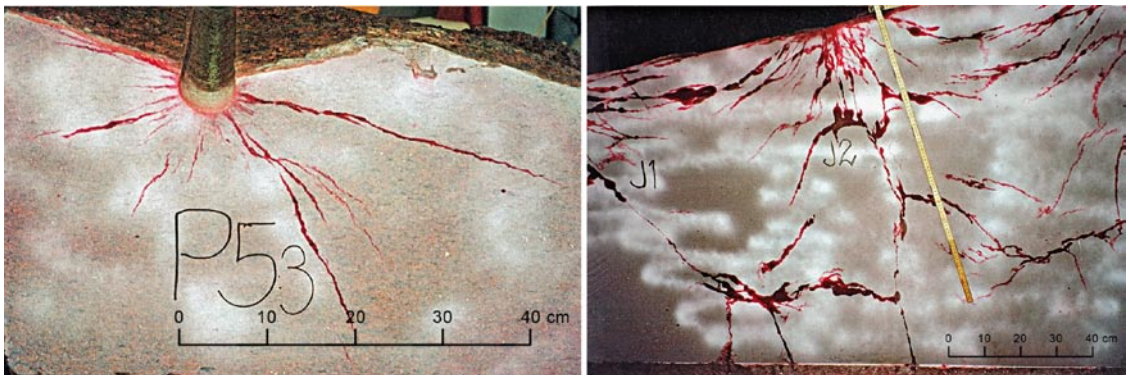

Figure 6-3. *Left: Fractures from a 22 mm Dynotex charge in a 64 mm hole. Right: Fractures from a 22 mm Dynotex charge in a 24 mm hole /Olsson and Bergquist 1996/ .*

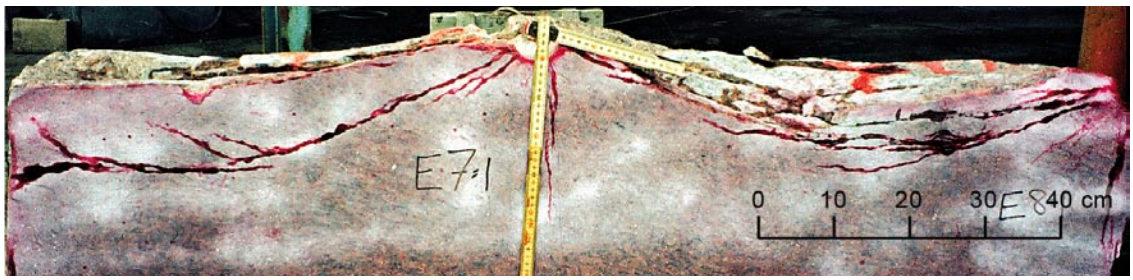

Figure 6-4. *Fracture pattern from increased spacing /Olsson and Bergquist 1996/.*

Some guidelines to reduce fractures from blasting are stated /Olsson and Ouchterlony 2003/:

- Use decoupled charges.
- Avoid water in holes (could extend fractures up to 3–4 times).
- Use simultaneous initiation (scatter less than 1 ms between holes).
- Explosives with a high detonation velocity often results in more and longer fractures and high fracture intensity close to the borehole.
- Increased spacing results in long fractures sub-parallel to the surface.
- Increased charge weight increases fracture length.

With the knowledge of the effects of these factors a new formula has been proposed /Olsson and Ouchterlony 2003/. The new formula emanates from measured fracture lengths in granite. Compensation factors for decoupling, spacing, initiation, water in holes and the rock are included in the formula. One important factor included in the formula is the variation of the detonation velocity due to decoupling in wet or dry holes.

Some typical fracture patterns from blasting in this study are shown in Figure 6-5. Here the differences in fracturing between the heavier bottom charges and the lighter column charges are obvious. The photo to the left shows a typical fracture pattern from the bottom charge. The charge weight from the bottom charge corresponds to a charge weight 5 times the weight of the column charge.

The fracture length from the bottom charge is 30–45 cm. The arrow in the left photo is 30 cm long. The fracture length from the column charge shown to the right is 10 cm, as shown by the arrow. Note also the differences in the fracture patterns. The bottom charge generates many more fractures than the column charge. Some of these blasting fractures pass the natural fractures and continue further into the rock mass. This is a rather typical behaviour for blasting fractures.

Now what kind of fracture pattern exists under the toe of a blast hole? Earlier studies /Ouchterlony et al. 2000/ show that the fracture pattern forms a cone, se Figure 6-6. This indicates that the fractures under the toe of a hole have about the same fracture length as the radial fractures from the charge. In the current investigation you might thus expect the fracture length from the bottom charge to be at least 40 cm.

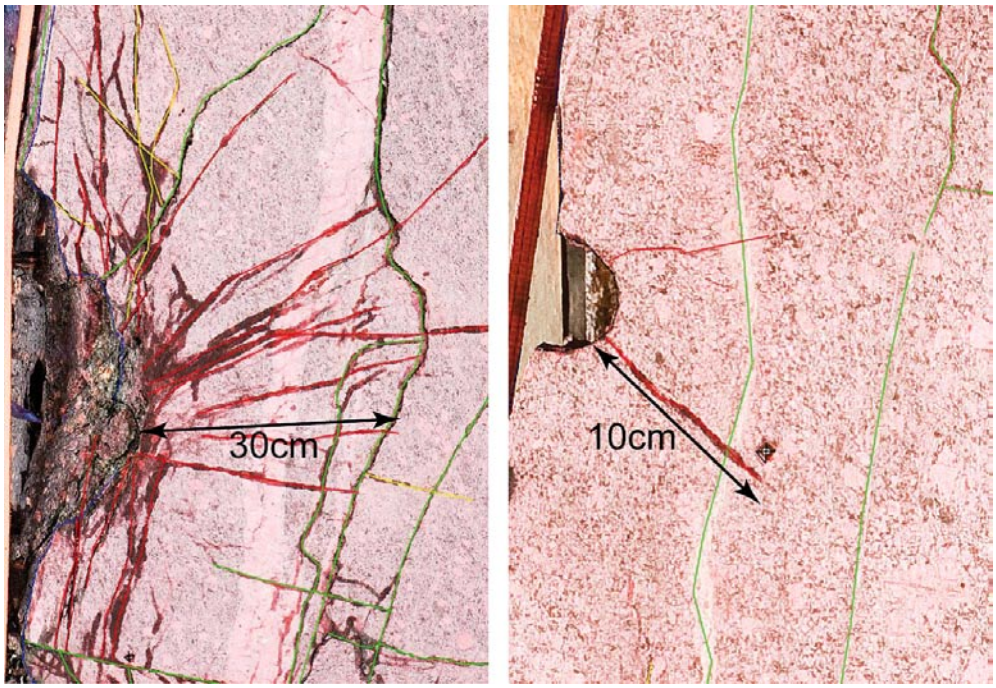

Figure 6-5. *Left: Fractures from bottom charge, arrow length 30 cm. Right: Fractures from column charge, arrow length 10 cm.*

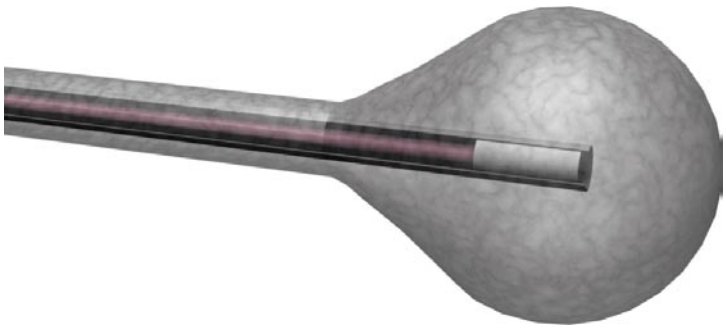

Figure 6-6. *Fracture envelope for a blast hole. The gray flask shaped surface contains in principle all radial and conical blasting fractures directed back into the remaining rock. The fractures that brakes the burden are obviously longer.*

6.2 The fracture modelling process

The fracture modelling process includes the following steps.

Figure 6-7. *The steps of the modelling process.*

6.2.1 Model setup

The fracture modelling work was performed in SKB's Rock Visualization System (RVS), an application based on Bentley MicroStation© /Curtis et al. 2007/, and also directly in Bentley MicroStation© 3D CAD.

A model was created covering the investigated volume. The model volume represented 10 m along the tunnel, with a depth of 1.2 m and height of 2 m. The model was created and saved in the Äspö96 local coordinate system.

6.2.2 Fitting of vectorized slab surfaces in 3D space

Prior to excavation, a large number of fixed point markers were surveyed on the rock wall at the site of the excavation, see also section 4.3.

Before cutting the blocks to slabs, each block was fixed and the fix point markers on the tunnel wall side of the blocks, with known Äspö 96 coordinates from the tunnel, were referenced to reference points near the sawing place. Using these reference points, new fix point markers on the investigated side could be marked and referenced into Äspö 96 coordinates. When vectorizing the fracture information, the position of the fix point markers as well as the block sides were also digitized.

The tunnel wall was also laser scanned before the block extraction and the inner wall of the niche created after excavation was surveyed on site in the tunnel to be used as reference planes when aligning the digitized surfaces into 3D space. The laser scan data used was preliminary data used for cross-checking only; these data were not reported at the time of the investigation.

As soon as a slab was examined, sawed and removed, the operation was repeated for the new surface on the block side (facing upwards at the sawing place). New fix point markers were attached and referenced to the reference points near the sawing place, thus obtaining tunnel coordinates in the Äspö 96 system. The process is described in detail in chapter 4.

To fit each digitized block side into the correct place in 3D space, the coordinates for the fix points on the investigated side were used to place corresponding fix points in 3D space and the view in the model was aligned with the plane formed by these points. The 2D design file with the digitized surface was then attached as a reference file aligned to the view plane. Finally the digitized surface was moved to the correct place, again using the fix point markers with known coordinates.

After all the sections for a block were fitted into 3D-space, a cross-check was performed using the laser scanned tunnel surface, the surveyed inner surface of the niche and the surrounding block sections as references. It was found that the sections of the two first and the two last blocks had to be adjusted a few cm to stay within the given boundaries.

Figure 6-8. *Block fixed at sawing place.*

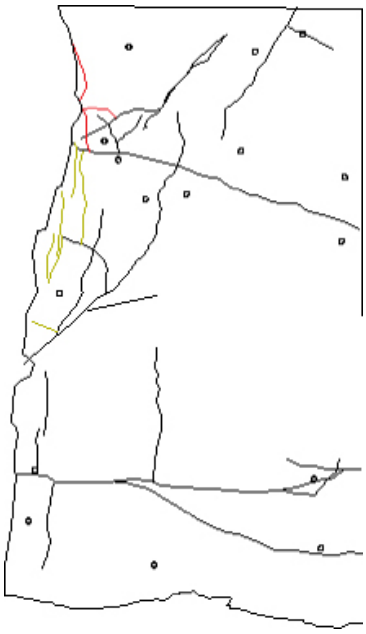

Figure 6-9. *Digitized slab surface with fractures, fix point markers and edges, 36B-05.*

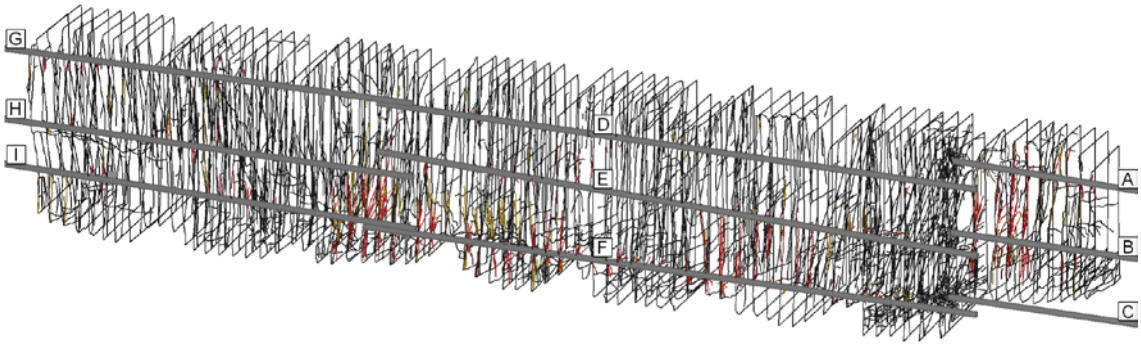

Figure 6-10. *All sections with digitized fracture traces fitted into 3D space.*

Given all possible error sources and the possibilities to adjust against known planes, the total accuracy of each placed section is estimated to be c. ± 1 cm.

6.2.3 3D modelling

Modelling technique

The fracture planes were created using the RVS modelling function *Surface by Profiles,* which connects selected line strings to an undulating surface, spanning the area between the line strings without extrapolation.

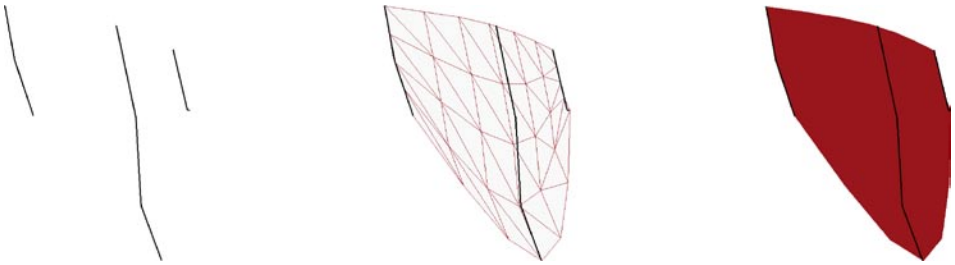

Figure 6-11. *Connecting fracture traces to undulating fracture planes.*

Interpretation

There are a number of criteria used to interpret which fracture traces to connect into a fracture plane, of course, herein lies also the biggest uncertainty in the model, see also section 8.2.

All fractures are classified when digitizing as is described in chapter 5. This classification is used as an input when deciding, which fracture traces to connect into fracture planes. However, when interpreting the fracture pattern in a 3D view, some re-evaluation of the classification from the digitizing is made since a clearer picture with more information becomes apparent when viewing the fracture traces together in 3D and also together with the 3D location of the boreholes.

The first criterion for connecting fracture traces is the visual interpretation. When slowly rotating a 3D view with the fracture traces, a pattern develops where larger natural fractures, which are visible through several slab surfaces, are quite easy to follow and interpret. These can therefore be modelled first with a quite high confidence and the fracture traces can then be eliminated from the view, making it easier to see and follow the traces of the smaller fractures.

As an aid to the visual interpretation, the perspective photographs of the blocks are of great help. These photos of the slabs show the investigated upper surface and one or two of the sides, where it often is possible to see the perpendicular direction of the observed fracture trace. Naturally, smaller fractures are harder to follow and unfortunately some of the sides are obscured by the straps holding the blocks together. Also notes of observed directions when digitizing are supportive in the visual interpretation of the fractures.

The next criterion is the observed properties of the fractures, noted when documenting the slabs, see section 4.6. This can be physical properties such as open-closed, mineral filling, oxidation etc. The physical properties were mostly used for early interpretations between sections when digitizing and, to some extent, for verification of visual interpretations. These properties together with the placement and the geometry of the fractures were also guiding when distinguishing between natural and blast induced fractures in the classification process.

The last criterion is the knowledge and the experience of the nature of the blast fractures and of the nature of the natural fracture pattern at the site.

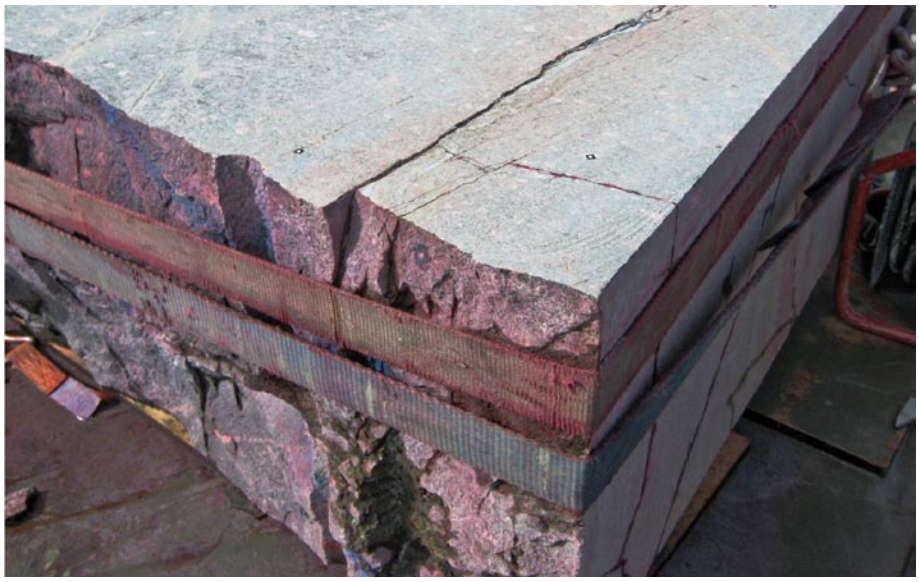

Figure 6-12. *Block with block side with visible fracture traces.*

Figure 6-13. *Block section with fractures with and without mineral fillings.*

When connecting blast fractures there are of course many ways the fracture traces can be connected, since the pattern is similar between the different sections and it is hard to know how far to connect a single fracture plane through the sections. Some guidelines were used:

- Planarity
- Persistence
- General geometry

All these points depend on how fractures are formed and this is discussed in detail in chapter 6.1.

Regarding planarity a basic assumption is that blast and blast induced fractures are almost planar. This is due to how the blast and blast induced fractures are formed. When connecting blast fractures, the fracture is stopped before it changes directions, so that 'wobbling' or twisted fractures are avoided. This geometry for the fractures is also confirmed by the detailed investigation, see 6.2.4.

Regarding persistence the fact that the formation of the fractures starts at a number of different points along the borehole makes it probable separate fractures (ears) are forming along the borehole and propagating independent of each other, at least to begin with.

Regarding general geometry the knowledge of how blast induced fractures are formed is guiding for the interpretation of how the fractures interact with and stop when they encounter the network of natural fractures.

Modelling blast and blast induced fractures is the trickiest part of the modelling and the part where the model is most uncertain. To verify the modelling, six representative areas were selected for detailed investigations. The result of this investigation is presented in section 6.2.4. The knowledge gained was used to re-evaluate some of the fractures modelled prior to the detailed investigations.

Another lesson that was learned when creating fracture planes from fracture traces was to correctly interpret the geometry of the fracture trace.

Fractures with a strike direction near perpendicular to the investigated section will generally be seen as straight or almost straight lines whereas fractures crossing the investigated section at an acute angle will be more winding, and for very sub-parallel fractures, the fracture trace will almost form a half circle, Figure 6-14.

Naturally, also information about the orientation of a fracture, observed when digitizing, was used when trying to connect fracture traces from one section to the next.

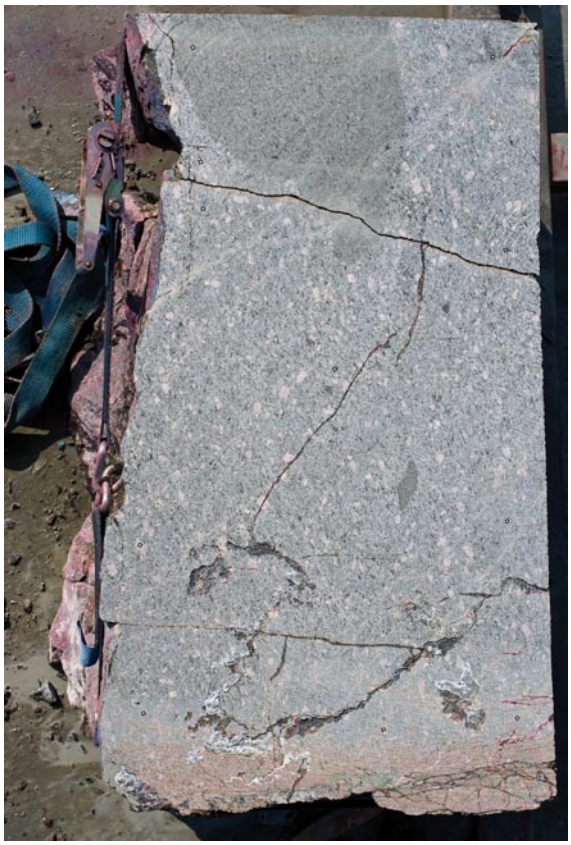

Figure 6-14. *Section 36B-06. The nearly straight fracture trace at the top belongs to a fracture intersecting the section at a near perpendicular angle. The irregular fracture trace below belongs to a fracture, which is sub-parallel to the section, intersecting the section at an acute angle.*

Single trace, forming fractures with very low confidence

When all fracture traces possible to connect between different sections are used, there are a number of fracture traces left which we were not able to connect to any adjacent section. In order to get a complete model regarding the number of fractures, these fractures were modelled simplified as rectangular planes. As the information regarding the strike direction of these planes were lacking, they were all modelled with a strike direction more or less perpendicular to the investigated sections, i.e. a strike value of 50° or 230° towards Äspö north (38° and 218° towards RT90 north). For some fractures, this value was slightly altered to match surrounding modelled fractures. The dip was set to correspond with the apparent dip on the mapped section.

The length of the plane side in the dip direction was set to the length of the fracture trace and the length of the perpendicular side, in the strike directions was set to the same value, however with a maximum width of 20 cm since the fracture was not observed in adjacent sections. Thus, all fractures modelled corresponding to a fracture trace of 20 cm length or shorter were modelled as squares. Fractures modelled from singular fracture traces longer than 20 cm are rare, since all longer fractures are more likely to be found in any of the adjacent sections.

The cut-off for these fractures was set to about 5 cm for natural fractures, i.e. fracture traces of 5 cm length or smaller were disregarded. For blast or blast induced fractures, all observed fracture traces were used.

The individual fracture traces have a high confidence in their position; however, the 3D modelled fracture surfaces based on these isolated actual observations have only a very low confidence in their geometrical form. Therefore, all these fractures are named in a different way, see below, and carefully filtered out from all statistics regarding fracture orientations. Their level of confidence is set to very low, cf. Table 7-1.

Naming of modelled fractures

When modelling the fractures they were all given different names. All natural fractures have the prefix N followed by a serial number starting from 001 and running upwards in the order they were modelled. Natural fractures modelled from single fracture traces have the prefix n followed by a serial number starting from 501 and running upwards in the order they were modelled.

For blast and blast induced fractures, the names were given to distinguish from which borehole they are judged to origin. Hence, the nine boreholes involved in this investigation were labelled A-I running top-down from the first section and forward, see Figure 6-10.

To distinguish between blast and blast induced fractures, the prefix for the latter included the letter I for induced. The prefixes for the fractures were thus A or AI for fractures originating from the top borehole of the first round. Also here followed by a serial number starting from 001 and running upwards in the order they were modelled. Fractures modelled from singular fracture traces also have the prefix in lower case and a serial number starting from 501.

Re-evaluation of digitalization when modelling

When joining fracture traces onto fracture planes, re-evaluation of the digitized data is sometimes necessary. Fractures can appear as two separate fractures in one section, as a continuous fracture in the next and again as separate fractures in the following section, see example in Figure 6-15. In this case, the continuous fracture must be cut into two different fractures in order to make the modelling of two separate fractures with different orientation possible. Information from the block sides is here very helpful.

An example of the opposite is when a fracture might be continuous in surrounding sections but fragmented in an intermediate section, se example in Figure 6-16. What can be suspected then is that the fracture is partly sealed and has not absorbed any penetrant. When this is suspected, the high-resolution photo is reviewed to see if the fracture is continuous and is sealed. If this is the case, the broken-up fracture trace has been connected and the fracture has been modelled as continuous since it is not possible to model fractures with holes representing sealed parts. But normally, sealed fractures are not modelled.

There is also some re-classification of fracture traces when 3D-modelling. When the 3D pictures emerge, and the 2D fracture traces are seen in the larger context, the level of information is increased and in some cases the fracture traces are re-classified when tied together with other fracture traces to form fracture planes.

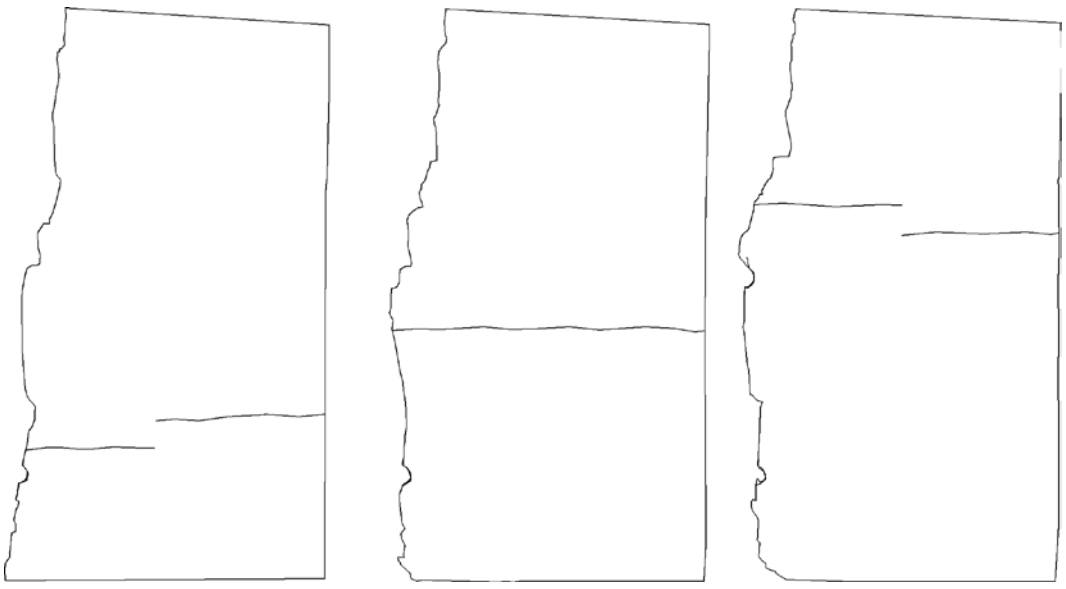

Figure 6-15. *Hypothetical appearance of two fractures in three sections.*

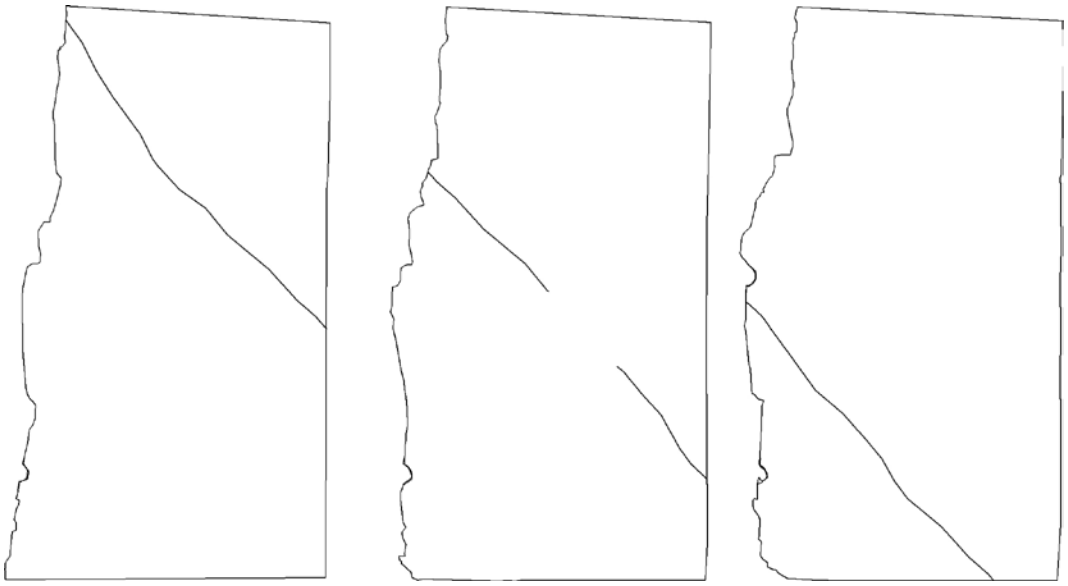

Figure 6-16. *Hypothetical appearance of a fracture in three different sections.*

One example of this is section 37B-01, shown in appendix 1 (VS0037B01), which is located ahead of the bottom charge in round number 9. The original classification of the fractures as natural was revised when modelling, see Figure 8-1.

6.2.4 Evaluation and verification

Confidence in geometry

The confidence in existence is very high for all observed and modelled fractures. All fractures are built on observed fracture traces. The classification refers to confidence in orientation and extension. The confidence in geometry and extension of the modelled fractures are classified in accordance to the definition given by the methodology study /Olsson et al. 2008/.

The level of confidence of a modelled fracture depends on how many slab surfaces the fracture is observed in and if the lateral extent of the fracture can be validated by any observation of perpendicular fracture traces e.g. surface mapping of the tunnel wall or excavated rock block. In the methodology study, three confidence classes, numbered 1–3 in Table 6-1, were suggested. During the modelling work, two extra classes, 0 and 4 were added to describe fractures with many observation where the geometry is certain and fractures with only one observation where only the existence is verified but where the orientation is unknown.

In the RVS model, all modelled fractures are labelled in the description field with type of fracture, followed by confidence class within brackets.

Table 6-1. Confidence classes.

Confidence class	Description
4) Very High	Identified in at least 8 sections **or** in at least 5 sections in combination with supportive information in a perpendicular section. Similar appearance in all sections. Forming semi-planar fracture planes.
3) High	Identified in at least 5 sections **or** in at least 3 sections in combination with supportive information in a perpendicular section. Similar appearance in all sections. Forming semi-planar fracture planes.
2) Medium	Identified in at least 3 sections. Similar appearance in all sections. Forming semi-planar fracture planes.
1) Low	Identified in 2 or 3 sections. Fairly similar appearance in all sections.
0) Very Low	Identified in only one section. Existence verified but orientation unknown.

Detailed study

Planning

After completing about half of the model, a detailed study was carried out to evaluate the modelling and to give input to the rest of the modelling. Six cases or typical places of special interest were selected.

1. Modelled fracture A004. Of principal interest. This fracture has been connected through many (7) sections. Is this correct?
2. Modelled fractures B006 and B007 in the transition zone between round 9 and 10.
3. Fracture F003. Of principal interest. This fracture has been connected through many (4) sections. Is this correct?
4. Fracture F024. Of principal interest. This fracture has been connected through many (4) sections. Is this correct?
5. Modelled fractures E010 and E011. Here we selected to model two separate fractures not connected through slab 40B-06. Is this correct?
6. Fracture FI007. Of principal interest. This fracture has been connected through many (5) sections. Is this correct? This fracture was later classified as natural and renamed N071.

Field investigation

For each investigation, the slabs concerned were identified and collected. The fractures of interest where identified on both sides of the slab. To make it possible to follow a single fracture from one side of the slab to the other, the slab was cut with an angle grinder, or in some cases a drillcore was drilled through the fracture of interest.

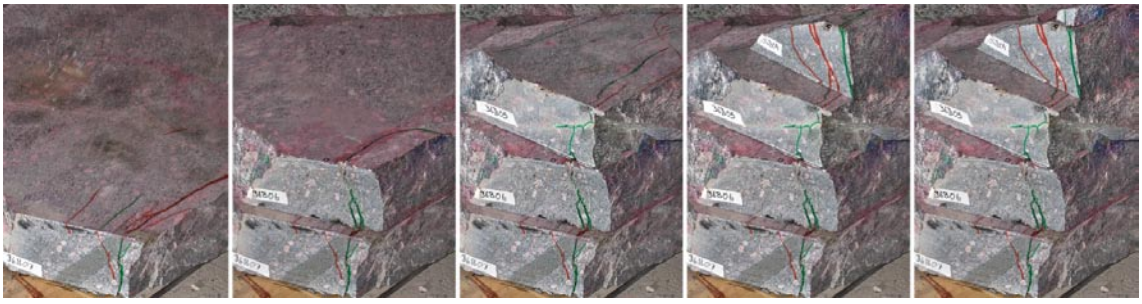

Figure 6-17. *Detailed investigation, case 1.*

Figure 6-18. *Detail of case 1. A blast fracture which comes from above meets an intersecting fracture, jumps to the side and continues.*

Result

The investigation revealed that in four of the six cases the modelled fractures were accurate. In two of the investigations, 1 and 3, the modelled fractures had to be revised.

The investigated blast fracture A004 in case 1 was first modelled as quite long, spanning over 7 sections. It was also slightly wavy, bending faintly to one side and then shifting to the other and back again, see Figure 6-19.

The detailed investigation showed that this was instead a set of sub-parallel fractures intersected by small crossing fractures as shown in Figure 6-18. The fractures also often connected with the edge of adjacent sections, thus forming the tunnel wall. The crossing fractures could not be detected, and hence not modelled, since they are sub-parallel to the investigated sections, the result of the remodelling is shown in Figure 6-20.

Regarding the investigated fracture F003 in case 3 the detailed investigation showed that the modelled fractures around the investigated area had a slightly different direction than the actual fractures. Some remodelling was done to correct the fractures but these are small changes that do not affect the overall fracture pattern. The original model of fracture F003, and also to some extent that of F005, show the twisted or wobbling appearance that normally was avoided when modelling. The detailed investigation showed, however, that the actual geometry of the fractures around the area was more planar. This confirms the initial assumption that blast induced fractures are more or less planar. This is also in agreement with the conceptual understanding of the blasting process, see section 6.1.

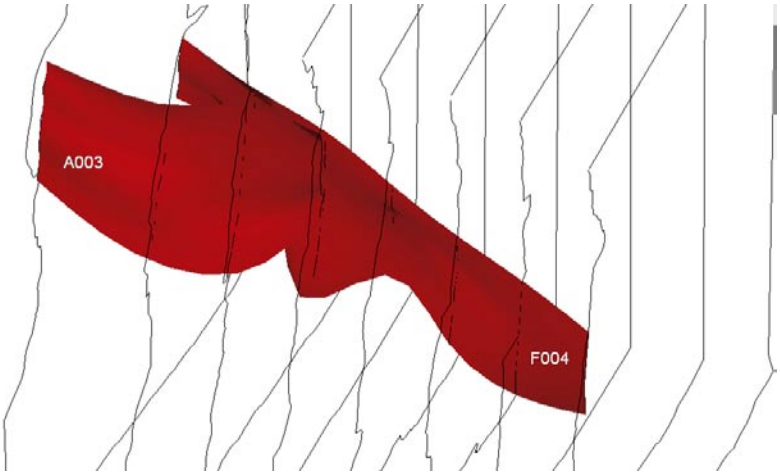

Figure 6-19. *Case1. Modelled fractures before detailed investigation.*

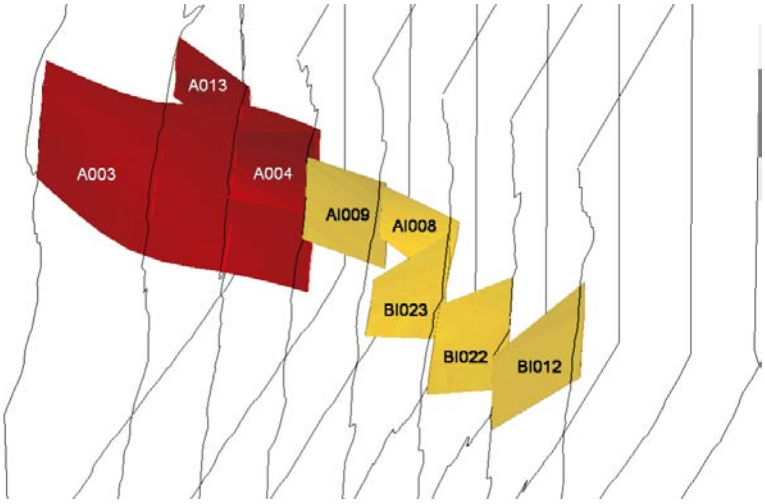

Figure 6-20. *Case 1. Modelled fractures after detailed investigation.*

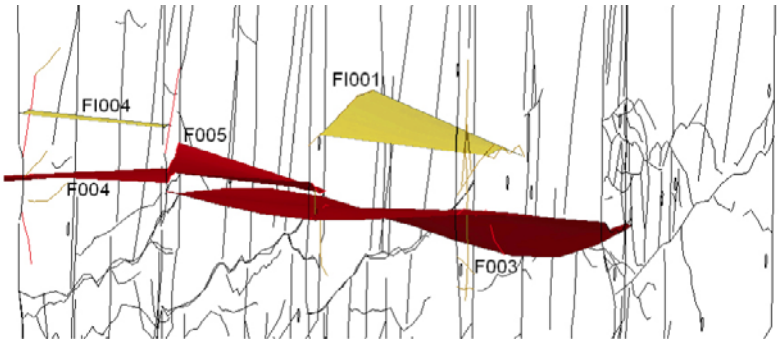

Figure 6-21. *Case 3. Modelled fractures before detailed investigation.*

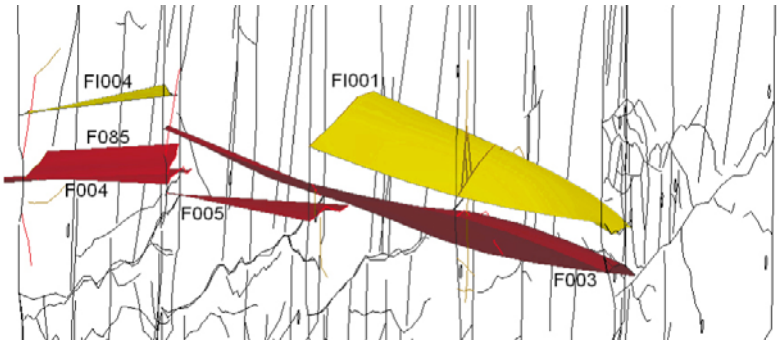

Figure 6-22. *Case 3. Modelled fractures after detailed investigation.*

Conclusions

The lesson learned from the detailed investigation was that the modelling was quite successful for the blast fractures and that no major revision of the model was necessary. Regarding the two cases where the modelled fractures had to be revised they also gave important knowledge that was applied to the model.

The most important implication on the modelling was the experience from case 2 that blast fractures often connect with the edge of adjacent sections, thus forming the tunnel wall. The entire model was reviewed implementing this knowledge, which led to the revision of a large number of blast and blast induced fractures where they were extended to the edge of the adjacent section where this fitted with the modelled fracture. Also, a large number of single fracture traces that could not be connected to fracture traces in adjacent sections did instead fit well to the edge of an adjacent section, thus avoiding the need to model single trace fractures with unknown orientation.

Limitations

It is sometimes not enough just to study the surfaces of the sawed slabs. Although the distance is only 10 cm fractures could join other fractures in the middle of a slab or be connected to the tunnel wall. Information can be missed or misinterpreted. Studying the slab sides is one way to obtain further information.

7 Results

7.1 Result from digitizing

7.1.1 General

The results from the digitizing differ much between different blocks or slabs. Some of the slabs are rather easy to digitize, with only a few and very distinct fractures where others are very difficult with a network of natural and blast fractures. It was found that the highest number of fractures and also the longest blasting fractures were found from the bottom charge. The fractures from the column charge were relative few and shorter.

A surprising observation was that in some parts of the holes, where there should be blasting fractures, there were no blasting fractures at all. It is not easy to explain this. It is most obvious in the upper contour hole, which seems to have fewer blast fractures. In blocks 41 to 43 the two upper holes have almost no blast fractures. From a blasting point of view it seems like the charges did not detonate properly, but there was no detonation failure reported and no undetonated explosives were found. Another, speculative explanation is an unexpectedly large scatter in the initiation times of electronic detonators. Then, if a neighbouring contour hole detonated some milliseconds before, this might have ejected the charge before it detonated. This has happened in cut blasting /Ouchterlony 1992/ but we have no physical evidence that it happened here.

In some of the slabs it is very difficult to classify the fractures as blast, blast induced or natural fractures. Generally there is a large difference in the fracture pattern from slabs near the bottom of a round compared to that in slabs from the middle of a round. The much higher charge concentration from a bottom charge forms a complicated network of blast/blast induced fractures. The picture is even more complicated when influenced by a crushed zone of natural fractures as in block 37. The result from some different slabs will now be discussed.

Figure 7-1. *Example of a section with a lot of blasting fractures at the lowest hole and hardly any at the two upper holes. Section 40B-03.*

7.1.2 Results from some of the slabs

Start of a round

An example from the start of a round is shown in Figure 7-2. The left photo shows the fracture pattern from section 41B-10 and the right photo is a zoomed photo from section 42B-03. There are no visible fractures coming from the boreholes and there should also be no fractures because the holes in this section should have been uncharged, see more details of this in chapter 3.2. The only fracture types in this section are natural fractures.

Because of uncertainties of the start point and end point of the holes and the exact lengths of charging or not it was sometimes difficult to know what kind of fracture type it was. A fracture originating from a hole should probably be classified as a blasting fracture but if the information from charging tells you that this section has not been charged the information is contradictory.

The middle of a round

Figure 7-3 shows two examples of fracture patterns in the middle of a round. In the left photo from section 39B-01 there are more blasting fractures from the lower borehole. This is probably caused by the vicinity of a vertical natural fracture. On the other hand one should expect more fractures from the lower hole in section 37B-07 in the right photo due to the nearby zone of natural fractures.

However the figures generally show that there are only a few radial blasting fractures from the boreholes. That's typical for the situation along the contour holes charged with 17 mm Dynotex and initiated simultaneously. The maximal blasting fracture length in the left photo of Figure 7-3 is less than 15 cm and in the right photo it is less than 10 cm. In general the blasting fractures from the column charge in our investigation are less than 15 cm.

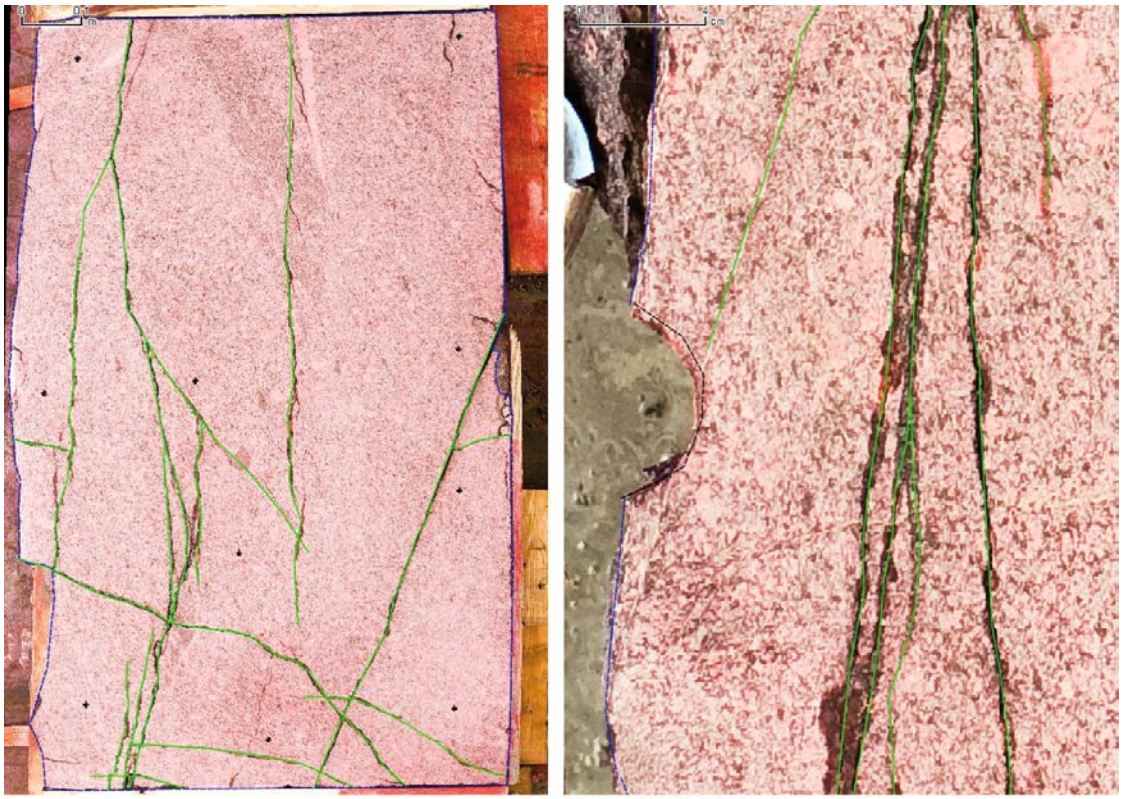

Figure 7-2. *Examples from the first section of a round. The fracture originating from contour hole on the right photo has infillings and is hence classified as natural.*

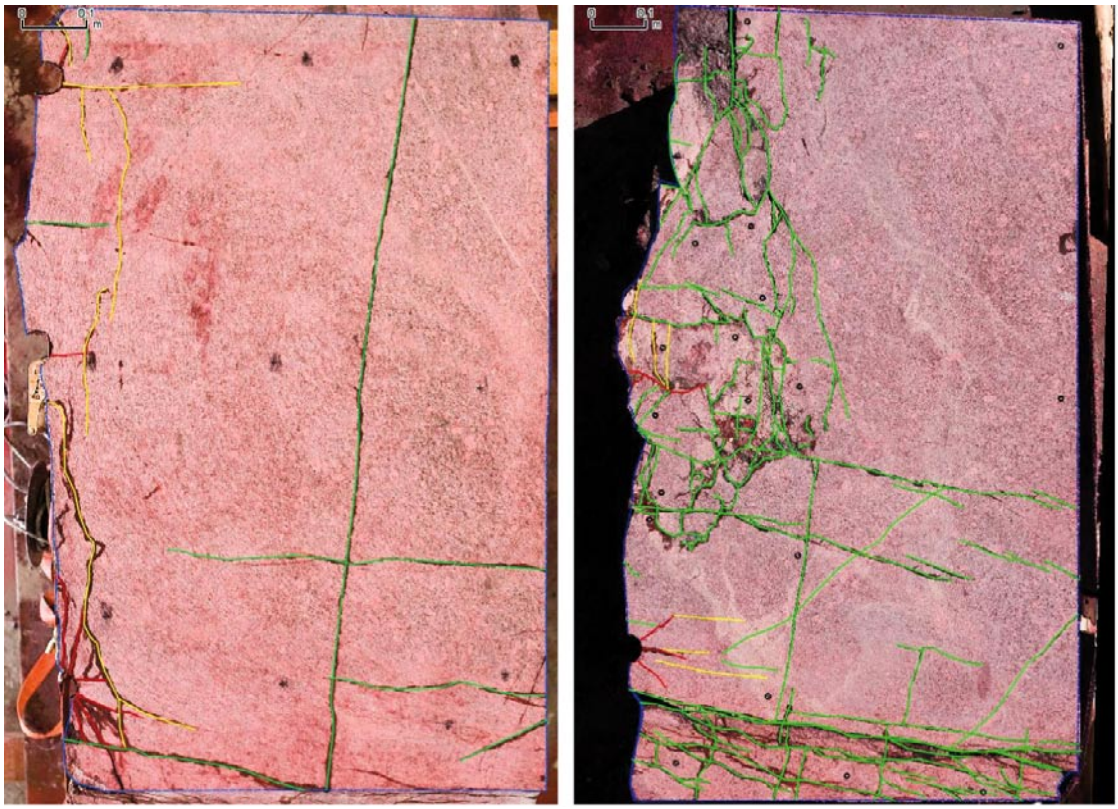

Figure 7-3. *Sections in the middle of a round 39B-01 and 37B-07.*

The bottom of a round

Due to a higher charge concentration the fracture pattern is more dramatic near the bottom of a round, compared to other sections in a round. Unfortunately there is a lack of information where exactly the contour holes started and ended. Furthermore the position of the charges and the position of the uncharged sections are unknown due to the lack of precise information regarding the position of the hole bottoms. Therefore it is almost impossible to be sure of how the bottom charge in one round affects the fracture pattern in the next round. However, a typical situation of the influence of a bottom charge is shown in Figure 7-4 in section 36B-09 (left photo) and in section 41B-06 (right photo).

The blasting fractures in section 36B-09 have an average trace length of nearly 20 cm with the longest fracture trace of 26 cm. The fractures are mainly orientated sub-parallel to the tunnel wall. In the upper part of section 36B-09 there are also many fractures, classified as blast induced fractures instead of as blast fractures due to the lack of a visible half-cast. The blasting fractures in section 41B-06 have an average trace length of nearly 25 cm with the longest fracture trace being 45 cm. The blasting fractures from this section are of special interest as this is the only visible bottom of a hole of all our sections and hence the only place where the exact position is known. From this fracture pattern it is therefore possible to estimate the fracture length from a bottom charge. The fracture length from the bottom charge could here be at least 3 times the fracture length from the column charge. An experience from earlier tests indicates that a conical pattern of fractures are produced under a hole, see more in chapter 7.1.

Section 41B-06 shows another example of how blasting fractures approach natural fractures and even cut across them. The fracture directions in this section are more symmetrical than in section 36B-09.

Fracture distribution

The total number of fracture traces identified in all of the slabs was 2,509 of which 1,801 were natural fractures, 436 were blasting fractures and 272 were blast induced fractures. Figure 7-5 shows the distribution of different fracture types in all of the blocks. Block 37 has the highest number of natural fractures, the other blocks seems to have about the same number of natural fractures.

Figure 7-4. *Sections at the bottom of a round (36B-09 and 41B-06).*

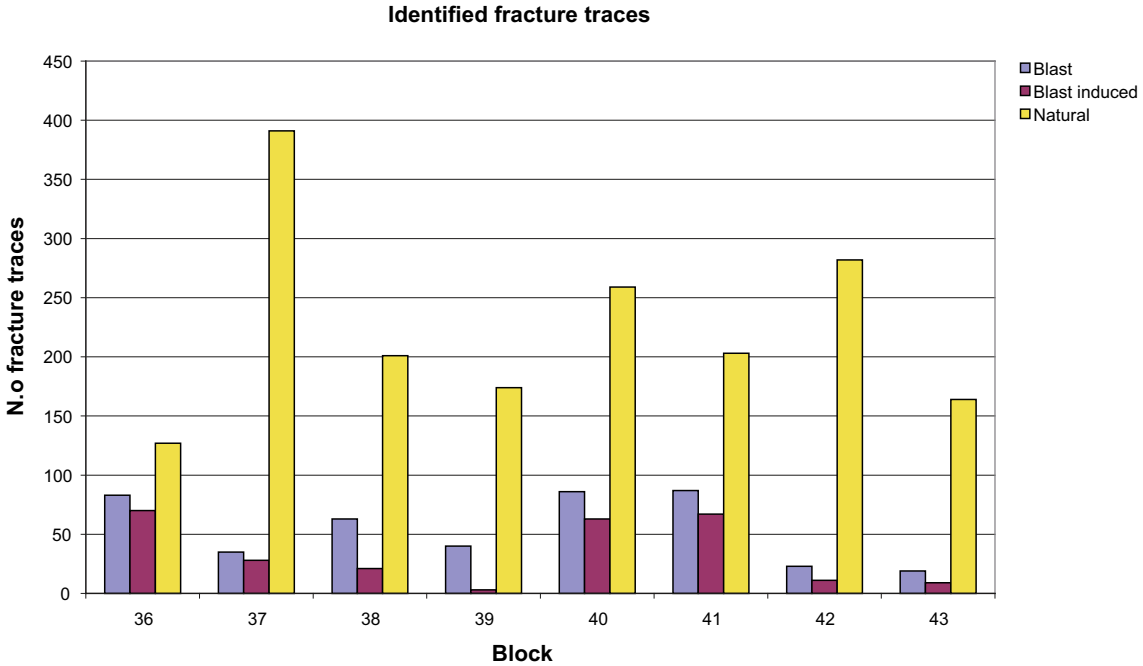

Figure 7-5. *Total number of identified fracture traces.*

Figure 7-6 shows the fracture trace distribution of natural fracture traces in all the blocks. The distribution is divided into six groups, < 10 cm, 10–<15 cm, 15–<20 cm, 20–<30 cm, 30–<40 cm and < 40 cm. There exist a large number of short natural fracture traces in block 37. Blocks 40 and 42 also have a high number of the shortest fracture traces. Block 37 is outstanding and seems to have the highest frequencies of short, medium and long fracture traces.

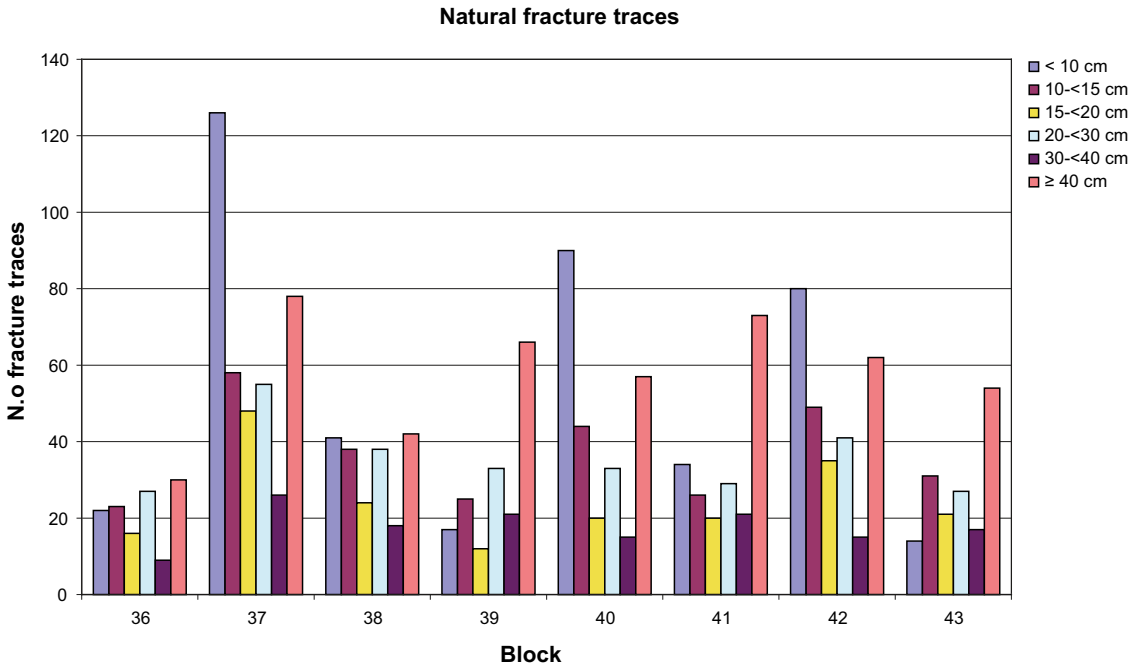

Figure 7-6. *Distribution of natural fracture traces.*

In Figure 7-7 the distribution of blast fracture traces is shown. Block 40 has the by far highest number of short blast fracture traces. One would sooner expect this to occur in blocks 36–37 and 41–42 since they are affected by the bottom charges. On the other hand blocks 36, 38 and 41 seems to have the highest proportion of medium long blast fracture traces. Block 43 has the lowest number of blast fracture traces.

Figure 7-8 shows the distribution of blast induced fracture traces. Blocks 40 and 41 have the highest number of short fracture traces while block 39 has the smallest number of fracture traces of all the blocks. Block 36 has the highest number of medium long fracture traces.

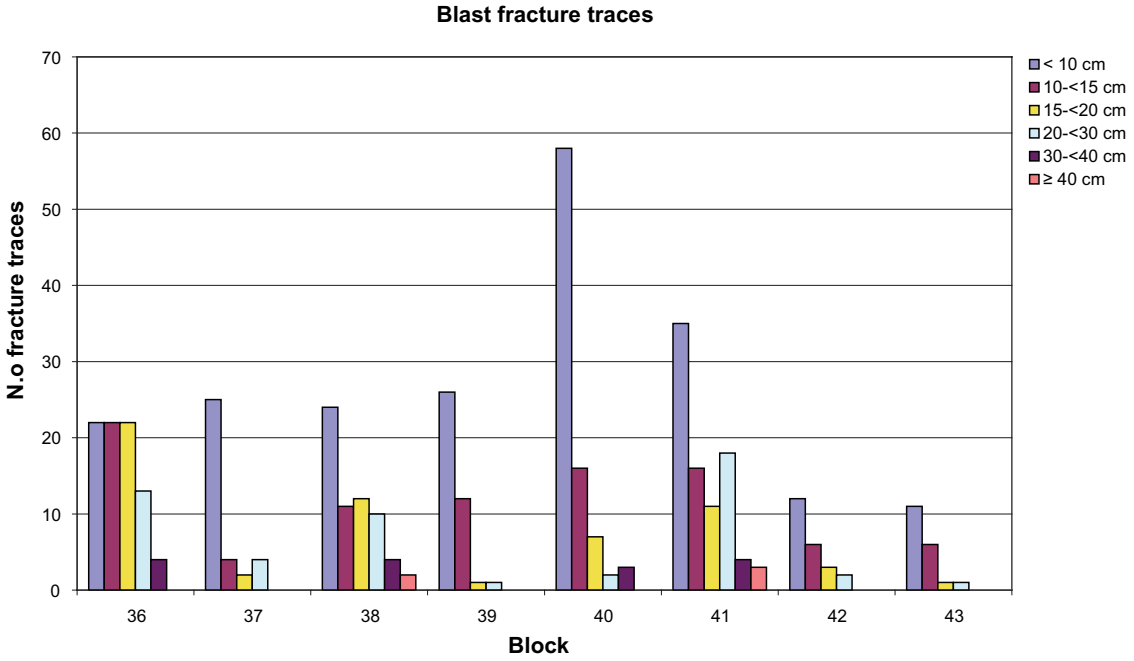

Figure 7-7. *Distribution of blast fracture traces.*

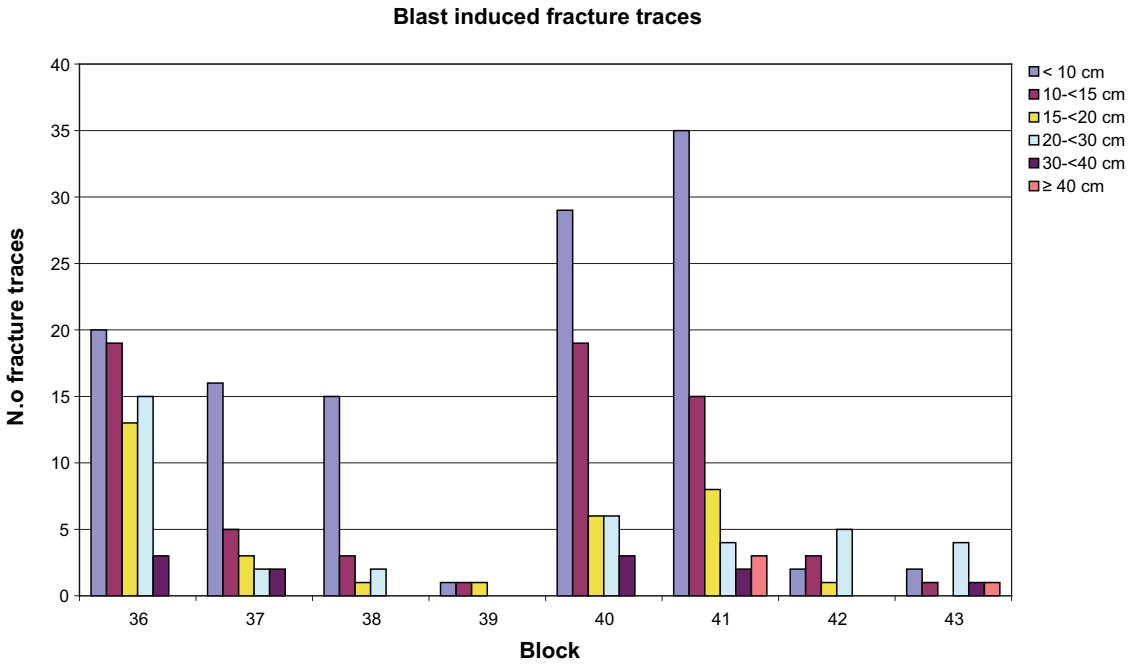

Figure 7-8. *Distribution of blast induced fracture traces.*

7.2 Modelling result

7.2.1 Modelled fractures

In the model there are a total of 1,218 modelled fractures. There are 773 modelled natural fractures, 260 blast fractures and 185 blast induced fractures.

The classification of the confidence in geometry and extension is described in section 6.2.4. All modelled fractures are confidence classed accordingly. The distribution of the different types of fractures in the five confidence classes is shown in Table 7-1.

For all types of fractures, the fractures with low or very low confidence, i.e. fractures constructed from one or two traces, dominate. For the natural fractures, the percentage of fractures with high or very high confidence is significantly higher than for the blast or blast induced fractures. This is as expected since the confidence for the geometrical properties of a modelled fracture is directly linked to the number of adjacent slab surfaces on which the fracture is observed and as the natural fractures in general are larger they are much easier to model with a higher level of confidence.

The low confidence in geometry and extension is hence a direct consequence of the fact that most of the fractures are very small. The difficulties of connecting fracture traces between the sections for blast and blast induced fractures are further discussed in section 6.2.3. All modelled fractures are shown in Figure 7-9, natural fractures are shown in green, blast fractures in red and blast induced fractures in yellow. In Figure 7-10 only the fractures from blasting are shown.

Table 7-1. Distribution of fractures with respect to confidence in geometry and extension.

Confidence class	Blast	Blast induced	Natural	All
4) Very High	0 (0%)	0 (0%)	14 (2%)	14 (1%)
3) High	1 (<1%)	1 (<1%)	38 (5%)	40 (3%)
2) Medium	18 (7%)	7 (4%)	70 (9%)	95 (8%)
1) Low	150 (58%)	92 (50%)	302 (39%)	544 (45%)
0) Very Low	91 (35%)	85 (46%)	349 (45%)	525 (43%)
Total	260 (100%)	185 (100%)	773 (100%)	1,218 (100%)

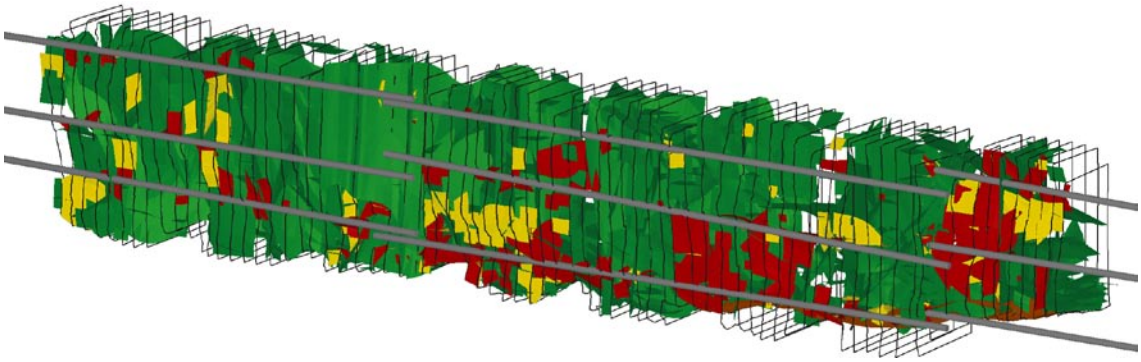

Figure 7-9. *All modelled fractures, section outlines and blast holes.*

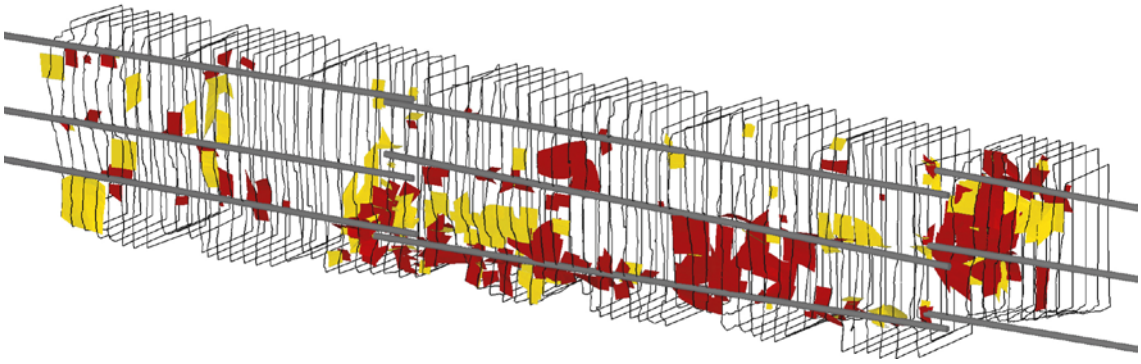

Figure 7-10. *Modelled blast (red) and blast induced (yellow) fractures.*

The longest blast fracture plane we have modelled goes through five sections, and is about 50 cm long. It does not shortcut any of the modelled natural fractures. However, since the extension in the edges of the modelled surface is somewhat underestimated, see section 7.2.5, it is possible that the fracture could shortcut two modelled natural fractures.

As the majority of the blast fractures are sub-parallel to the tunnel wall, see Appendix 1, their contribution to the overall fracture connectivity is very small.

Natural fractures are also often sub-parallel to the tunnel. Natural fractures are open, nearly open, closed or mineral filled. They could be influenced by the blasting process and as a result a filled fracture could open up.

Regarding connectivity between rounds, this aspect is discussed in section 8.1.

7.2.2 Modelled fracture orientations

The orientations of the modelled fractures are shown below, note that the strike reference direction is RT90 north. The fractures modelled from only one fracture trace are not included since no information about their orientation is available and as they generally are modelled with a strike of 50°/230° (Äspö96) and a dip corresponding to the apparent dip of the fracture trace. The use of these orientations would distort the orientation assessment.

The predominant orientation for all fracture types is 130°/310° (RT90), which is nearly parallel to the tunnel direction or perpendicular to the sampling planes. The implication of this is further discussed in section 7.2.3 below.

7.2.3 Geometrical uncertanties

The confidence in geometry is low or very low for the majority of the modelled fractures. This is due to the fact that the majority of fractures are too small to be detected in more than a few sections. This must be considered when using the model.

The sampling also, as any sampling method, discriminates fractures parallel or sub-parallel to the sampling sections. This is also clearly visible when comparing the orientations of the modelled natural fracture pattern, see Figure 7-11, with the expected orientations of the fractures in the investigated area, see Figure 2-5 (note that in Figure 2-5 the north reference is Magnetic north which is 2.3° east of RT90 north used in Figure 7-11). This effect is enhanced by the fact that for the small fractures, the modelling method tends to favour the interpretation of a fracture pattern where you look for similar fracture traces to connect to in roughly the same position in the adjacent sections, hence creating factures with a strike direction perpendicular to the investigated sections.

This conclusion was not evident until the model was completed and the modelled fractures where analyzed statistically. It is not certain, however, that this knowledge significantly would have changed the modeller's bias for creating fractures with a strike direction perpendicular to the investigated sections, it could well be that the error is built into the modelling method. From that respect it would be very interesting to see what the result would be for an investigation performed in a perpendicular tunnel, using the same methodology.

A comparison between the orientations of natural fractures with very high or high confidence, Figure 7-13, to the orientations of all natural fractures, Figure 7-11, also shows that the fractures with higher confidence tends to better follow the expected general direction of the fractures in the area. This is what could be expected if we suspect that the methodology bias is less for the larger fractures that are easier to detect and follow. The sampling bias is still there, however, for these fractures, but it should also be less for more extensive fractures, than for smaller fractures, since we have a lot of parallel sampling sections. The orientations of the natural fractures with medium to very high confidence also confirm this picture, to some extent, Figure 7-14.

7.2.4 Model uncertainties

The combined uncertainties from the digitizing and photo interpretation, the 3D fitting and the modelling together add up to the total uncertainty of the model.

Regarding digitizing and photo interpretation the uncertainties in interpretation and classification of fractures are described in section 5.4.

Regarding measurement of section coordinates and 3D fitting, this matter is elaborated in section 6.2.2 and the total accuracy of each placed section is estimated to be about ±1 cm.

Regarding the uncertainties in modelling, the difficulties to connect fracture traces between sections are discussed in sections 6.2.3 and 6.2.4.

The geometrical uncertainties are further elaborated in section 7.2.3 above.

7.2.5 Limitations in use of the model

As discussed in section 6.2.3 the model is built using the RVS function Surface from Profiles, which is a function that interpolates a surface between selected profile lines as shown in Figure 6-11. No extrapolation beyond the identified sections lines, or mapped fractures, is done, see Figure 7-15.

Since a fracture which is cut off by a crossing fracture, and ending in the intersection with this fracture, is only visible on one side of the intersecting fracture it will end before reaching the intersecting fracture as in Figure 7-16.

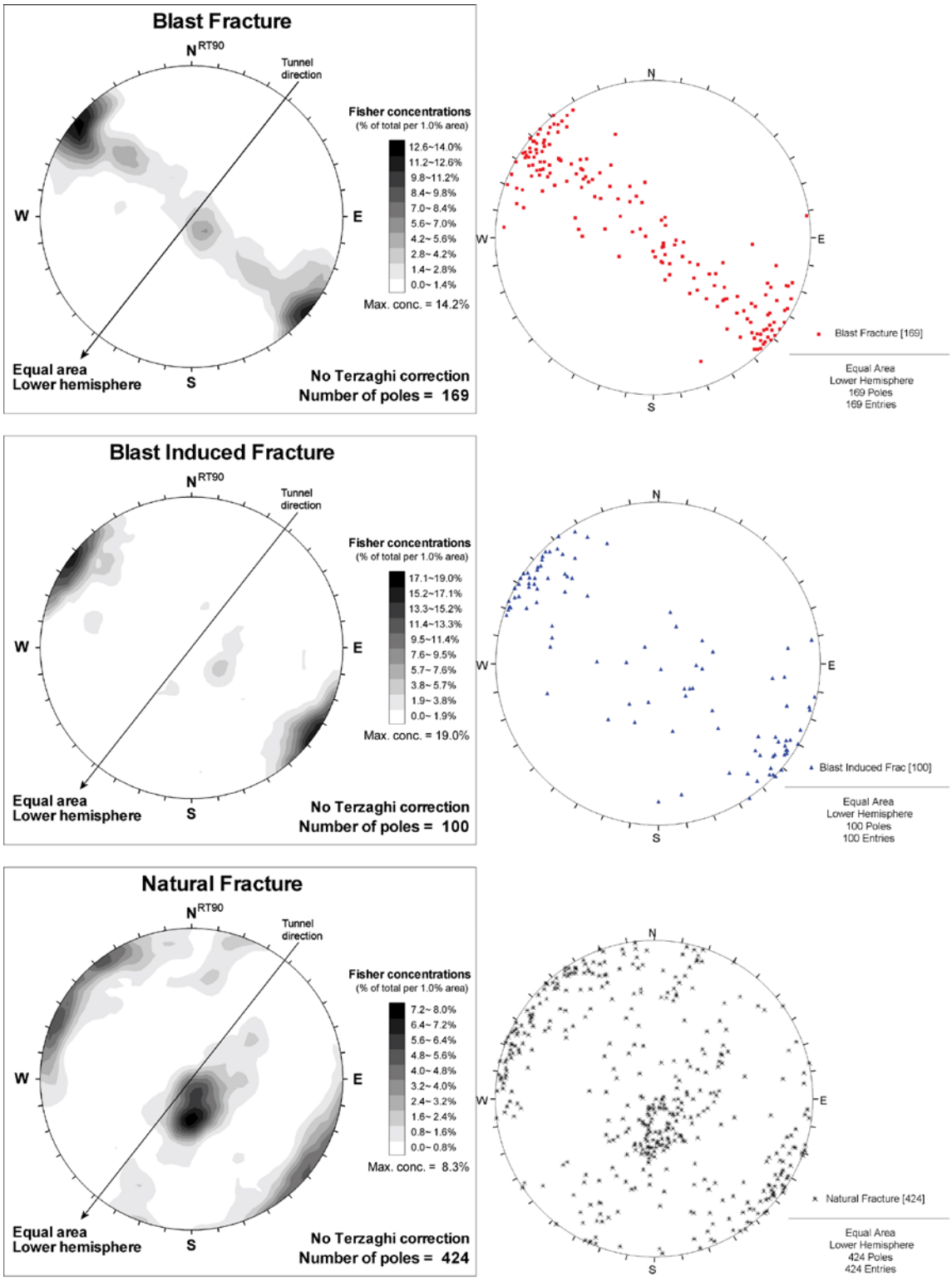

Figure 7-11. *Stereoplots (Fisher) of Blast, Blast Induced and Natural Fractures.*

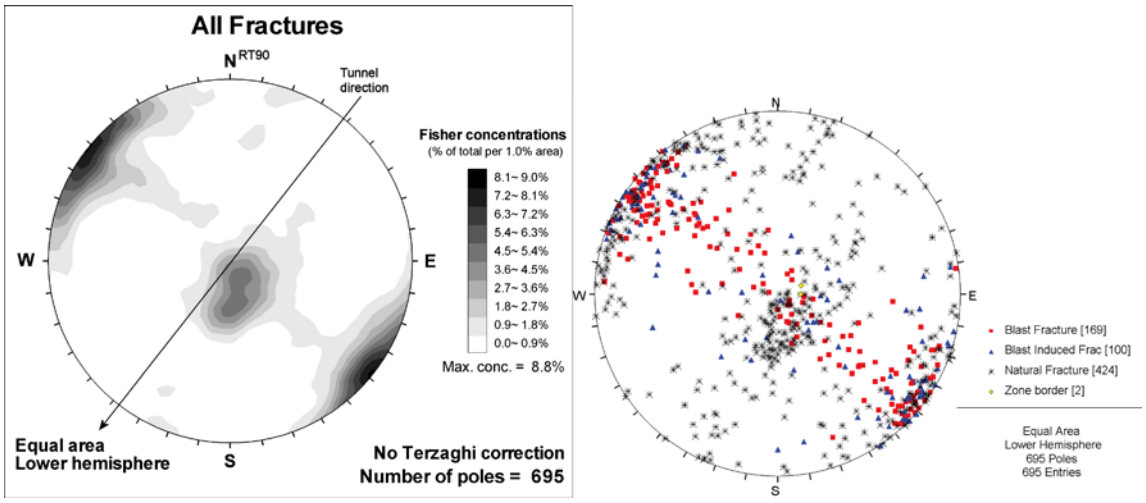

Figure 7-12. *Stereoplots (Fisher) of all modelled fractures.*

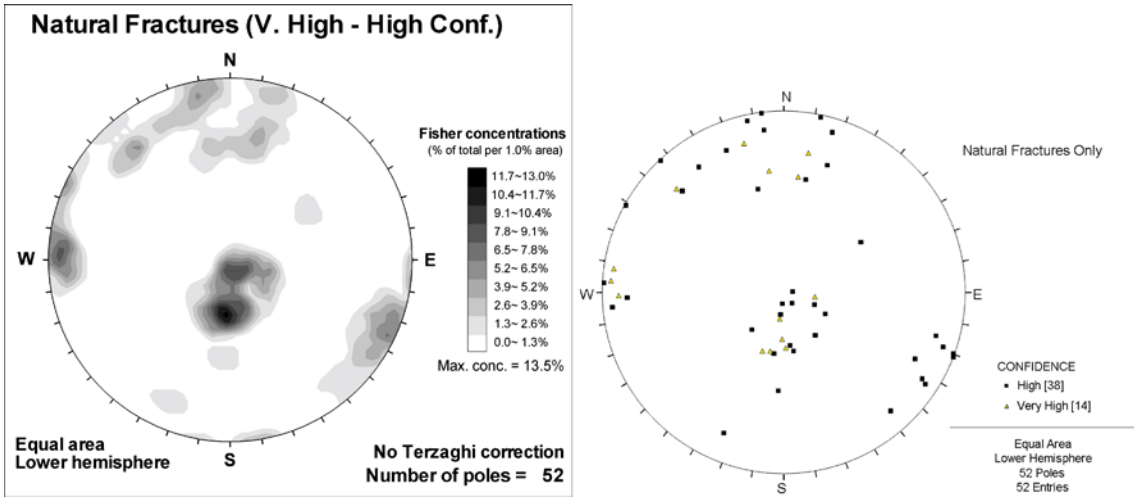

Figure 7-13. *Stereoplots (Fisher) of Natural Fractures with very high or high confidence.*

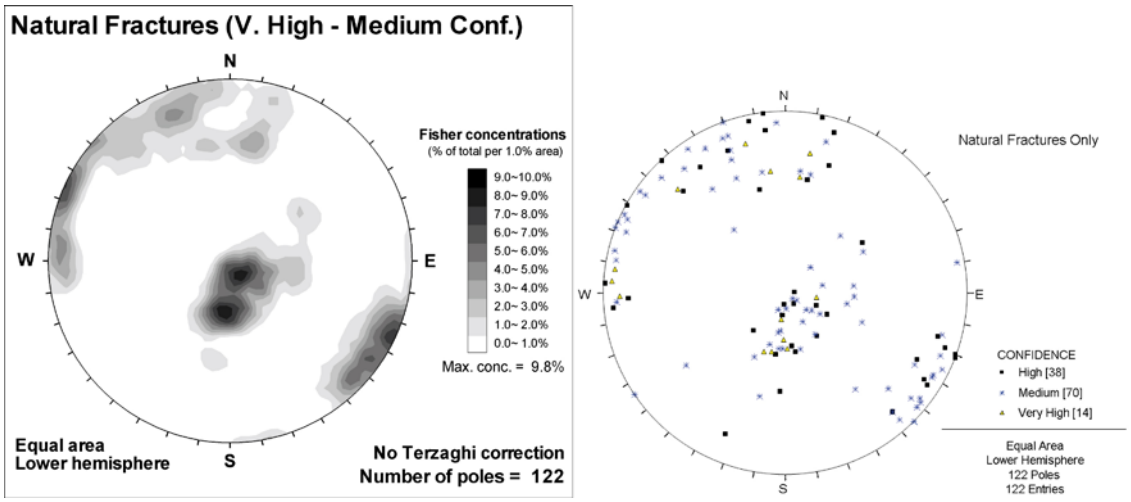

Figure 7-14. *Stereoplots (Fisher) of Natural Fractures with very high, high or medium confidence.*

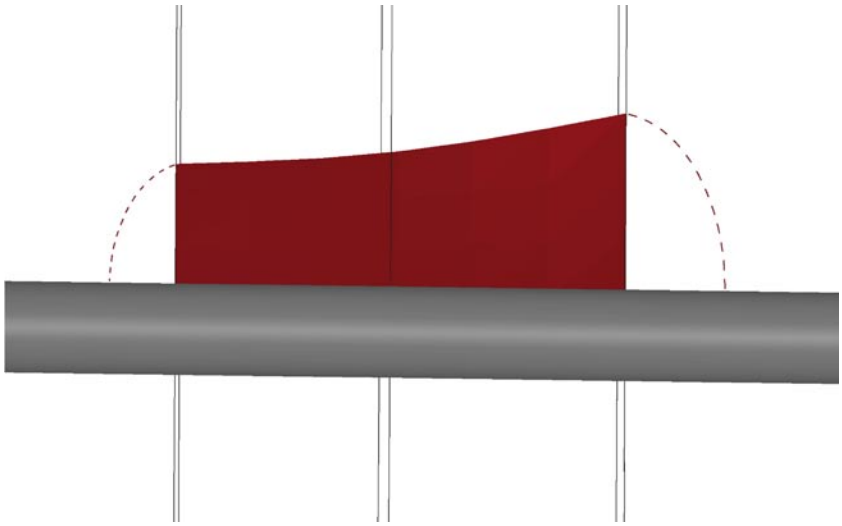

Figure 7-15. *Fracture interpolated between three vertical sections, no extrapolation. The borehole is shown in grey.*

Figure 7-16. *The fracture on the left is only detected on one side of the intersecting fracture, resulting in a gap between the fractures.*

This means that the fractures in the model do not form a fracture network of fractures which are connected with mathematical precision but rather a fragmented set of non-connected fractures whose total persistence is slightly underestimated. This is particularly true for the smaller blast and blast induced fractures, whereas the larger natural fractures more often intersect forming a connected fracture network. However, it is of no big importance that the fractures are not connected with mathematical precision when evaluating the fracture network visually.

These limitations are important to be aware of since they lead to the important knowledge of how this model can, and should be viewed and used. Since the extension of and connection between the fractures are underestimated, the connectivity in the model is much less than could be expected for the actual situation. Thus the model is not suitable for e.g. hydrological modelling without revision.

Due to the geometrical uncertainties regarding fracture orientations, see section 7.2.3, and 8.2 it is not recommended to use the model as a representative description of natural fracture network in the investigated rock mass. At least not until it is analyzed how the sampling bias and the methodology bias affect the result. This is, however, outside the scope of this study.

8 Conclusions

8.1 Blasting results regarding the EDZ

The following conclusions regarding the EDZ are drawn from this investigation.

No evidence is found of a continuous EDZ in the investigated area. Blasting fractures appear like a number of smaller disconnected planes along the contour holes.

No evidence is found that blasting fractures from different rounds are connected. The lateral offset between the hole bottom of a round and the hole start of the next round and the fact that the first part of a round is uncharged makes the distance larger than the extent of the blast fractures, see Figure 8-1.

Blasting fractures are strongly influenced by the presence of natural fractures or a fracture zone and the fracture length from the blasting fractures could be increased when blasting fractures are affected by and drawn to natural fractures. Blasting fractures often stop as they reach natural fractures but they could also cut across the natural fractures.

Since the blasting fractures are connected to the natural fracture network they could open up for potential water transport ways but since they by themselves do not form a continuous network, the main water conductors are still the longer natural fractures, and their capacity is the limit of potential water flow in the rock mass.

The blast and blast induced fractures have a near-planar geometry and should not be expected to be winding or twisted. In section 6.1.1 it is stated that a blast fracture that reaches a fracture can jump sideways and continue on the other side of the intersecting fracture. It is also stated that what appears to be a single wavy fracture probably often constitute a number of fracture fingers. This is supported by what was found in the detailed investigation, see section 6.2.4, Figure 6-18.

A surprising observation is that in some parts of the holes, where there should be blasting fractures, there are none; this is further elaborated in chapter 7.

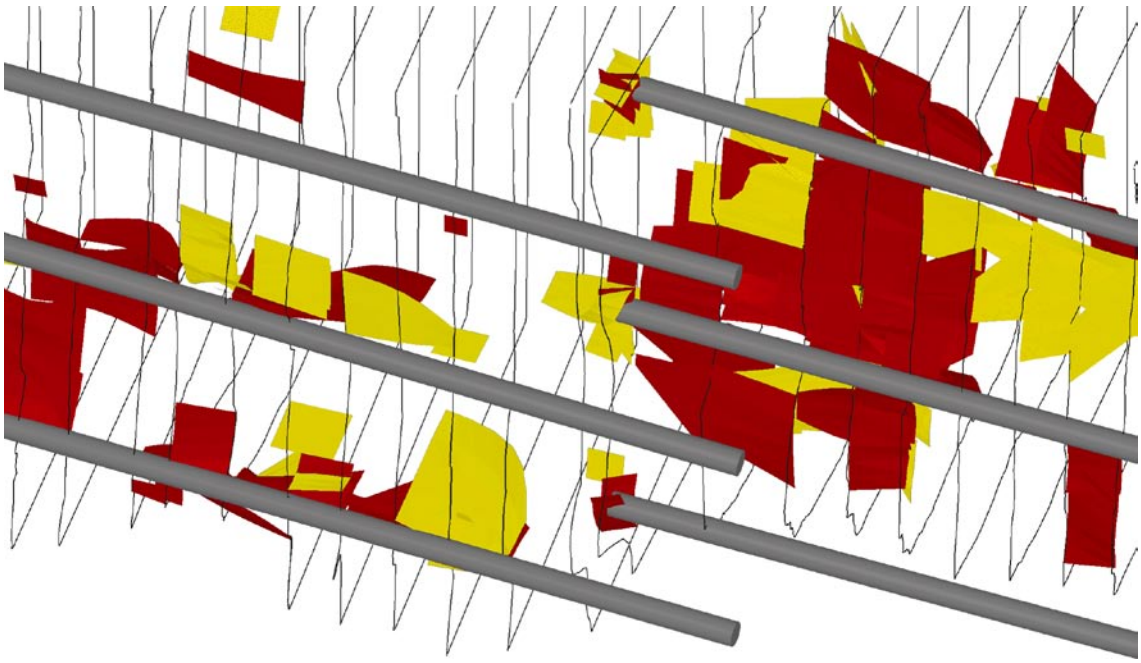

Figure 8-1. *Modelled blasting fractures at the transition zone between round 9 and 10.*

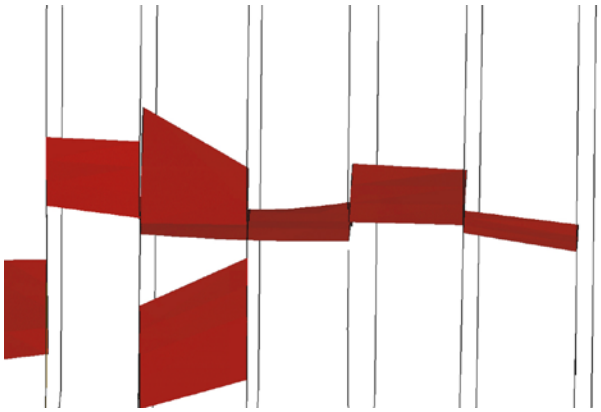

Figure 8-2. *Blast fractures interpolated between sections.*

Figure 8-3. *Fractures detected in only one section modelled as planes on the left and the same fractures shown together with surrounding fractures on the right.*

All fracture traces are modelled into fracture planes, also those where no connections were found in adjacent sections. This is done to give a better image of the distribution of primarily the blast and blast induced fractures as they otherwise would be completely nonexistent in the sections where they are very small. All these fractures have the confidence class very low and should not be used in any analysis concerning fracture orientation since their true orientation cannot be modelled from a single fracture trace.

Since the fractures are not extrapolated beyond the observations in the sections, it is not possible to see how the fractures terminates along the contour blast holes, see Figure 7-15.

As fractures with a width < 20 µm cannot be detected, no such fractures are modeled.

8.2 Uncertainties regarding the EDZ

As discussed earlier, most modelled fractures are small and are not detectable in more than a few sections. Hence the confidence in geometry is low or very low for the majority of the modelled fractures.

However, the uncertainties regarding the geometries of the individual fractures do not affect the overall conclusions concerning the EDZ since the fracture traces in the transition zones are so far apart in 3D space, see Figure 8-1.

Regarding the natural fractures there is a difference of about 10°–20° between the predominant orientation for the modelled natural fractures, about 130°/310°, which is near parallel to the tunnel direction or perpendicular to the sampling planes, and the expected orientation for fractures in the investigated area, about 140°–150°/320°–330°. This can be caused either by sampling bias or methodology bias as described in section 7.2.3.

Also the blasting fractures are small and there are numerous ways of connecting them between the sections. However, the detailed investigation showed that four out of six investigated fractures were correctly interpreted and for one of the other two fractures, only a minor correction was necessary. Even if the detailed investigation is limited, this implies that the general interpretation is fairly correct.

9 Discussion

9.1 Positive experiences from the used method

Method with wire sawing and block removal is a good method for large scale characterisation of the EDZ. The earlier proposed method of drilling longer holes behind the area would probably save time though.

The technique of sawing blocks to slabs worked fine. Mapping the block side before sawing is better than mapping the slab side after sawing since there is a big risk that the slab falls apart when moving it after sawing.

It is possible to detect fractures, natural, blasting or blast induced fractures with the dye penetrant method being used.

The photo documentation with modern SLR camera equipment was very successful and the images were very informative and were very useful for digitizing.

The program used for digitizing worked fine for the purpose intended.

The technique for georeferencing the investigated slab sides worked fine too. The surveyed points in the tunnel could be used for referencing the blocks at the sawing place and later for referencing each slab side as the block was sawed. The minor additive systematic errors that had to be corrected were very small. Surveying the corner of the sawed out volume vas invaluable for verification and correction.

The modelling in RVS worked well. The handling of views, reference files and objects made it fairly easy to use RVS for the evaluation of the fractures. The modelling function, which creates fracture surfaces from slab surface trace lines, is suitable for this task. Some weaknesses are elaborated below.

9.2 Limitations of the used method

In more damaged rock it can be difficult to get intact blocks. Hence, this method of investigation is limited to sites with relatively good rock quality.

The modelling function in RVS, which creates fracture surfaces from trace lines proved suitable for the task at hand but does not create a continuous fracture network. This limits the usability of the model for other purposes, such as hydrological modelling. In order to achieve a continuous fracture network, a fracture extrapolation functionality must be added.

9.3 Possible improvements

The information regarding the position of the hole bottoms was inaccurate and contradictory. The second transition zone proved hard to evaluate as a large fracture caused the block to split in half. This indicates that the documentation of the tunnel wall prior to block excavation must be improved. (e.g. detailed geological mapping of the area and thorough surveying of blast hole bottoms). The importance of this was not evident before the evaluation of the modelling.

When excavating the blocks, drilling and transportation were limited due to an injection test that was carried out in the same tunnel at the same time. Unlimited access to the investigation site without disturbance of other activities is vital for effective work.

In this investigation it was revealed after the investigation that the lowest hole of the first investigated transition zone, hole C of round 9, was re-blasted. This indicates that more time for planning is necessary to give time to evaluate all site specific information prior to investigation.

All information concerning charging was limited to the planned charging. The documentation of the actual charging in each hole was insufficient and this must be improved for the holes in the test area in future investigations.

The time for digitizing in parallel with the documentation of the slabs was limited as time had to be spent on handling the slabs. This could have been handled by an extra hand.

The technique for turning blocks must be improved, to avoid damaging the blocks.

Differences in interpretation when digitizing showed that when two or more persons are doing this job, an early follow-up must be made to harmonize their interpretations.

The detailed investigation gave a lot of information, which affected the interpretation and modelling. It could be advantageous to investigate more details and maybe at an earlier stage in the process. When performing the investigation, core drilling in combination with sawing proved to be a suitable method.

If the block sides had been photographed in UV light, calcite filled fractures could easily had been identified.

Information regarding fracture directions on perpendicular surfaces is invaluable when modelling. In the first block penetrants were sprayed on all sawed sides except the bottom side, this should have been done on all blocks, and the block sides should have been investigated. This must be considered from the start so that the block sides are as free as possible when strapping the block for transport.

When digitizing in QGIS, see chapter 5, each fracture trace was given a unique ID. Unfortunately, when converting the digitized files to MicroStation dgn-files the ID's were lost. In future investigations, this must be solved.

9.4 Experiences from modelling

During the evaluation process, the knowledge of how to interpret and connect fracture traces has grown.

- When fracture traces appear curved and wide it is most likely a fracture intersecting the investigated section at an acute angle.
- It is important to review adjacent sections and other interpreted fractures when modelling.
- Blasting fractures are affected by nearby natural fractures and fracture zones. They can be drawn towards open fractures.
- Perpendicular surfaces, such as the block sides, are very informative when modelling in 3D and should be investigated when possible.
- The penetrant does not reveal closed fractures, which is unfortunate since their presence could affect the formation of the blasting fractures.
- The fracture pattern near the bottom charge is complicated and difficult to model.
- The knowledge of the handling of blocks, the interpretation of photos and the 3D modelling grows during the work. Thus, it is better to start an investigation with the least important area and to save the more important areas to the end when the work process has improved.
- The selected distance between sections of 10 cm makes it difficult to detect many fractures in more than one section since the fractures are fairly small. A distance of 5 cm had probably given a better basis for modelling, but had increased the workload since it had increased the amount of data. It could be an idea to slice thinner slabs in areas of particular interest such as in the end of a blast round.
- Detailed investigations of selected areas are important and informative.
- There is a difference between the predominant orientation for the modelled natural fractures and the expected orientation for fractures in the investigated area which can be caused either by sampling bias or methodology bias as described in section 7.2.3.

9.5 Other experiences and recommendations

Other experiences and recommendations from this investigation are listed below:

- When core drilling in poor rock small pieces of rock became wedged and got stuck in the bore-hole leading to significant delays. The use of a temporary casing, along with a triple-tube core barrel with a split liner, would have saved time and improved core recovery.
- I would have been interesting to let an independent team digitize and model a part of the model volume as a test of consistency. This would be very informative regarding the uncertainty of the model.
- It was initially planned to saw the slabs first and to move them indoors for investigation. The methodology developed during the project was to map the block surface prior to sawing. This means that the investigation must be done at the sawing place. To cover the equipment from rain a tent was used. This tent was, however, sensitive for wind and sunlight also disturbed the lighting conditions with shadows etc. In retrospect, a better solution would have been to set up the sawing and investigation place in the tunnel. This would decrease the distance the blocks have to be transported, give better control over lighting, give better possibility to create a steady platform and would be less weather sensitive. An issue is then the height of the tunnel, the setup used requires that the camera is mounted at least 2.5 m above the investigated surface.
- There turned out to be much interest for the photographs from other parties. Hence it would have been good to photograph the investigated surfaces wet and dry prior to applying penetrant dye.

10 Acknowledgements

We greatly acknowledge the following people:

- Ann Bäckström, Stefan Grandin-Svärd, Gerry Johansson and the personnel of DWT for invaluable help with the field work.
- Mats Elfström for his help with setting up a system for digitalization, preparation and conversion of digitizing files and for input to this report.
- Christer Andersson and Rickard Karlzén for input regarding the tunnel excavation.
- Phil Curtis, Carl Henric Wahlgren and Aaron Fox for their contributions to this report.
- Pär Kinnbom for providing us with background data regarding tunnel geometry.

We also want to express our appreciation to Finn Ouchterlony for his review of the original draft of this report and for input regarding the process of blasting fracture propagation.

A special thanks to Rolf Christiansson who conceived, initiated, supported and supervised this investigation.

11 References

Andersson C, 2007. Äspö Pillar Stability Experiment, Final Report. Rock mass response to coupled mechanical thermal loading. SKB TR-07-01, Svensk Kärnbränslehantering AB.

Berglund J, Curtis P, Eliasson T, Olsson T, Starzec P, Tullborg E-L, 2003. Update of the geological model 2002. SKB IPR-03-34, Svensk Kärnbränslehantering AB.

Curtis P, Elfström M, Markström I, 2007. Rock Visualization System. Technical description (RVS version 4.0). SKB R-07-44, Svensk Kärnbränslehantering AB.

Drake H, Tullborg E-L, 2007. Fracture mineralogy. Results from drill cores KLX03, KLX04, KLX06, KLX07A, KLX08 and KLX10A. Oskarshamn site investigation. SKB P-07-74, Svensk Kärnbränslehantering AB.

Johansson C J, Persson P-A, 1970. Detonics of High Explosives. Academic Press, London.

Malmtorp J, Andersson C, Karlzén R, 2008. Berguttag i TASS-tunneln-Delresultat t o m september 2008. SKB R-08-122, Svensk Kärnbränslehantering AB.

Nisca D, 1987. Aerogeophysical interpretation. SKB Progress Report 25-87-04. Swedish Hard Rock Laboratory.

Olsson M, Bergquist I, 1993. Crack lengths from explosives in small diameter boreholes. In Fragblast 4, Proc 4thIntnl Symp on Rock Fragmentation by Blasting 193–196. H P Rossmanith ed. Balkema, Rotterdam.

Olsson M, Bergqvist I, 1995. Sprickutbredning vid flerhålssprängning. SveBeFo Rapport 18.

Olsson M, Bergquist I, 1996. Crack lengths from explosives in multiple hole blasting. In: Fragblast 5, Proc 5thIntnl Symp on Rock Fragmentation by Blasting 187–191. B Mohanty ed. Balkema, Rotterdam.

Olsson M, Bergqvist I, 1997. Sprickutbredning vid flerhålssprängning – Sammanfattande rapport av försöksperioden 1993–1996. SveBeFo Rapport 32.

Olsson M, Ouchterlony F, 2003. Ny skadezonsformel för skonsam sprängning. SveBeFo Rapport 65.

Olsson M, Niklasson B, Wilsson L, Andersson C, Christiansson R, 2004. Experiences of blasting of the TASQ tunnel. SKB R-04-73, Svensk Kärnbränslehantering AB.

Olsson M, Markström I, Pettersson A, 2008. Methodology study for documentation and 3D modelling of blast induced fractures. SKB R-08-90, Svensk Kärnbränslehantering AB.

Ouchterlony F, 1983. Analysis of cracks related to rock fragmentation. In Rock Fracture Mechanics (H P Rossmanith ed.) pp 31–67. CISM Courses and Lectures No. 275. Springer, Wien.

Ouchterlony F, 1992. Some recent research and developments in Swedish tunnel blasting. Report DS 1992:1, Swedish Detonic Research Foundation, Stockholm.

Ouchterlony F, Olsson M, Båvik SO, 2000. Perimeter blasting in a 130 m road cut in gneiss with holes with radial bottom slots. Proceedings of the 1th world conference on explosives & blasting technique, Munich Germany. Balkema.

Ouchterlony F, Olsson M, Bergqvist I, 2002. Towards new Swedish recommendations for cautious perimeter blasting. Int J for Blasting and Fragmentation 6, 235–261.

Wahlgren C-H, Curtis P, Hermanson J, Forssberg O, Öhman J, Fox A, La Pointe P, Drake H, Triumf C-A, Mattsson H, Thunehed H, Juhlin C, 2008. Geology Laxemar. Site descriptive modelling SDM-Site Laxemar. SKB R-08-54, Svensk Kärnbränslehantering AB.

Appendix 1

Images

Photos of block sides without and with digitized fracture traces classified as natural fractures (green), blast fractures (red) and blast induced fractures (yellow). The digitized fracture traces have their original classification; however, some were re-evaluated when modelling.

VS0036B01

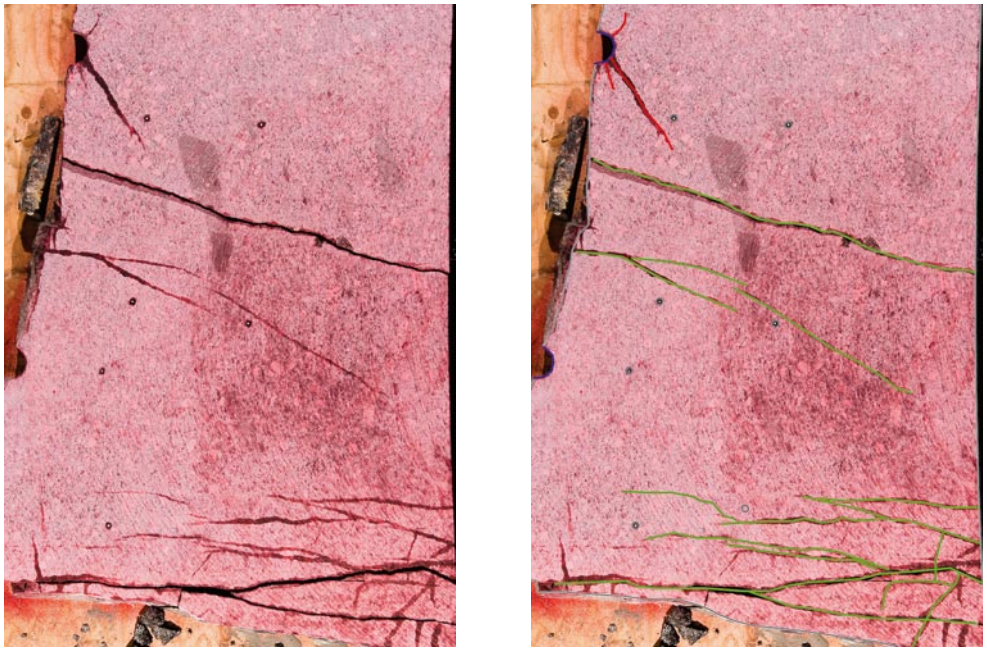

VS0036B02

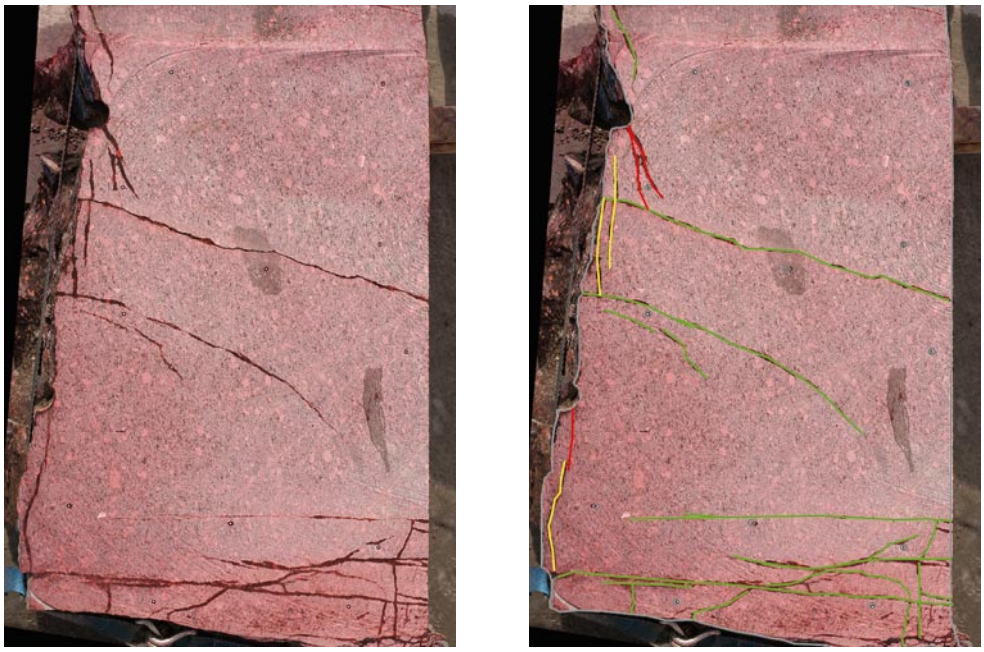

VS0036B03

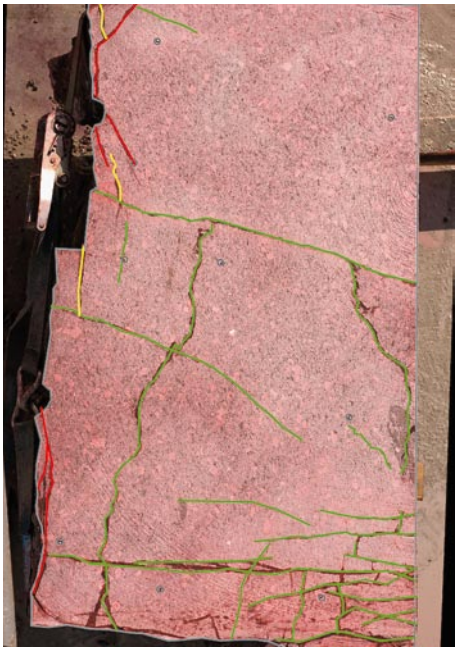

VS0036B04

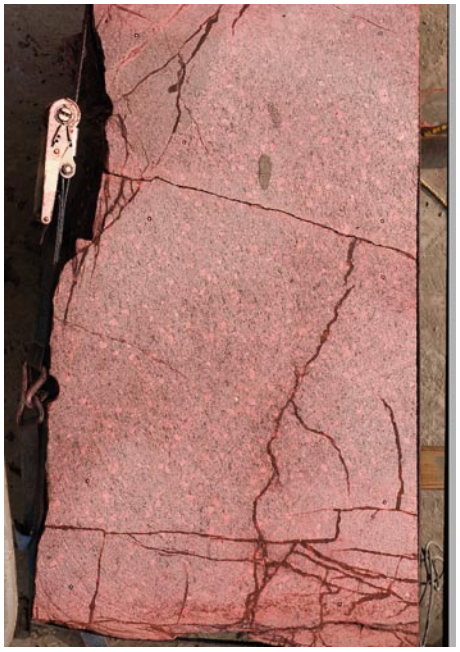

VS0036B05

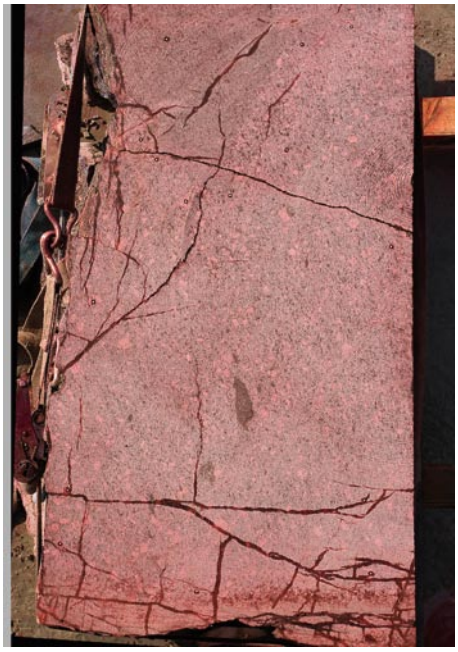

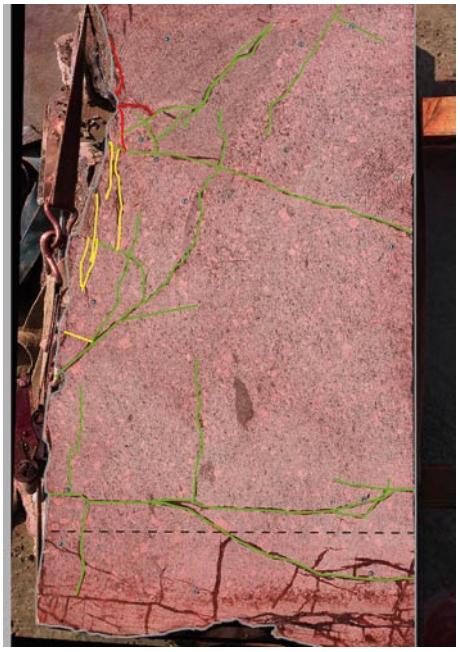

VS0036B06

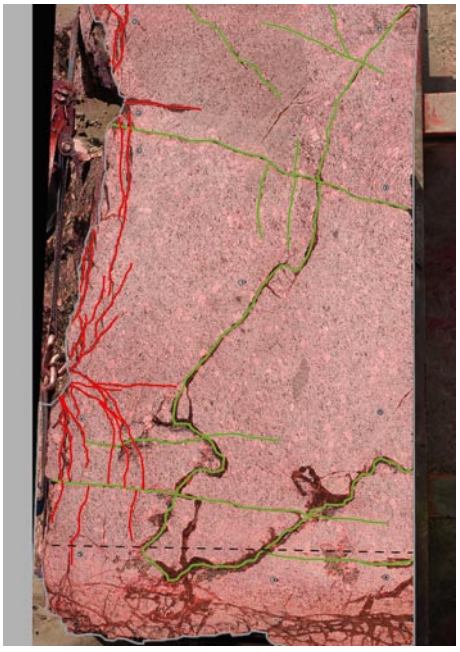

VS0036B07

VS0036B08

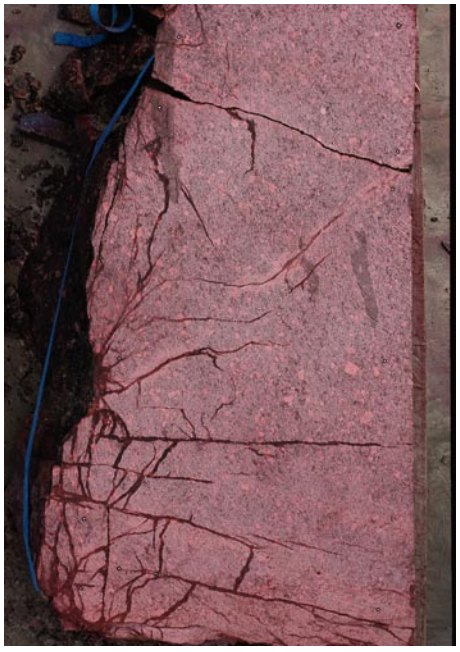

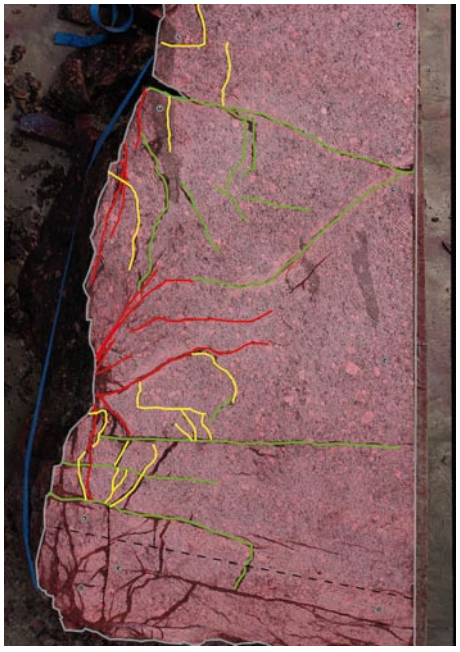

VS0036B09

VS0037B01

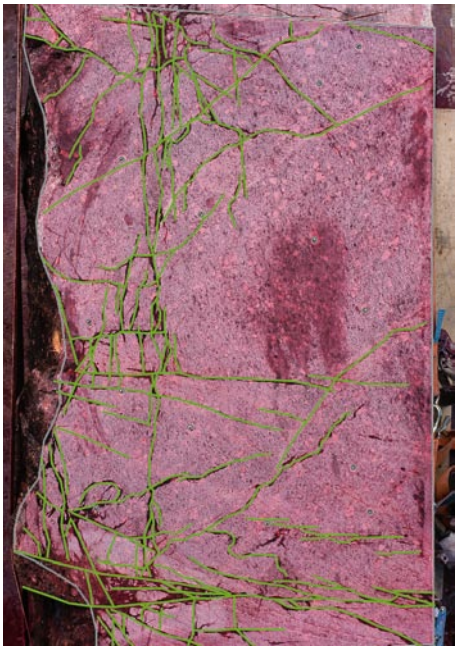

VS0037B02

VS0037B03

VS0037B04

VS0037B05

VS0037B06

VS0037B07

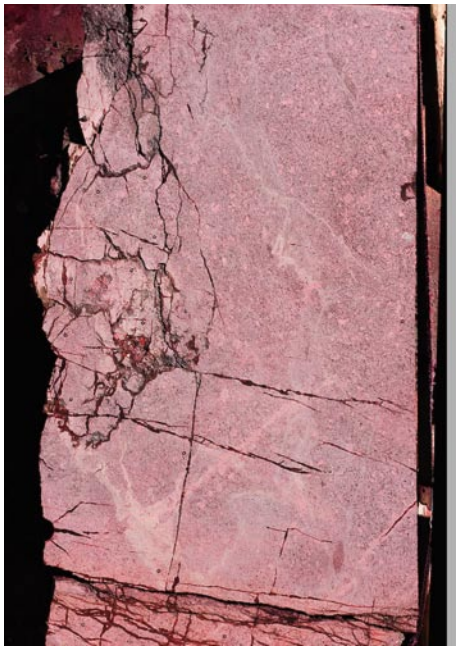

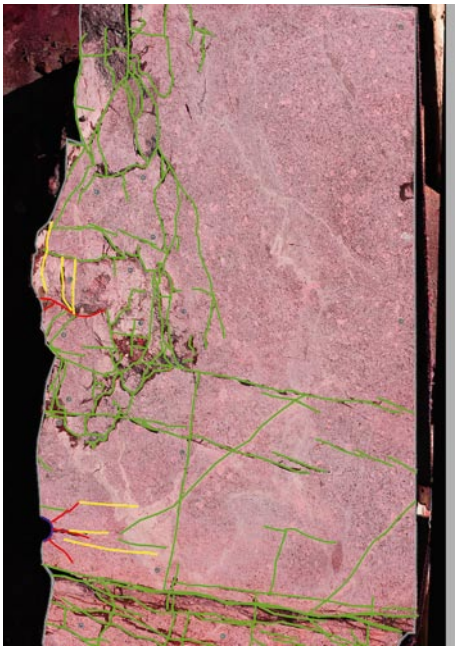

VS0037B08

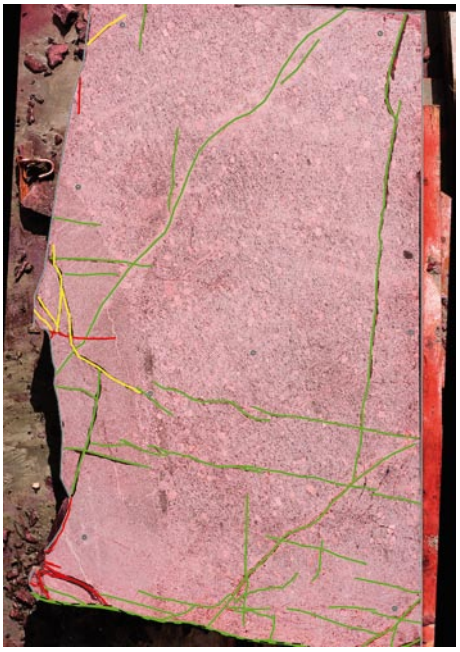

VS0037B09

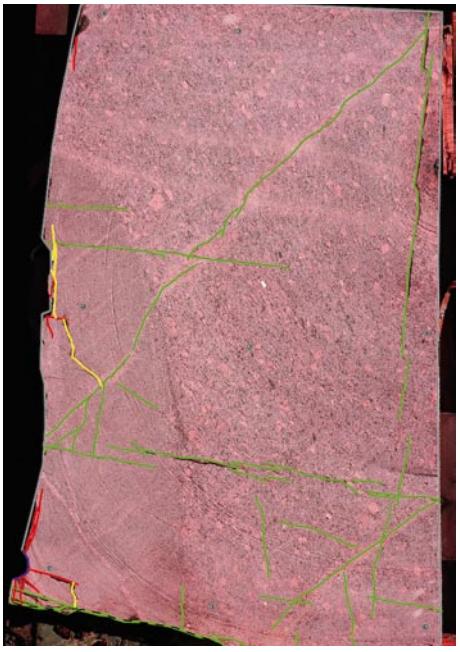

S0038B01

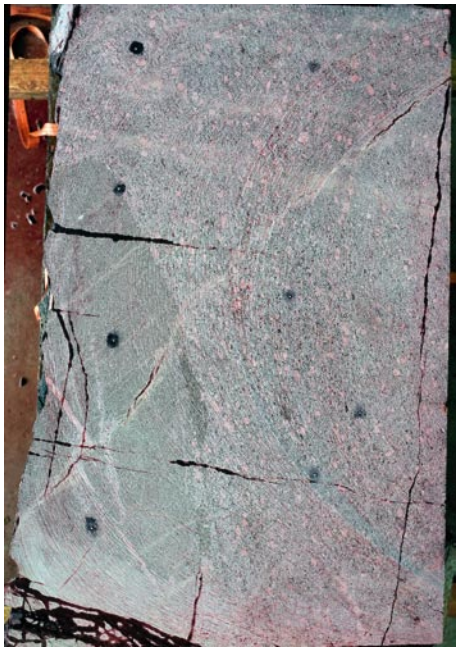

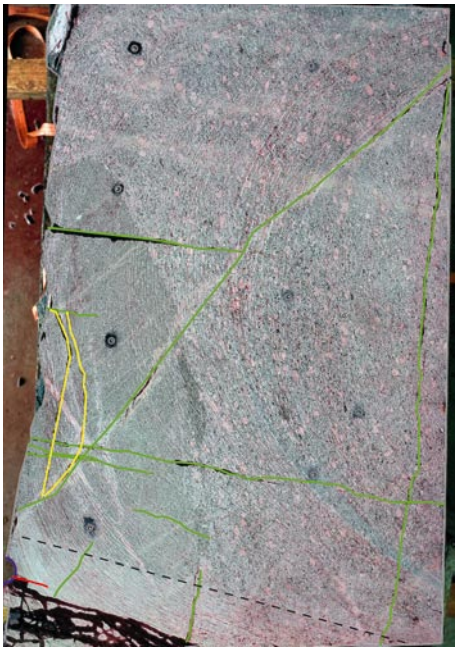

VS0038B02

VS0038B03

VS0038B04

VS0038B05

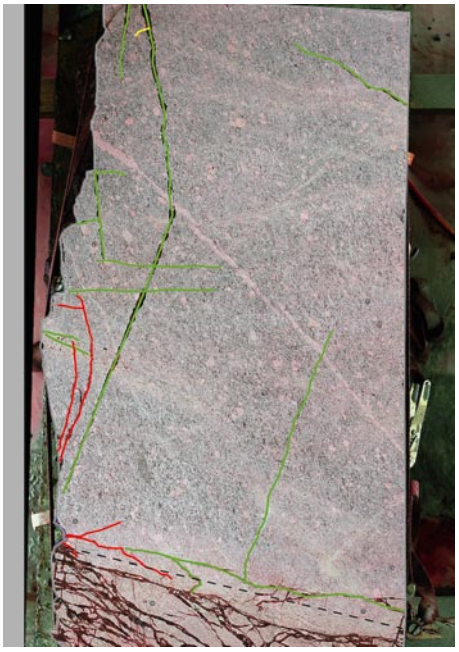

VS0038B06

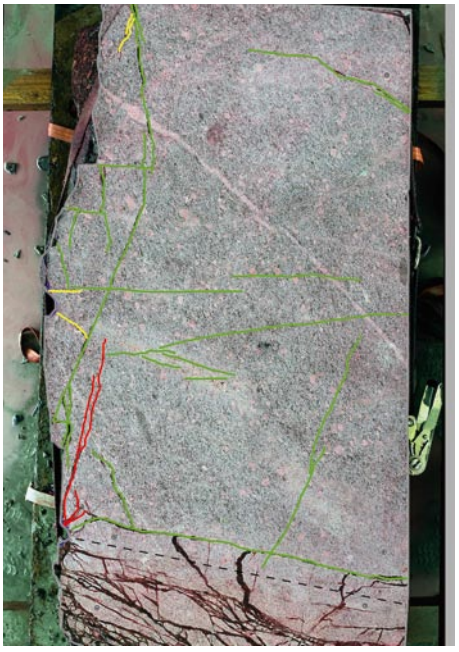

VS0038B07

VS0038B08

VS0038B09

VS0039B01

VS0039B02

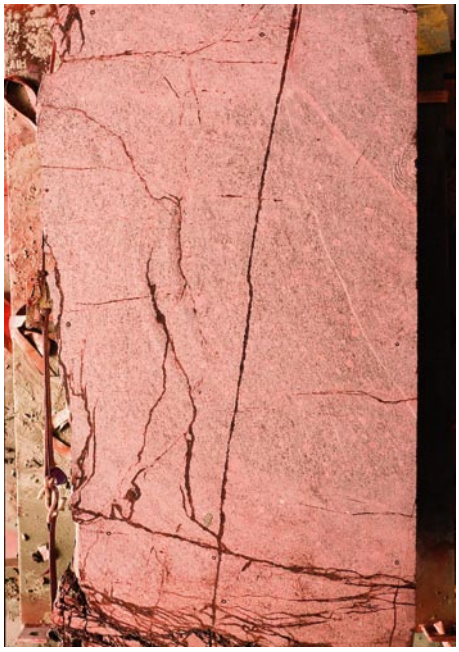

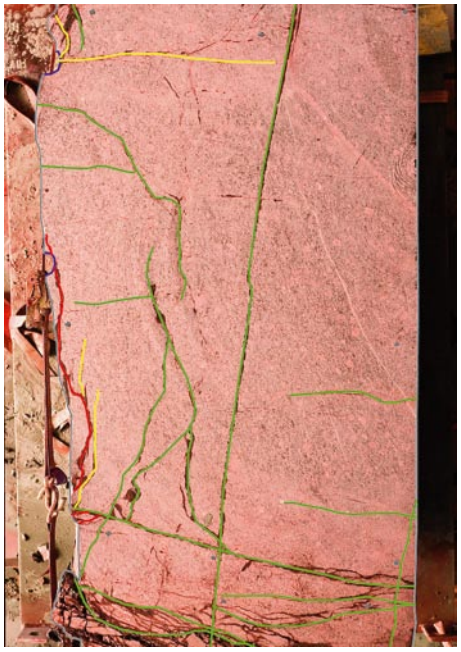

VS0039B03

VS0039B04

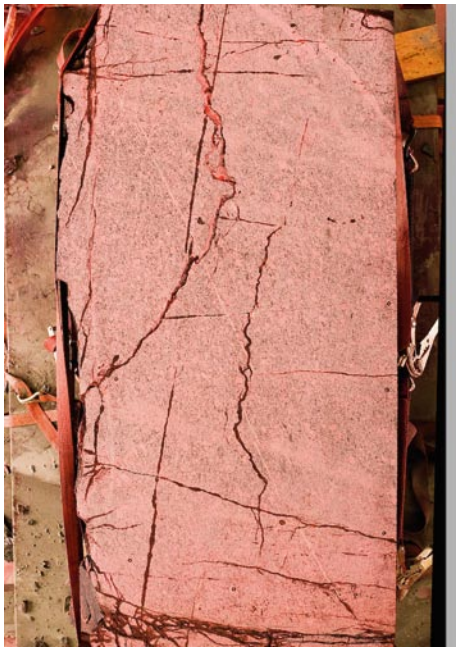

VS0039B05

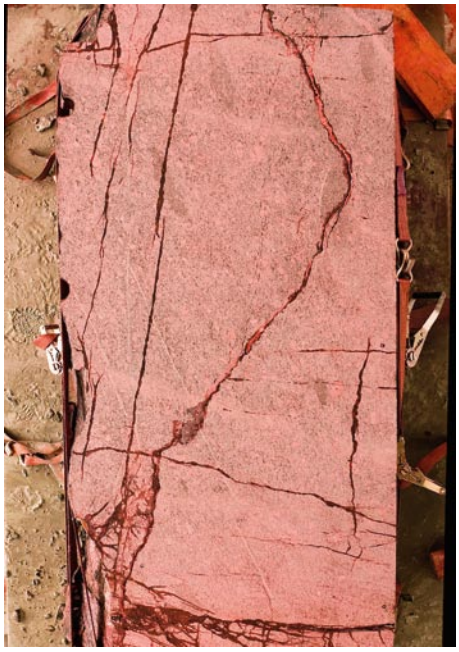

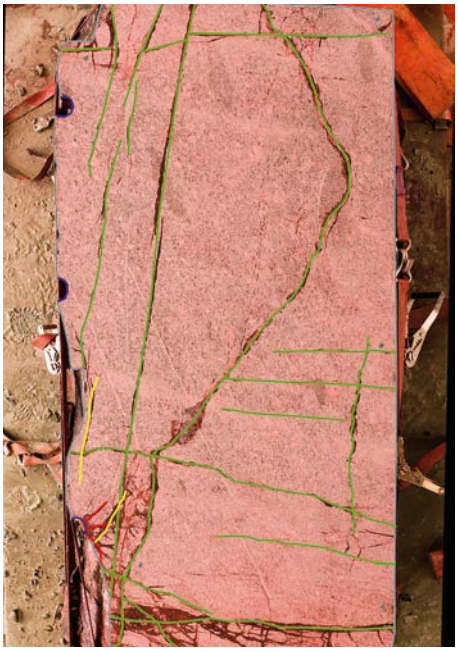

VS0039B06

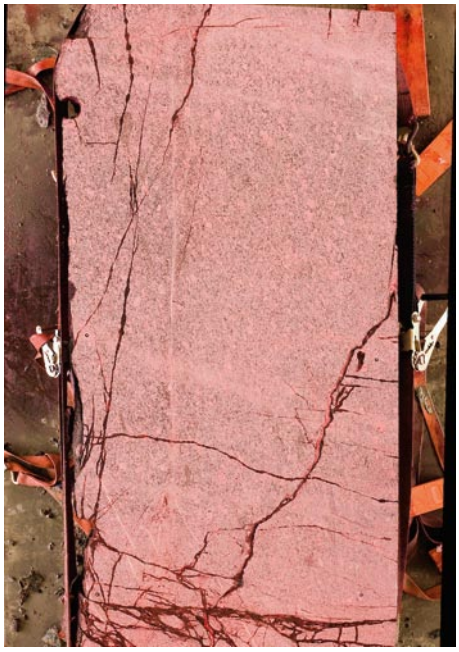

VS0039B07

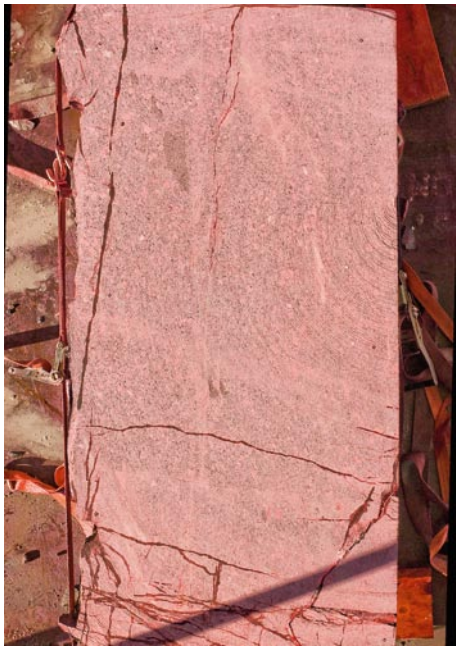

VS0039B08

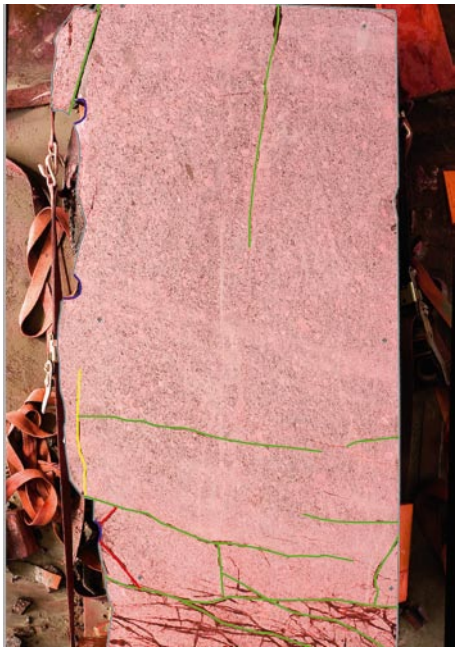

VS0039B09

VS0040B01

VS0040B02

VS0040B03

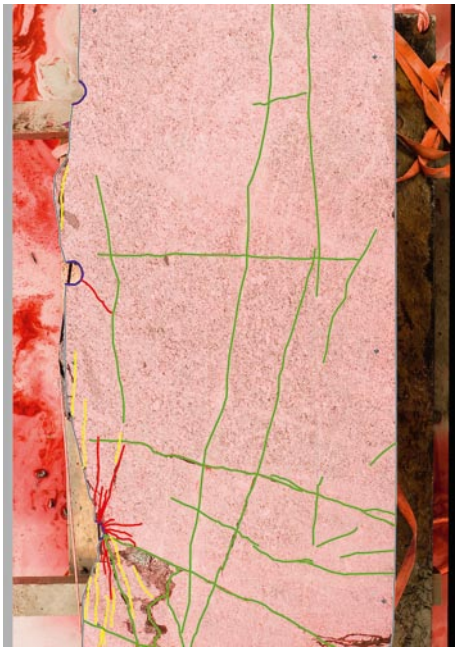

VS0040B04

VS0040B05

VS0040B06

VS0040B07

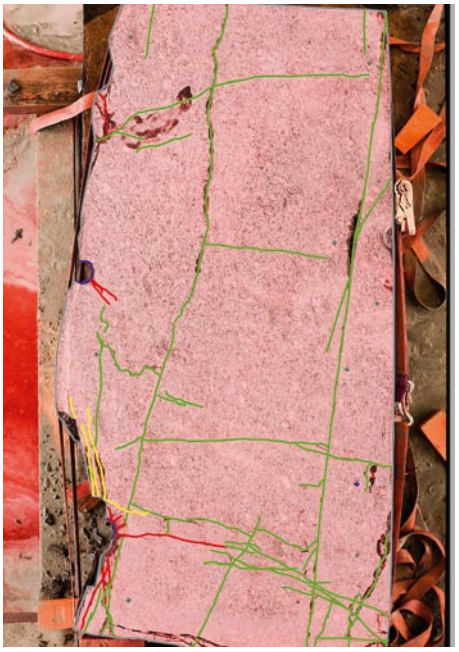

VS0040B08

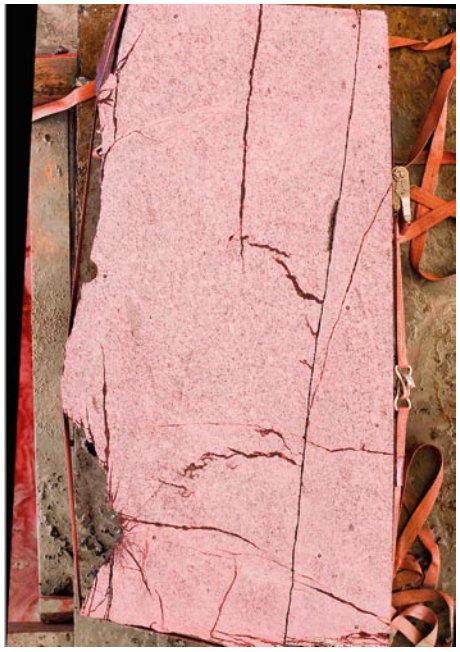

VS0040B09

VS0041B01

VS0041B02

VS0041B03

VS0041B04

VS0041B05

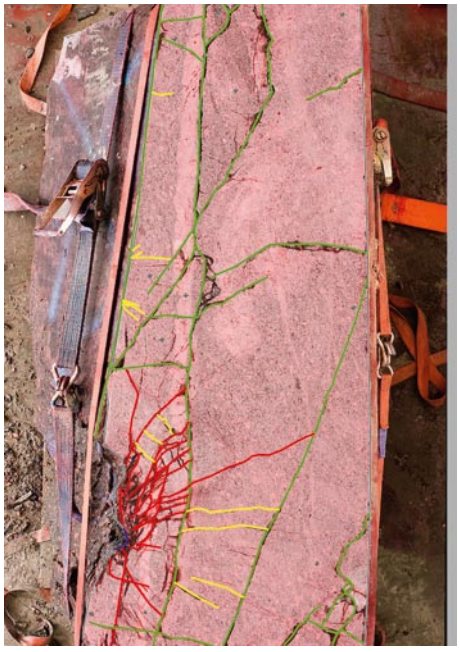

VS0041B06

VS0041B07

VS0041B08

VS0041B09

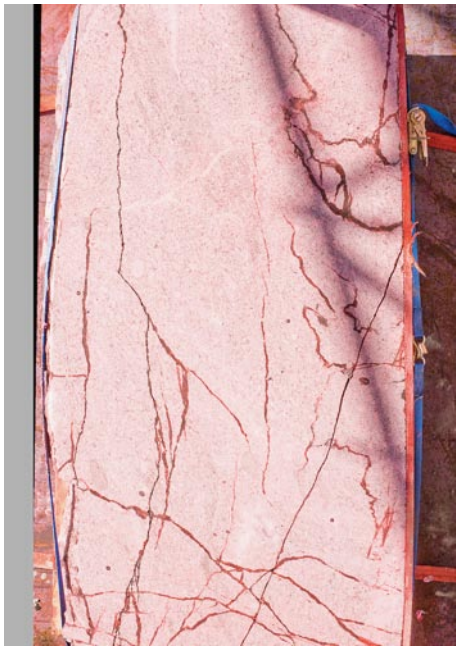

VS0041B10

VS0042B01

VS0042B02

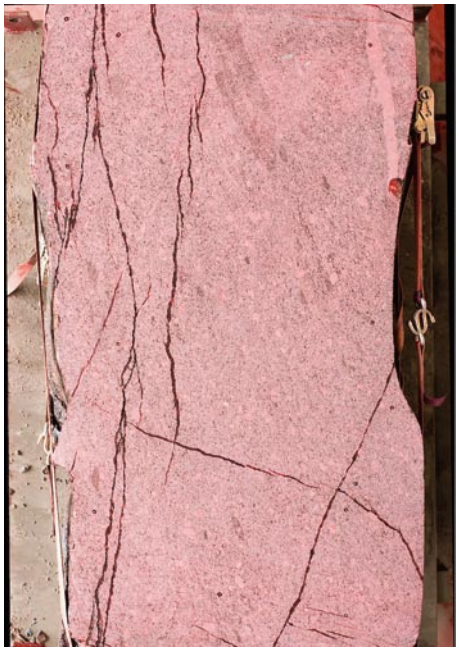

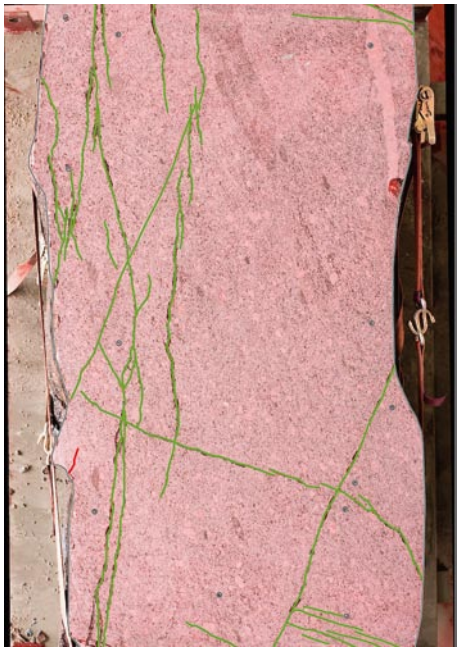

VS0042B03

VS0042B04

VS0042B05

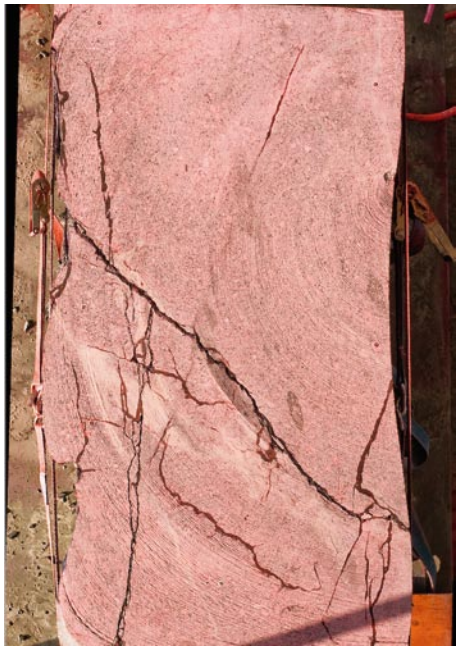

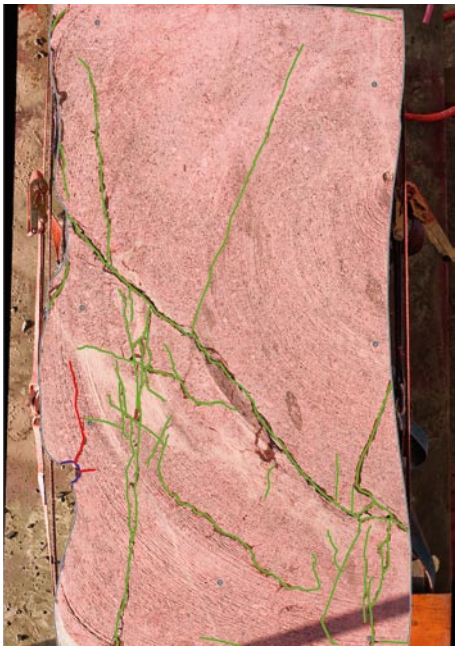

VS0042B06

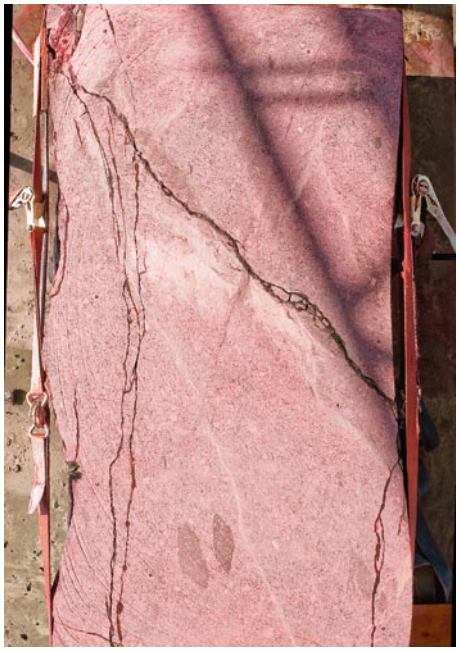

VS0042B07

VS0042B08

VS0042B09

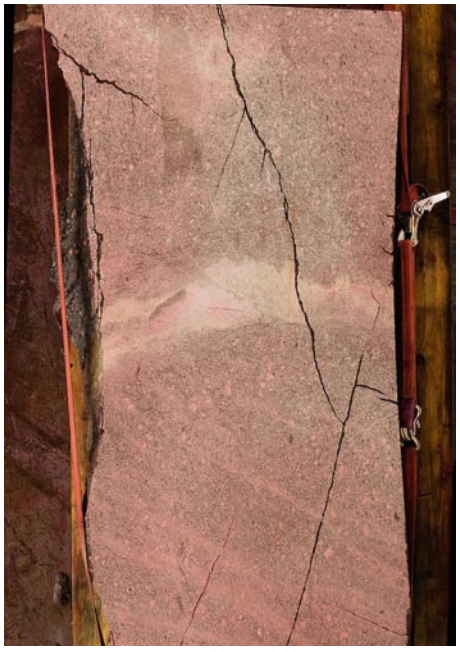

VS0042B10

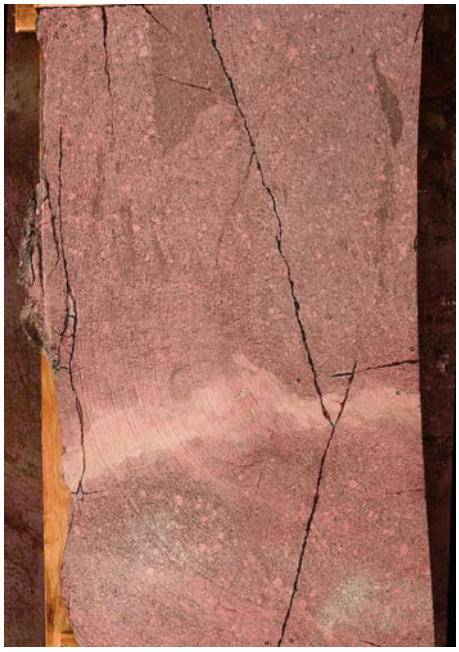

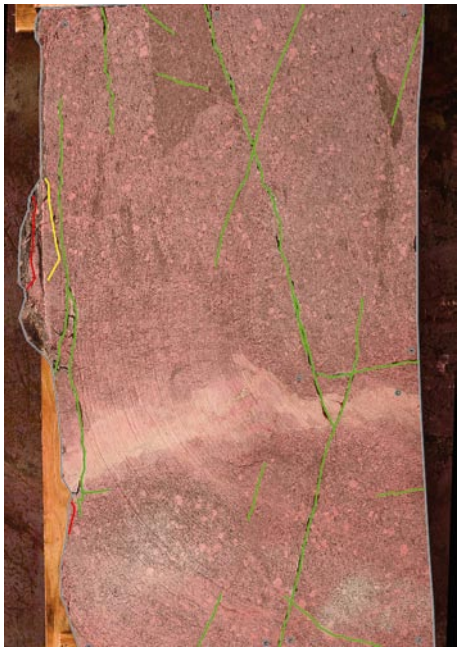

VS0043B01

VS0043B02

VS0043B03

VS0043B04

VS0043B05

VS0043B06

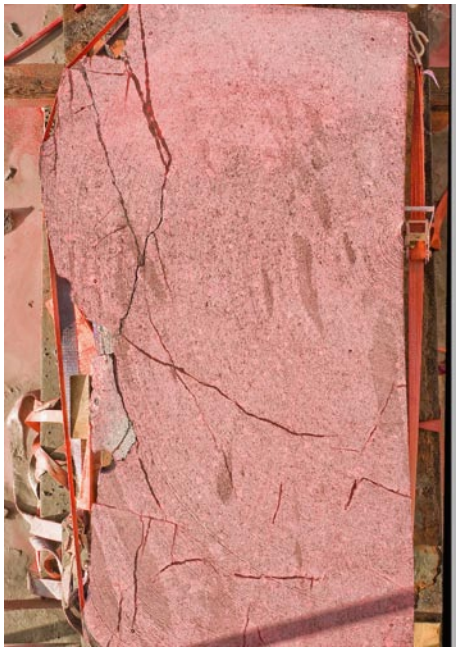

VS0043B07

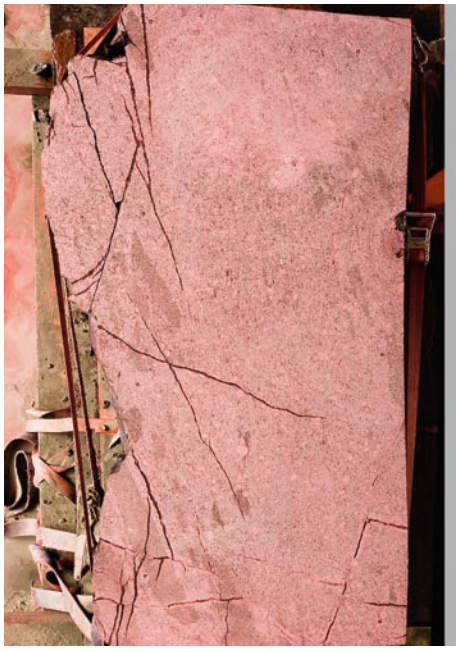

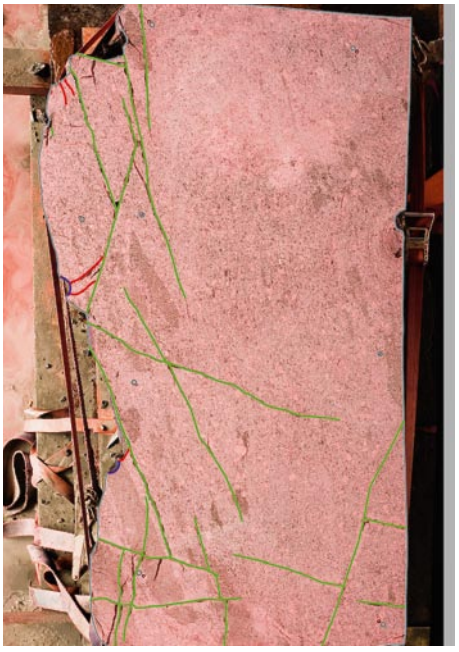

VS0043B08

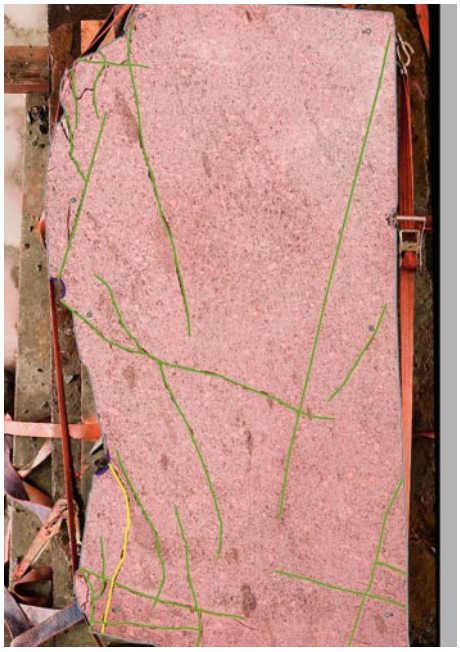

VS0043B09

VS0043B10